

SANDIA REPORT

SAND92-2272 • UC-212

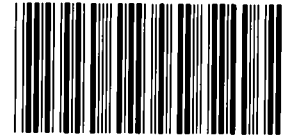
Unlimited Release

Printed January 1993

RETAIN HARDCOPY

MICROFICHE

Utility Battery Storage Systems Program Report for FY92



8541076

Paul C. Butler

SANDIA NATIONAL
LABORATORIES
TECHNICAL LIBRARY

Prepared by
Sandia National Laboratories
Albuquerque, New Mexico 87185 and Livermore, California 94550
for the United States Department of Energy
under Contract DE-AC04-76DP00789

Issued by Sandia National Laboratories, operated for the United States Department of Energy by Sandia Corporation.

NOTICE: This report was prepared as an account of work sponsored by an agency of the United States Government. Neither the United States Government nor any agency thereof, nor any of their employees, nor any of their contractors, subcontractors, or their employees, makes any warranty, express or implied, or assumes any legal liability or responsibility for the accuracy, completeness, or usefulness of any information, apparatus, product, or process disclosed, or represents that its use would not infringe privately owned rights. Reference herein to any specific commercial product, process, or service by trade name, trademark, manufacturer, or otherwise, does not necessarily constitute or imply its endorsement, recommendation, or favoring by the United States Government, any agency thereof or any of their contractors or subcontractors. The views and opinions expressed herein do not necessarily state or reflect those of the United States Government, any agency thereof or any of their contractors.

Printed in the United States of America. This report has been reproduced directly from the best available copy.

Available to DOE and DOE contractors from
Office of Scientific and Technical Information
PO Box 62
Oak Ridge, TN 37831

Prices available from (615) 576-8401, FTS 626-8401

Available to the public from
National Technical Information Service
US Department of Commerce
5285 Port Royal Rd
Springfield, VA 22161

NTIS price codes
Printed copy: A06
Microfiche copy: A01

SAND92-2272
Unlimited Release
Printed January 1993

Distribution
Category UC-212

Utility Battery Storage Systems Program Report for FY92

Paul C. Butler, Manager
Storage Batteries Department

Sandia National Laboratories
Albuquerque, New Mexico 87185

Abstract

Sandia National Laboratories, New Mexico, conducts the Utility Battery Storage Systems Program, which is sponsored by the U.S. Department of Energy's Office of Energy Management. In this capacity, Sandia is responsible for the engineering analyses, contract development, and testing of rechargeable batteries for utility-energy-storage applications. This report details the technical achievements realized during fiscal year 1992.

Contributors

Sandia National Laboratories:

Abbas Akhil, Battery Systems Analysis and System Integration

Roger Assink, Applied Research, Lead-Acid

Jeffrey Braithwaite, Battery Systems Engineering, Sodium/Sulfur

Nancy Clark, Battery Systems Engineering, Zinc/Bromine

James Freese, Testing and Field Evaluation

Sandra Klassen, Applied Research, Zinc/Bromine

Lana Lachenmeyer, Planning and Reporting

Contractors/Subcontractors:

Harrison Clark, Power Technologies, Inc.

Salim Jabbour, Decision Focus, Inc.

Prabhu Prabhakara, Power Technologies, Inc.

Hans Meyer, Omnion Power Corporation

Sanjay Deshpande, GNB Industrial Battery Co.

Joe Szymborski, GNB Industrial Battery Co.

Ben Norris, Pacific Gas & Electric Co.

Rick Winter, Pacific Gas & Electric Co.

Steve Eckroad, University of Missouri at Rolla

Phil Eidler, Johnson Controls Battery Group, Inc.

Al Koenig, Silent Power, Inc.

James Rasmussen, Silent Power, Inc.

Jeffrey Zagrodnik, Johnson Controls Battery Group, Inc.

Contents

Acronyms and Abbreviations	ix
1. Executive Summary	1-1
Introduction	1-1
Highlights	1-2
Utility Battery Systems Analyses	1-2
Battery Systems Engineering	1-2
AC Battery Development - Omnion	1-2
Technology Development - GNB	1-3
Applied Research - SNL	1-3
Zinc/Bromine Project	1-4
Technology Development - JCBGI	1-4
Technology Evaluation - SNL	1-4
Applied Research - SNL	1-4
Sodium/Sulfur Project	1-4
Technology Development - BPI	1-4
Technology Evaluation - SNL	1-5
Supplemental Evaluations and Field Tests	1-6
SNL Test Facilities	1-6
Nickel/Hydrogen Field Tests	1-6
Other SNL Activities	1-6
2. Utility Battery Systems Analyses	2-1
Background	2-1
Utility Selection and Study Guidelines	2-1
Chugach Electric Association	2-3
Findings	2-3
Generation Benefits	2-3
Reduced Load Shedding	2-3
Transmission and Distribution Benefits	2-3
Cost/Benefit Analysis	2-4
Recommendations	2-4
San Diego Gas and Electric	2-5
Findings	2-5
Generation Benefits	2-5
Transmission and Distribution Benefits	2-5
Cost/Benefit Analysis	2-6
Recommendations	2-6

Oglethorpe Power Corporation	2-6
Recommendations	2-9
Bonneville Power Administration Puget Sound Area	2-9
Combustion Turbine Displacement	2-10
Cross-Cascades 500-kV Line Deferral	2-10
Local Benefits of Battery Energy Storage	2-10
Generation Benefits of Battery Energy Storage in the Northwest	2-11
Conclusions	2-12

3. Battery Systems Engineering 3-1

AC Battery Development - Omnion	3-1
Tasks/Milestones	3-1
Container Development	3-1
PCS Design and Development	3-3
PCS Waveform Control	3-3
Integrated Transformer and Reactor Design	3-4
Software Control	3-5
Container Thermal Management	3-6
Test Summary	3-6
Technology Development - GNB	3-7
Task 1. Phase 1: VRLA Battery Improvements	3-8
Vent Valve Reliability	3-8
Positive Plate Growth	3-11
Thermal Management and Charging Profiles	3-12
Ground Fault Elimination	3-13
Plate Pasting Process Control	3-17
Positive Active Material	3-18
Task 1. Phase 2: VRLA Battery Advancements	3-19
Cell Design	3-19
Copper Negative Grid	3-20
Positive Plate Design	3-21
Electrolyte Immobilization	3-25
Manufacturing Processes	3-25
Task 2. Baseline Design and Economics Study	3-25
Specifications and Design Requirements	3-26
Baseline Conceptual Designs	3-26
Economic Analyses	3-27
VRLA Battery Storage Plant Preliminary Design Specification for PG&E	3-27
Market Assumptions/Cost Estimates	3-27
System Requirements	3-27
PCS Performance Requirements	3-27

Balance of Plant	3-30
Physical Site Characteristics	3-30
Battery Siting Study - Stockton Division	3-31
Lodi Planning Area - Colony Substation	3-31
Corral Planning Area and Substation	3-32
Applied Research - SNL	3-32
4. Zinc/Bromine Project	4-1
Technology Development - JCBGI	4-1
Battery Fabrication and Testing	4-2
Stack and Battery Assembly	4-2
Status of 8-Cell Battery Testing	4-2
50-Cell Battery Results	4-3
Minicell Battery Tests	4-4
Results of Other Testing	4-5
Zinc-Loading Study	4-6
Low-Temperature Study	4-7
Full Discharge Without Strip	4-7
Reverse Polarity Test	4-9
Shunt Current	4-9
Electrolyte Utilization	4-10
Stand Heating Study	4-10
Engineering Development	4-11
Electrode Substrate Resistivity	4-11
Cathode Activation Layer	4-11
Terminal Electrode	4-11
Separator Development	4-12
Zinc Plating	4-12
New Battery Design	4-12
Cell Stack Design	4-12
Heating/Cooling Requirements	4-12
Environmental Impact	4-15
Technology Evaluation - SNL	4-16
Task 1. Evaluation of 8-Cell Battery	4-16
Task 2. Evaluation of Two 50-Cell Stacks in Parallel	4-18
Applied Research - SNL	4-20
Durability of Carbon-Plastic Electrodes for Zinc/Bromine Storage Batteries	4-20
Complexing Agents for the Zinc/Bromine Battery Electrolyte	4-21

5. Sodium/Sulfur Project	5-1
Utility-Battery Technology Development - BPI	5-1
Results	5-2
Task 1. UES Applications Assessment	5-2
Task 2. UES Cell and Battery Development	5-3
Task 2.1 UES Battery Design Study	5-3
Task 3. Design and Fabrication of UES Module	5-15
Task 4. Full-Scale Battery Plant Design	5-15
Technology Evaluation - SNL	5-15
Task 1. 40-Cell XPB Module	5-16
Task 2. XPB Single Cells	5-19
6. Supplemental Evaluations and Field Tests	6-1
SNL Test Facilities	6-1
Nickel/Hydrogen Field Tests	6-1
FSEC Tests	6-1
7-kWh Battery	6-1
Appendix: Presentations and Publications	A-1
Presentations	A-1
Publications	A-1

Figures

2-1	Geographic Distribution of Utility Systems Studies	2-2
2-2	Comparison of Benefits to Cost for 5 Battery Locations	2-7
2-3	Percent of Benefits for 5 Battery Locations	2-8
2-4	Load Shapes for High-Load Days of Concern to BPA	2-10
2-5	Typical Wind Tunnel Load Profile and Battery Energy Required to Limit Load Changes to 50 MW/min	2-11
3-1	AC Battery Container Configuration (all dimensions are in inches)	3-2
3-2	AC Battery Module	3-2
3-3	Typical AC Waveform without Skewing	3-3
3-4	Two Modules with Skewing and Resultant Waveform	3-4
3-5	Current THD vs Number of Skewed Modules	3-5
3-6	Experimental Setup for Thermal Test of AC Battery	3-7
3-7	Operation of a Production ABSOLYTE Pressure Relief Vent on a Cell at Constant Overcharge	3-10
3-8	Operation of Another Randomly Selected ABSOLYTE Pressure Relief Vent Valve on a Cell at Constant Overcharge	3-10

3-9	Various Positive Grid Configurations	3-11
3-10	Bead Smoothing Process	3-16
3-11	Initial High Rate Discharge Testing of the Advanced Design (LSB) VRLA	3-20
3-12	Several Grid Alloy Compositions	3-21
3-13	Grid Corrosion Test, Grid Growth	3-22
3-14	Grid Corrosion Test, Grid Growth vs Ult. Tensile Strength	3-22
3-15	Positive Plate (Alloys/Paste Additives)	3-23
3-16	Peak Load Day Profile	3-28
3-17	Battery Discharge Profile	3-28
3-18	Top View of PG&E Unit Battery	3-29
3-19	Side View of PG&E Unit Battery	3-29
3-20	Electrical Diagram of the PG&E Unit Battery	3-29
3-21	PG&E Colony Substation	3-31
3-22	Corral Substation	3-32
3-23	The Modulus of the Virgin Stopper and Electron Beam-Treated Stopper	3-33
4-1	Cycle-Life Efficiencies for 8-Cell Battery V1-53	4-2
4-2	Cycle-Life Efficiencies for 8-Cell Battery V1-54	4-3
4-3	Cycle-Life Efficiencies for 8-Cell Battery V1-55	4-3
4-4	Effect of Current Density on Efficiency in the Minicell	4-5
4-5	Frequency Regulation Test Using 8-Cell Battery V1-64	4-6
4-6	Effect of Zinc Loading on Efficiency Measured in 8-Cell Battery V1-54	4-7
4-7	Resistances Measured in Samples of Terminal Electrode Materials (Carbon/Plastic/Metal Screen) when Immersed in Brominated Electrolyte at 40°C	4-12
4-8	8-Cell, 1-kWh Battery (SNL #518)	4-17
4-9	Battery Efficiencies, SNL #518	4-17
4-10	15-kWh Unit, Consisting of Two 50-Cell Stacks in Parallel (SNL #526)	4-19
4-11	Battery Efficiencies, SNL #526	4-19
4-12	SNL #526 Voltage Plot for Cycle 201	4-20
5-1	300-kW NAS-P _{ac} Unit (2-hr Rated Duration)	5-3
5-2	75-kWh NAS-P _{ac} Module Performance at 2-hr Constant Power Discharge	5-4
5-3	Power Discharge 75-kWh BES Module Performance, Temperature vs Depth of Discharge	5-4
5-4	UES Battery Module, Cut-Away Side View	5-5
5-5	UES Battery Module, Cut-Away Top View	5-5
5-6	UES Central Sulfur Cell Design	5-7
5-7	Typical Corrosion Cell Test Set-Up	5-8
5-8	Electrical Performance for Chrome-Plated 446 Electrode Over the Life of the Experiment	5-9
5-9	Electrical Performance for Flame-Sprayed Molybdenum on Aluminum Electrode, Over the Life of the Experiment	5-9

5-10	Electrical Performance for a Pure Molybdenum Electrode in a Sulfur-Saturated Melt Over Life of the Experiment	5-9
5-11	Cell Resistance at the Beginning of Discharge and Beginning of Charge vs Cycle Number for Cell 017	5-13
5-12	Depth of Discharge and f1 vs Cycle Number for Cell 017	5-13
5-13	Depth of Discharge Plots of Cycles 7, 38, and 75 for Cell 017	5-13
5-14	Cell Resistance vs Cycle Number for Cell 019	5-14
5-15	Depth of Discharge and f1 as a Function of Cycle Number for Cell 019	5-14
5-16	Depth of Discharge Plots of Cycles 6, 20, 31 and 50 for Cell 019	5-14
5-17	Depth of Discharge and f1 vs Cycle Number for Cell 022	5-14
5-18	Cell Resistance vs Cycle Number for Cell 022	5-15
5-19	Forty-Cell XPB Sodium/Sulfur Module	5-17
5-20	Schematic of Electrical Configuration of the 40-Cell Sodium/Sulfur Module	5-17
5-21	SPL 40-Cell XPB Module Test Results	5-18
5-22	SPL 40-Cell XPB Module, Currents for Strings 1-5 (Cycles 167 and 168)	5-18
5-23	SPL 40-Cell XPB Module, Currents for Strings 6-10 (Cycles 167 and 168)	5-19
5-24	XPB Cells, Parametric Tests with Charge and Discharge Current Varied	5-20
5-25	XPB Cells, Constant Power Tests	5-20
6-1	Performance Summary of Batteries PV1 and PV2 (Batteries Series-Connected)	6-3
6-2	Performance Summary of Batteries PV3 and PV4 (Batteries Series-Connected)	6-4

Tables

2-1	Utility-Specific Systems Studies	2-3
2-2	Benefits Summary for CEA System	2-4
2-3	Benefits Summary for SDG&E System	2-6
2-4	Selected Battery Sizes	2-7
2-5	VOS or Outage Cost for 1-hr Interruption	2-8
2-6	Battery Attributes	2-12
3-1	Current from Sampled Waveforms	3-5
3-2	Battery Thermal Test Results	3-7
3-3	ABSOLYTE Vent Baseline Characterization	3-9
3-4	Alternate Positive Grid Designs	3-12
3-5	Thermal Management Product Characterization	3-14
3-6	Results of ABSOLYTE II Automatic Electrolyte Fill by Weight Study	3-15
3-7	Capabilities of Leak Test Methods	3-16
3-8	Pasted Plate Improvement	3-18
3-9	Performance Comparison	3-19

3-10	Comparison of Material Resistivities	3-24
4-1	Cell Stack Orientation V1-15(50)	4-4
4-2	Experimental Separators Tested in Minicell	4-5
4-3	Constant Power Discharge Steps	4-5
4-4	V1-64 Frequency Regulation Discharge	4-6
4-5	V1-50 Frequency Regulation Efficiencies	4-7
4-6	Loading Study Efficiencies and Energy Losses	4-8
4-7	V1-60 Full-Discharge Cycles Without Strip	4-8
4-8	V1-14 High-Efficiency Electrolyte Full-Discharge Cycles Without Strip	4-9
4-9	Shunt Current Calculation for a Cycle	4-9
4-10	Calculated Shunt Currents	4-10
4-11	Zinc Utilization Study V1-62	4-10
4-12	Properties of Experimental Separator Compositions	4-13
4-13	Calculated Heat and Electrical Power in a Single Cell for a Constant Current Cycle at 25 A	4-14
4-14	Battery Cooling	4-15
4-15	Final Average Efficiencies of SNL #518	4-18
5-1	300-kW x 2 hr ACUnit Battery Specification	5-4
5-2	c/S UES Cell Design Characteristics	5-8
5-3	Summary of UES Cell Testing and Status	5-12
5-4	Typical Cell Performance Test Results	5-15
6-1	7-kWh Battery Discharge Rate Tests	6-2
6-2	7-kWh Battery Charge Rate Tests	6-3

Acronyms and Abbreviations

ANL	Argonne National Laboratory
AR	area regulation
BESS	battery energy storage system
BOL	beginning of life
BOP	balance of plant
BPA	Bonneville Power Administration
BPI	Beta Power, Inc.
CAEDS	computer-aided engineering design system
CATIA	computer-graphics aided three-dimensional interactive application
CDAS	control and data acquisition system
CE	coulombic efficiency
CEA	Chugach Electric Association
CPV	common pressure vessel
c/S	central sulfur
CSM	copper-stretch-metal
CT	combustion turbine
CV	cyclic voltammogram
DOD	depth-of-discharge
DOE	Department of Energy
EE	energy efficiency
EMC	electric membership corporation
EOC	end of charge
EOD	end of discharge
EOL	end of life
EPDM	ethylene-propylene-diene monomer
EPR	ethylene-propylene rubber
EPRI	Electric Power Research Institute
EV	electric vehicle
FSEC	Florida Solar Energy Center
FOP	fixed origice paster
FR	frequency regulation
FPGA	field programmable gate array
FSEC	Florida Solar Energy Center
GNB	GNB Industrial Battery
HDPE	high-density polyethylene

HVAC	heating, venting, and air conditioning
ICEA	Insulated Cable Engineers Association
IHPTF	induction heated post terminal fusion
IR	infrared
ISOA	improved state-of-the-art
JCBGI	Johnson Controls Battery Group, Inc.
LSB	large sealed battery
MEM	methylethyl morpholinium bromide
MEP	methylethyl pyrrolidinium bromide
O&M	operating and maintenance
OEM	DOE/Office of Energy Management
OPC	Oglethorpe Power Corporation
OPE	Omnion Power Engineering
OSHA	Occupational Safety and Health Administration
PAM	positive active material
PBT	polybutylene terephthalate
PCS	power conversion system
PG&E	Pacific Gas & Electric
PREPA	Puerto Rico Electric Power Authority
PTFE	polytetra-fluoroethylene
PTI	Power Technologies, Inc.
R&D	research and development
RF	radio frequency
RPM	revolutions per minute
SCL	Seattle City Light
SDG&E	San Diego Gas & Electric
SES	stationary energy storage
SFR/SR	Simplified Frequency Regulation/Spinning Reserve
SFUDS	Simplified Federal Urban Driving Schedule
SNL	Sandia National Laboratories
SOA	state-of-the-art
SOC	state-of-charge
SOW	statement of work
SPL	Silent Power Limited
SR	spinning reserve
T&D	transmission and distribution
TAG	Technical Assessment Guide
TBD	to be determined
TCAP	transformer capacity model

TDI	Southwest Technology Development Institute
TES	thermal energy storage
THD	total harmonic distortion
TIG	tungsten inert gas
TOC	total oxidizable carbon
UBC	Uniform Building Code
UBS	Utility Battery Storage Systems Program
UES	utility energy storage
UMR	University of Missouri at Rolla
UPS	uninterruptible power supply
VOS	value of service
VRLA	valve-regulated lead-acid

1. Executive Summary

Introduction

This report documents the fiscal year 1992 activities of the Utility Battery Storage Systems Program (UBS) of the U.S. Department of Energy (DOE), Office of Energy Management (OEM). The UBS program is conducted by Sandia National Laboratories (SNL). See SAND91-2694, *Utility Battery Exploratory Technology Development Program Report for FY91*, for a description of the previous year's activities. UBS is responsible for the engineering development of integrated battery systems for use in utility-energy-storage (UES) and other stationary applications. Development is accomplished primarily through cost-shared contracts with industrial organizations. An important part of the development process is the identification, analysis, and characterization of attractive UES applications.

Paul C. Butler is the Project Manager for UBS activities at SNL. He also supervises the Storage Batteries Department under Gary N. Beeler, Energy Components Directorate. Nicholas J. Magnani is the Sector Program Manager.

UBS is organized into five projects:

- Utility Battery Systems Analyses
- Battery Systems Engineering
- Zinc/Bromine
- Sodium/Sulfur
- Supplemental Evaluations and Field Tests.

The results of the Utility Systems Analyses are used to identify several utility-based applications for which battery storage can effectively solve existing problems. The results will also specify the engineering requirements for widespread applications and motivate and define needed field evaluations of full-size battery systems.

The Battery Systems Engineering and specific technology projects have emphasized four battery systems development contracts, all cost-shared with industry. SNL conducts program management, technology evaluation, and applied research activities. Battery Systems Engineering is focusing on improving the lead-acid battery technology and on the development of electronic components for and design of complete utility battery systems. The other two development projects involve

the progression of two advanced battery technologies, zinc/bromine and sodium/sulfur. These contracts utilize a phased development approach from fundamental electrochemical research and development (R&D), to component development, and through several steps of battery engineering (conceptual, prototype, and product). An integrated battery system suitable for commercialization and deployment at utilities is the desired final product. At SNL, program management involves formulating specific near- and long-term plans, placing the industrial development contracts, monitoring and guiding progress, solving programmatic issues, and coordinating reporting. Under technology evaluation, contract deliverables are tested primarily at SNL to determine performance, lifetime, and failure mechanisms. These data are reported to the developers for use in optimizing designs and resolving problems. Applied research is performed in certain projects in which SNL has specific technical expertise to address critical problems facing a technology. This applied work is closely coordinated with the prime industrial contractor.

A separate testing project enhances and maintains the SNL battery evaluation facilities. Specialized hardware and software are developed to support unique test capabilities and needs. In addition, this project directs field test work for nickel/hydrogen batteries no longer being developed by SNL and ensures that appropriate technology transfer is completed.

For continuity, this report is organized by project, with one chapter devoted to each. Specific topics covered in Chapters 2 through 6 include

2. Utility Battery Systems Analyses
3. Battery Systems Engineering
 - AC Battery Development by Omnion Power Engineering (OPE)
 - Technology Development by GNB Industrial Battery (GNB)
 - Applied Research at SNL
4. Zinc/Bromine Project
 - Technology Development by Johnson Controls Battery Group, Inc. (JCBGI)
 - Technology Evaluation at SNL

- Applied Research at SNL
5. Sodium/Sulfur Project
 - Technology Development by Beta Power, Inc. (BPI)
 - Technology Evaluation at SNL
 6. Supplemental Evaluations and Field Tests

A summary of the FY92 highlights follows.

Highlights

Utility Battery Systems Analyses

Four systems studies were started in late FY91 to identify all possible benefits of battery energy storage in specific utility applications. Utility partners were selected based on primary considerations of ownership and operating conditions to include a broad diversity of candidate utilities. The four utilities selected were San Diego Gas & Electric (SDG&E), Oglethorpe Power Corporation (OPC), Chugach Electric Association (CEA), and Bonneville Power Authority (BPA).

SDG&E represented a large, investor-owned utility. OPC represented a large, electric member cooperative, serving a large rural area. CEA also represented a cooperative structure, but a smaller service area interconnected to a relatively small power pool in Alaska. BPA represented a large, non-investor-owned, public power marketing utility. BPA's study area was restricted to study battery applications only in the Puget Sound area. All these utilities had an interest in or a strong potential for battery energy storage application, and all except BPA shared the cost of the study with direct and in-kind contribution.

The methodology adapted was generally the same for each utility, but the study details were different for each utility due to differences in internal planning and operating procedures and financial structure. The studies were originally intended to last no more than three months each, but the period extended well beyond this timetable, not due to the time required for the analysis itself, but due to the time required to acquire utility planning data and review interim and final study findings.

Applications were identified for each utility, with benefit-to-cost ratios ranging from less than one to greater than two. Unit decommitment and spinning reserve were the two most cost-effective applications on

the generation side, even for utilities with relatively flat marginal costs. In the transmission and distribution cases, battery energy storage could potentially defer new distribution lines and transformer upgrades. Benefits for this application were greater if the line traversed difficult terrain or went through expensive urban areas. Generation capacity credits were not significant unless the battery was sized for discharges of 6 hr or more, which increased the installed cost of the battery beyond the break-even point. This supported prior prevailing assumptions that smaller sized batteries were the most cost-effective. In the case where sensitivity studies were performed, service life and salvage value had minor effects on the benefit-to-cost ratios.

These studies were screening-level studies and did not include detailed simulations of the impact of battery storage over the entire study period. Instead, the studies relied on a snap-shot approach of examining the effect of incorporating a battery in a few representative days from three or four selected years. Further, the mutual exclusivity of the benefits was not considered. These details were recommended for the next phase, which would be a feasibility study for battery energy storage. Two of the four utilities have indicated an interest in performing the feasibility studies that will include these needed refinements to accurately quantify the economic value of battery energy storage benefits. These feasibility studies would also include the conceptual design and cost estimate of the complete battery energy storage system for specific sites selected by the utility.

Battery Systems Engineering

AC Battery Development - Omnion

The AC Battery is a patented, modular battery system design concept that splits the battery into small groups, with each group containing its own power conversion electronics, factory-packaged as "modules." Several modules are packed in a truckable "container," and their power is aggregated to obtain the rated output of the container. One of the key advantages that the AC Battery concept offers is that it shifts the large on-site labor component to the factory floor, where tight quality controls can be maintained and cost savings realized by the repetitious manufacture of similar components.

Since initiation of the development of the AC Battery in December 1991, the implementation of this integrated system has evolved substantially. As development proceeded from the initial concept toward realization in hardware, the product took a refined form, incorporating new techniques for power conversion, heat

transfer, and packaging. This report highlights the progress made on the AC Battery contract.

- Resizing of the container for easier transportation, installation, and thermal management.
- Reconfiguration of the modules for higher dc voltage, higher energy density, and reduced power conversion subsystem (PCS) cost.
- Skewing of the module outputs for lower distortion and higher power conversion efficiency.
- A new transformer design that replaces the reactors in the PCS while delivering a 480-VAC output.
- A battery thermal test that has led to a dual circuit heating, ventilating, and air conditioning (HVAC) system tailored to the differing needs of the PCS power train and the batteries.
- Software control of the PCS using FPGAs (Field Programmable Gate Arrays) to replace numerous discrete logic devices.
- Centralized high-level control providing greater system flexibility while minimizing the cost and complexity of the PCS.

Technology Development - GNB

The initial efforts in this contract have focused on implementing manufacturing process techniques that can have a significant effect in the improvement of valve-regulated lead-acid (VRLA) battery system reliability. These have included an improved electrolyte-filling technique, an improved jar-to-cover heat-sealing process, and an improved leak detection method, all of which are meant to reduce the possibility for electrolyte leakage from the cell and the potential for development of electrical ground faults that can impact both battery performance and personnel safety. The improvements resulting from the implementation of these processes are reported herein. Work has also begun on a full characterization and demonstration of the pressure relief valve system, a critical element of any VRLA battery design to ensure performance and design life of the battery.

Prototype cells incorporating design modifications to increase the energy density and specific energy of the current ABSOLYTE VRLA cells have been fabricated, and preliminary discharge testing is confirming a 12 to 17% improvement at the discharge rates typically used for utility battery energy storage systems. Initial experimental builds of an advanced lead-acid battery with exceptional high-rate discharge capabilities have not

met design expectations, however, and modifications to this cell's grid and active materials are planned to bring performance up to expected levels.

Experimental plans have been prepared to research radical modifications in cell design and electrochemistry, including the use of copper-cored negative grids, positive active material pastes with additives and binders to increase material utilization, positive grid alloys with improved corrosion and "growth" resistance, and electrolyte immobilization/separator systems to reduce the cost of the principal item in VRLA cells that cause them to be more expensive than their flooded electrolyte counterparts. Manufacturing processes that can be upgraded to improve throughput and product reliability have been identified and alternative processing techniques are being reviewed and evaluated.

The battery improvement tasks are supplemented by other tasks that require the conceptual design of battery systems for specific utility applications and the economic analysis of existing designs over improved and advanced battery designs. These tasks require the involvement of "host" utilities to provide the design input and the parameters for the economic analysis. These tasks are being performed by Pacific Gas & Electric (PG&E) and Puerto Rico Electric Power Authority (PREPA), the two utilities on the GNB team. Each utility has identified specific battery energy storage applications in its network and is using these applications as representative cases for the GNB contract. The host utility input and the related design and economic study effort are being coordinated by the University of Missouri at Rolla (UMR).

Applied Research - SNL

This effort supports the vent valve reliability improvements in Task 1 of the GNB contract. SNL applied research is attempting to find suitable surface treatments that will overcome the valve sticking problem observed in the valves used for venting GNB batteries. Two types of surface treatments have been applied to sample plugs and returned to GNB for environmental testing. These surface treatments include a plasma process which creates a chemically resistive coating and crosslinks the surface of the rubber plug, thus increasing its modulus. The second process uses an e-beam to crosslink the rubber surface.

Results of the environmental testing of the samples at GNB will indicate a preferred process or may require investigation of additional research to find a suitable coating or surface treatment.

Zinc/Bromine Project

Technology Development - JCBGI

JCBGI is in the second year of a cost-shared contract to fabricate, evaluate, and optimize a zinc/bromine battery system suitable for electric utility applications. In early FY92, Phase 1, which demonstrated the feasibility of the existing zinc/bromine technology, was completed. This included building and testing several 1-kWh batteries that demonstrated energy efficiencies of >75% with <10% capacity loss in 100 cycles. Many of these batteries cycled between 250 and 350 cycles before failure. In addition, a 15-kWh battery was built and tested to 200 cycles before it was damaged during a power failure. Safety and cost analysis studies were initiated. These data together showed that zinc/bromine could be built at low cost, have potentially long lifetimes, be recycled, and still offer 2-3 times the specific power of lead-acid batteries.

Once feasibility was demonstrated in Phase 1, the majority of effort in Phase 2 has been to optimize the components of the battery system and to design a new battery stack that is large enough to form building blocks for a modular system that could be used for a variety of utility applications. Work has been done to improve the performance and manufacturability of the carbon plastic electrodes, the active carbon layer, separator materials, and terminal electrode materials. The design of a new cell stack has been essentially completed. Modeling techniques including computer-aided engineering design system (CAEDS) and a JCBGI-proprietary FORTRAN performance model have been used extensively in this design process. Finite element analysis has also been used to predict the end block stress and model potential flow of the electrolyte in the cell. There is confidence in this new design since these models have been used to validate the existing design.

Technology Evaluation - SNL

An 8-cell, 1-kWh zinc/bromine battery from the utility battery development contract with JCBGI was tested during FY92. Improved welding techniques were incorporated in this battery to prevent leaks. A total of 273 charge/discharge cycles (26 cycles at JCBGI and 247 cycles at SNL) was completed on the battery. A drop in coulombic and energy efficiency was observed immediately after 15 no-strip cycles were completed. Prior to that time, the battery performed well and experienced absolutely no leaks in the stack or in any of the auxiliary components.

A 15-kWh battery, consisting of two 50-cell stacks assembled in a parallel configuration, was fabricated by JCBGI as the next deliverable for the utility development contract. Twenty charge/discharge cycles, including several no-strip cycles, were performed at JCBGI. A total of 180 no-strip and baseline cycles was performed at SNL with only a slight downward trend in efficiency. During cycle 201, a lightning storm caused a temporary power outage that ultimately led to the failure of the battery. The projected life of this battery was approximately 300 cycles.

Applied Research - SNL

A durability study of electrode materials was completed. The six-month study examined the effects of electrolyte on glass-filled carbon plastic electrodes made of high density polyethylene (HDPE), and accelerated aging was carried out at temperatures up to 60°C. Results from this study show that electrode material with higher polymer content sorbs greater amounts of electrolyte. Higher glass content may increase dimensional stability (length and width). The electrode materials did not show evidence of chemical attack by the electrolyte, nor was the crystallinity of the polymer affected. The mechanical properties of the electrode materials decreased slightly due to sorption of electrolyte, and the electrical conductivity increased upon exposure to the electrolyte.

A project to reformulate the electrolyte was requested by JCBGI and is being carried out in collaboration with JCBGI personnel. The objective is to develop complexing agents that will allow further improvement in performance and safety. A contract has been placed with the University of New Mexico to synthesize candidate complexing agents. The compounds will be evaluated for bromine complexation and for electrochemical performance, and measurements of bromine vapor pressure will be made.

Sodium/Sulfur Project

Technology Development - BPI

During FY92, the majority of the activity focused on the following: 1) identification of UES applications and markets that are attractive for the sodium/sulfur technology, 2) design of a UES cell and battery, 3) development of the central sulfur (c/S) UES cell and selected battery components, and 4) fabrication and initial qualification of the UES cell.

The motivation for developing a c/S cell design is the promise for significantly greater calendar life compared with state-of-the-art electric-vehicle (EV) cells because the potential for corrosion of the cell container is effectively eliminated. Based on test results obtained by Silent Power Limited (SPL), c/S cells appear to offer a 75% improvement in characteristic life over standard, central-sodium cells. Many of the SPL c/S cells continue to cycle beyond eight calendar years. The cell development ongoing in this program is utilizing improved component technology and is being coupled with a well-conceived battery thermal design.

Of importance, cell design criteria are different for UES applications than those for electric vehicles. While both mandate safety first, the UES application must emphasize cost over weight- or volume-based performance. In stationary applications, lead-acid battery systems and other non-battery storage technologies are the competition. Therefore, sufficient benefit must exist relative to the advanced battery to justify the capital cost required to introduce a replacement technology into the market place. The most sensitive influence on the true cost measure, life-cycle cost, is the service life of the battery. This determines how many battery replacements will be required to maintain the power capability over the stated life of the equipment. Battery service life is intricately tied to three factors: the reliability characteristics of the cell, how cells are connected electrically to form the battery, and, lastly, the methodology by which cells are controlled within the battery. Each of these factors is being addressed in this project.

Relative to the battery system, a preliminary design of a battery module was completed. This module has an energy capacity of 75-kWh at 125 VDC and constitutes the basic building block of an integrated battery storage system. These modules have been given the designation NAS-P_{ac}, for sodium/sulfur-ac power. Similar to an EV battery, each module is autonomous and represents the smallest replaceable energy unit within the battery system. Local control over the thermal environment and the critical electrical control functions is provided. Eight of these NAS-P_{ac} modules are used with a power-conversion system to form an integrated battery system. The modules are arranged in a 4-series x 2-parallel configuration to provide 500 VDC and fit within a 7.5-ft-high x 7-ft-wide envelope set by the preferred power conversion system and the desire to transport the system via standard truck or seabox. These portable power units fit into the concept of distributed generation. In this respect, the use of advanced batteries (e.g.,

sodium/sulfur) is a definite benefit, requiring only 20% of the volume and weight of an equivalent lead-acid battery system. These same benefits accrue to the user in that the same energy storage can be accomplished in 1/5 the footprint. System-level specifications are 300 kW, three-phase 480 VAC. The battery is rated for a 2-hr operation (i.e., 600 kWh).

Based on a preliminary assessment of the c/S UES cell reliability, the module cycle life is expected to be 1500 cycles, or five years, depending on utilization. The module design is such that it can continue to operate with up to 38% of the cell strings failed. As part of a "no maintenance" battery philosophy, interstitial latent heat storage within the module and a standard, non-evacuated thermal enclosure are employed as passive methods to limit cell temperature rise. These features decrease the cost of the battery but also cause higher heat loss (12 W/kWh) compared with an EV-type evacuated enclosure. The actual impact on system efficiency, however, will depend on the application. For example, to satisfy the twin peak diurnal cycles of electrified rail transit applications, the make-up heat amounts to 6 to 8% of the stored electrical energy. This loss could be halved by using the more expensive evacuated insulation system.

Technology Evaluation - SNL

An 8-V, 40-cell XPB sodium/sulfur module was life-cycle tested during FY92. A total of 168 charge/discharge cycles was completed on the module. Cells from four strings failed or were close to failure when the module was removed from test. The capacity of the module at 100% DOD had declined from an initial 305 Ah to 190 Ah, a loss of 38%. The relative rapid decrease in capacity of this module is not consistent with the behavior observed in earlier 40-cell modules tested at SPL. However, this behavior was indicative of the inconsistent performance of the entire XPB cell population tested at SPL (e.g., the single cells and the 200-cell battery). A second 40-cell XPB module is presently being tested using the stationary energy storage (SES) test profile.

Two new XPB cells were placed on test in May. Break-in and baseline capacity tests were completed, and a test plan was developed to characterize the cells. A series of cycles was performed to characterize capacity loss with increasing charge and discharge rates and the effect of sustained power on cell energy content. These cells are presently performing SES life-cycle tests using the SES test profile.

Supplemental Evaluations and Field Tests

SNL Test Facilities

In preparation for upcoming evaluations of utility battery performance at SNL, improvements to the facilities have been in progress. This activity has included procurement of four large power supplies, three load units, a computer, and a stand-alone tester.

Nickel/Hydrogen Field Tests

During FY92, a much-reduced effort was continued with JCBGI to provide technical support for two 2-kWh common pressure vessel (CPV) nickel/hydrogen batteries on test at the Florida Solar Energy Center (FSEC). In addition, JCBGI continued to evaluate the 7-kWh module, which was previously on test at SNL.

Three out of four CPVs used to contain the 2-kWh nickel/hydrogen batteries experienced small leaks. These leaks were identified at the adhesive-bonded end

domes. The delivered capacities of these batteries were well above the rated value of 160 Ah.

A series of discharge and charge rate tests was completed on the 7-kWh battery at JCBGI. The battery capacity remained quite stable over the discharge rate range, varying from 190 to 195 Ah for the C/4 to C/20 rates. Even the highest rate tested, C/3, delivered over 183 Ah, well above the 160 Ah rating. The capacities were equally as stable over the charge range of C/5 to C/20.

Other SNL Activities

Chapters on sodium/sulfur and zinc/bromine battery technologies prepared in collaboration with personnel at SPL, JCBGI, and Exxon Research and Engineering Company were written for publication in the second edition of the McGraw-Hill *Handbook of Batteries and Fuel Cells*. The first edition of this handbook was published in 1984; thus, the chapters for the second edition represent a significantly updated source of information on zinc/ bromine and sodium/sulfur technologies.

2. Utility Battery Systems Analyses

Background

For several years, battery energy storage has predominantly been considered a load-leveling and peak-shaving resource, and its potential use in other utility applications has been largely overlooked. The fast-response capability of battery energy storage systems combined with other characteristics, such as modularity and ease of siting, makes this technology eminently suitable for providing support to the entire utility network for several applications such as spinning reserve, frequency control, and deferral of transmission and distribution facilities. Until now, the benefits and economic value of battery energy storage only for load leveling and/or peak-shaving have been well understood. But the application of battery storage and the methodology to evaluate its benefits in the other, non-load-leveling applications has not been as well documented. The Electric Power Research Institute (EPRI) estimated a range of benefits for these applications from general utility information. More specific benefit information derived from utility planning scenarios and operating conditions is necessary to demonstrate the feasibility of this technology for a wide range of utility applications. The widespread application of this technology by the utility industry is predicated on the availability of this information base.

Thus, the objective of the SNL effort was to undertake a set of studies that would identify numerous applications for batteries and estimate their value in the utility network. There were two possible approaches that could be adopted for performing studies to achieve these objectives:

- examine the needs of utilities on a regional basis to identify all possible applications in which battery energy storage can play a role and estimate the value

or

- examine specific utility networks and identify potential battery energy storage applications within each network and estimate the related benefits.

The results from each approach would have different meanings and would be interpreted accordingly. A study performed on the basis of the first approach would yield estimates of the value of battery energy

storage at the regional level, based not on the requirements of a particular utility, but on collective, regional conditions derived from general assumptions.

The second approach would be more focused, and identify real applications and estimate the value of the battery system based on utility-specific conditions and assumptions. The results of a study based on this approach would be immediately applicable to the host utility, while preserving the possibility that they are also applicable to other utilities with similar operating conditions. The results obtained from the second approach were deemed to be more valuable for the DOE/SNL UBS program and the utility community as a whole, and it was decided to structure the systems studies along those lines.

Utility Selection and Study Guidelines

Utilities with a diverse ownership structure and operating conditions were selected to gain insight into their process for evaluating and implementing technology options such as battery energy storage. The utilities that were finally selected included:

- Investor-owned utility - San Diego Gas & Electric (SDG&E)
- Rural electric cooperative - Oglethorpe Power Corporation (OPC)
- Municipal electric association - Chugach Electric Association (CEA)
- Public power administration - Bonneville Power Administration (BPA)

Figure 2-1 shows the utility locations.

Each of the four utilities either had an active interest in battery energy storage or had a strong potential for benefiting from its use. Cost-sharing was required from all utilities except BPA. SNL's share of the cost for each study and an approximate cost share from the utilities is shown in Table 2-1. This table also shows the start dates of each study.

The study period was initially limited to no more than 3 mo. It was felt that a longer duration could lead



Figure 2-1. Geographic Distribution of Utility Systems Studies.

Table 2-1. Utility-Specific Systems Studies

Utility	Sandia Contract	Utility Cost Share	Start Date	End Date
San Diego Gas & Electric	\$46K	Yes	8/91	12/92
Oglethorpe Power Corp.	\$47K	Yes	7/91	11/91
Chugach Electric (Alaska)	\$43K	Yes	9/91	1/92
Bonneville Power Administration	\$70K	No	2/91	11/91

to a lengthy, iterative refinement process with ever-changing input assumptions and planning scenarios in an attempt to obtain better and more accurate results, whereas the 3-mo time limit established a firm deadline and forced the use of only one set of assumptions and deferred refinement of results to future studies. In practice, the studies extended beyond this planned 3-mo duration. This delay was not caused by the length of time required for the analysis, but by delays in obtaining input information and feedback from utilities as the studies progressed.

The findings of each study are summarized in the following subsections.

Chugach Electric Association

This section describes the results of a screening study to determine the benefits of adding megawatt-scale battery energy storage to the CEA system. Generation, transmission, and distribution benefits of storage, with a primary focus on benefits that are typically difficult to quantify, are addressed. The potential benefits to the costs of adding battery storage are also compared.

The CEA analysis was primarily performed by Decision Focus, Inc., with support from Power Technologies, Inc., in the areas of transmission and distribution benefits.

Findings

Generation Benefits

Generation benefits were calculated for six representative days in each of 1994, 1996, and 2000. Projected system operation was based on MAINPLAN (utility system computer simulation) runs. The benefits were calculated for five gas-fired combustion turbine units whose operation is most likely to be affected by the

addition of batteries to the system. The focus was on using batteries to provide spinning reserve.

Load-Leveling

Because the marginal units on the CEA system are typically gas-fired combustion turbines for all hours, the system marginal energy costs do not differ much between on-peak and off-peak hours. Coupled with the assumed battery efficiency of around 80%, this means that no load-leveling savings could be achieved on the CEA system.

Dynamic Operating

For each of the 18 days, the potential reduction in load following, minimum loading, and start-up costs were calculated for each of the five generation units; reductions in these costs are achievable even though the battery is used only to provide spinning reserve. The most cost-effective unit for decommitment was identified on each day. A value of \$40 to \$70/kW-yr of battery capacity, levelized in current dollars, appears appropriate for dynamic operating benefits; this estimate was derived by calculating change from the MAINPLAN results that would be made possible by the addition of battery capacity. Of this total, more than two-thirds is from reduced minimum loading costs, and the remainder is from reduced load following costs.

Reduced Load Shedding

Addition of battery storage to the CEA system would be effective in reducing load shedding. The amount of the reduction would depend on the size of the battery. An approximate calculation indicates that the value of the reduced load shedding could be \$8 to \$16/kW of battery capacity per year.

Transmission and Distribution Benefits

Current CEA transmission and distribution (T&D) facility expansion plans were reviewed to identify T&D

investments that might be avoided or deferred as a result of adding battery storage to the CEA system. Several such investments were identified. The most attractive opportunities are at the Huffman, Hillside, and Girdwood substations and at the village of Hope. Based on a qualitative review of these investments and comparison with more detailed analyses for other utilities, potential T&D benefits of \$20 to \$200/kW of battery capacity appear reasonable. This is equivalent to a T&D benefit of \$3 to \$27/kW of battery capacity per year.

Cost/Benefit Analysis

Table 2-2 summarizes the findings. Summing the capacity (value of displacing other capacity additions), generation, reduced load shedding, and T&D benefits yields levelized current-dollar savings of \$81 to \$183/kW-yr, compared to a levelized current-dollar cost of \$50 to \$60/kW-yr. Note: For the purposes of this study, the cost estimates used are from EPRI's Technical Assessment Guide (TAG, 1989). The total cost is \$703/kW for a 3-hr battery, including land cost. Reducing the storage component in the TAG cost estimates for a 3-hr battery by two-thirds yields an estimated cost of \$350/kW for a 1-hr battery. With a levelized fixed charge rate of 13.7%, this is equivalent to \$50 to \$60/kW-yr for a 1-hr battery. These values suggest that batteries would be a cost-effective addition to the CEA system.

Some benefits may be mutually exclusive. The interactions between the various benefits, that is, whether they are additive or mutually exclusive, depends on storage size, location, system load profiles, and load profiles at individual substations and on individual T&D lines, how the system (including the battery) is operated, and on any equipment deferred as a result of adding batteries.

Recommendations

Based on the results of this screening-level study, it is recommended that CEA consider the addition of battery storage to its system. This screening study focused only on the benefits of battery storage and it was not intended to calculate the cost of the battery system that would provide these potential benefits. A follow-on feasibility study that would provide a preliminary cost estimate of the battery system and include a detailed study to verify and refine the findings of this initial screening study by calculating the benefits more precisely is recommended. Such a study should include the following aspects:

- T&D expansion studies should be carried out, with and without batteries. Potential sites for installing batteries should be identified. Interactions among the various benefits should be considered to ensure that batteries are not being justified on the basis of benefits that may be mutually exclusive.
- More detailed calculation of generation-dynamic operating costs and benefits should be carried out, including examination of multiple weeks of system operation during each of a larger number of years than was considered here. Such calculation should fully account for changes in system operation as load grows and should identify all possible operation savings, not only those that arise when a unit is completely decommitted.
- Comparative evaluation of the economics of battery storage with other capacity additions under consideration by CEA should be carried out. Such detailed study would also allow a better assessment of the "optimum" battery size and the best time for adding the battery plant to the CEA system.

Table 2-2. Benefits Summary for CEA System

Category	Annual Benefit (\$/kW-yr)
• Capacity	30-70
• Generation	40-70
Dynamic Operating (Spinning Reserve/Unit decommitment)	
• Reduced Load-Shedding	8-16
• T&D	<u>3-27</u>
TOTAL	81-183

- Identify a preferred site for locating the battery based on the findings above. Based on these findings, develop the conceptual design of the battery system and estimate its cost. Perform a cost/benefit evaluation based on the total benefits and battery system cost.

These recommendations were provided to CEA at the conclusion of this study.

San Diego Gas and Electric

This section describes the results of a screening study to determine the benefits of adding megawatt-scale battery storage to the SDG&E system. Generation, transmission, and distribution benefits of storage, with a primary focus on benefits that are typically difficult to quantify, are addressed. The potential benefits to the costs of adding battery storage are also compared.

The SDG&E analysis was primarily performed by Decision Focus, Inc., with support from Power Technologies, Inc., in the areas of transmission and distribution benefits.

Findings

Generation Benefits

Generation benefits were calculated for eight days during 1990 and 1991, one week day and one weekend day for each season, using actual SDG&E data. The benefits were calculated for five gas-fired steam turbine units whose operation is most likely to be affected by the addition of batteries to the system. Two modes of battery operation were considered: daily charge/discharge with a 3-hr battery, and provision of spinning reserve only with a 1-hr battery. The spinning reserve mode appears to be more cost effective.

Load-Leveling

Because the marginal units on the SDG&E system are typically gas-fired steam turbines for all hours, the system marginal energy costs do not differ much between on-peak and off-peak hours. With the assumed battery efficiency of 80%, this means that no load-leveling savings could be achieved on the SDG&E system.

Dynamic Operating

For each of the eight days, the potential reduction in load following, minimum loading, startup, and spinning reserve costs was calculated for each of the five units. The most cost-effective unit for decommitment was identified on each day. For the 1990-1991 period, the savings were about \$23 to \$26/kW-yr of battery capacity; the biggest component of the savings is from reductions in load-following costs. That is, each kilowatt of battery capacity would reduce annual system operating costs \$23 to \$26. Accounting for inflation and increases in natural gas prices, this is equivalent to an annual savings of about \$50, levelized in current dollars, per kW/yr. The savings are likely to increase in the future as load growth forces increasing utilization of less economic units.

Environmental

Storage in general, and batteries in particular, has the potential to shift the type and location of emissions of NO_x, SO_x, and CO₂; NO_x is of greatest concern in Southern California. Even if providing only spinning reserve, batteries have the potential to reduce NO_x emissions by allowing the system to be operated more efficiently. The addition of batteries to the system might also make it unnecessary to retrofit expensive pollution controls to an existing gas-fired unit, if that unit's operation would be sharply reduced as a result of adding batteries. These benefits could be worth up to about \$20/kW of battery capacity per year.

Transmission and Distribution Benefits

This project identified the potential role battery storage could play in providing equal or better performance than other T&D options, such as adding new T&D facilities and equipment. Current SDG&E T&D facility expansion study results and transmission and distribution system design practices were reviewed with SDG&E personnel to identify anticipated and potentially needed transmission additions.

The findings of this initial study indicate that strategically installing battery storage on the SDG&E system may result in large T&D system benefits up to \$1200/kW, equivalent to as much as \$200/kW of battery capacity per year. The actual magnitude of the site specific T&D benefits and corresponding battery

storage requirements should be determined on a case-by-case basis from more detailed analysis. Further analysis should include the development of load profiles for substations that are candidate battery sites so that the number of hours of storage required for equipment deferral can be determined.

Cost/Benefit Analysis

Table 2-3 summarizes the findings. Summing the capacity, generation, environmental, and T&D benefits yields levelized current-dollar savings of \$100 to \$370/kW-yr, compared to a levelized current-dollar cost of \$60 to \$130/kW-yr. These values suggest that batteries would be a cost-effective addition to the SDG&E system.

Some benefits may be mutually exclusive. The interactions between the various benefits, that is, whether they are additive or mutually exclusive, depends on storage size, location, system load shapes, and load shapes at individual substations and on individual T&D lines, how the system (including the battery) is operated, and on any equipment deferred as a result of adding batteries.

Recommendations

Based on the results of this screening-level study, it is recommended that SDG&E consider the addition of battery storage to its system. A detailed study to verify the findings of this initial screening study and to calculate the benefits more precisely is recommended. Such a study should include the following aspects:

- More detailed calculations of generation-dynamic operating costs and benefits should be carried out, including examination of multiple weeks of system operation during the course of the year and consideration of how system

operation, and especially the operation of marginal units, is likely to change in the future.

- Detailed T&D expansion studies should be carried out, with and without batteries. Potential sites for installing batteries should be identified. Interactions among the various benefits should be considered to ensure that batteries are not being justified on the basis of benefits that may be mutually exclusive.
- Comparative evaluation of the economics of battery storage with other capacity additions under consideration by SDG&E should be carried out.

Such detailed study would also allow a better assessment of the "optimum" battery size and the best time for adding the battery plant to the SDG&E system.

Oglethorpe Power Corporation

The methodology for the OPC study consisted of evaluating and quantifying the reasonable benefits attainable from the battery storage application and comparing the total benefits against the cost of the battery storage system. Several benefits and the particular characteristics of OPC system were reviewed and analyzed including:

- Load profile with and without direct load control,
- Future generation expansion plan,
- Role of pumped hydro storage and its impact on load leveling,
- Cost of purchased power and energy,
- Future transmission projects,
- Future distribution projects,

Table 2-3. Benefits Summary for SDG&E System

Category	Annual Benefit (\$/kW-yr)
• Capacity	40-75
• Generation	
Load-Leveling	0
Dynamic Operating	50-75
• T&D	10-200
• Environmental	<u>1-20</u>
TOTAL	100-370

- Radial transmission lines/substations,
- Need for backup power source.

Five specific substation locations within the OPC system for battery storage to defer T&D projects were selected for this study: Habersham (H), Egypt (E), Satilla (S), Vidalia (V), Warrenton (W). The battery sizes used for these five locations are shown in Table 2-4.

The results of a benefit-to-cost comparison are presented in Figure 2-2. The methodology used for benefit-to-cost comparison is essentially based on calculating the present worth of all the annual cost savings/benefits accruing due to the battery and the annual cost of owning and operating the corresponding battery plant.

Only four major benefits due to battery storage are included in these benefits-to-cost ratios. They are:

- Generation capacity,
- Transmission deferment,
- Distribution deferment,
- Value of service or cost of outage.

The battery storage identified in this study is mostly in the form of a backup or reserve source. It is not used in the general sense of load leveling. A generation capacity (kW) credit based on a 10-hr discharge rating is applicable. This battery kW (based on 10-hr discharge rating) is essentially a generation reserve source. A 10-hr discharge rating is used so that even if this reserve is called upon during the annual peak load condition, the battery will be able to provide the power (kW) equal to the credit it has received for the longest peak load period of 10 hr. Thus, for example, a 10-MW, 1-hr battery is given a credit of 1 MW. The cost of the battery credit is based on the least expensive generation alternative, which is a combustion turbine. The annual cost savings from avoiding the investment in this generation is credited to the battery.

The transmission credit is computed on the basis of the cost of deferring T&D projects. The actual capital cost expenditure is considered to be postponed by a number of years. The annual cost savings due to the postponement is credited to the battery benefits. The distribution benefits are also calculated similarly.

The fourth and last benefit computed in this study is the value of service or cost of outages. The interruption cost, or value of service (VOS) data, is considered to be

Table 2-4. Selected Battery Sizes

	OPC Substation Locations (designated by letter code)				
	H	E	S	V	W
MWh	7.5	26.0	9.0	217.0	218.0
MW	1.5	6.5	1.5	31.0	43.6
hr	5	4	6	7	5

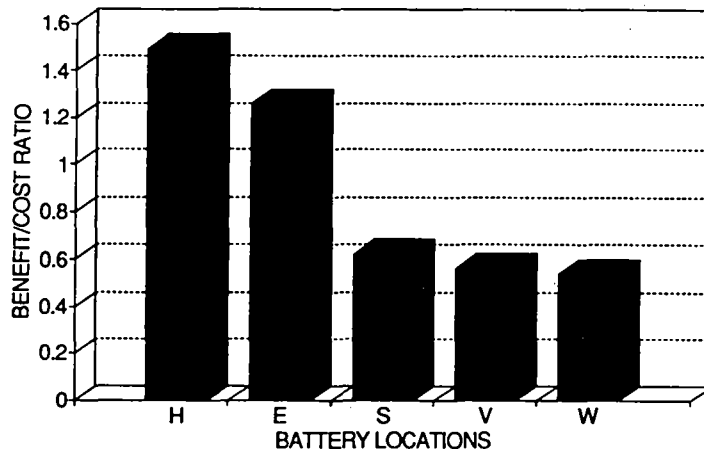


Figure 2-2. Comparison of Benefits to Cost for 5 Battery Locations

suitable to relate the worth of service reliability to the cost of service. The VOS or outage costs depend upon type of load, frequency and duration of interruption, and timing of the interruption. However, some of these costs have a wide range. The cost range for 1-hr interruption has been reported in the literature.

The actual cost or VOS used in this study is shown in Table 2-5. For each of the five types of battery applications analyzed in this study, it is assumed that the total amount of energy not served or kWh interrupted per year is equal to the total battery kWh rating. This means that, on the average, the sum of energy supplied to the customers by the battery during the interruptions over a period of 1 yr is equal to its total energy rating.

After computing benefits, the battery storage system costs were calculated. For the battery alone, a different life is used than for the entire battery storage plant. The operating and maintenance (O&M) cost used is 0.25% of the capital cost. Amortizing the capital cost is levelized over the plant life. The salvage value of the battery is included in computing the levelized annual cost. The replacement cost of battery cells is included as needed. The converter and BOP are assumed to have a 30-yr life and no salvage value.

The benefit-to-cost ratio for batteries application at five different locations for T&D deferral was computed. The percentage benefit of the four items is shown in Figure 2-3.

- Backup source (considering cost of outage, VOS, or value of unserved energy) credit was the most significant benefit from battery storage. In terms of customer loads on the OPC/electric membership corporation (EMC) system, the poultry industry loads are considered to suffer high damage when service interruption occurs. Hence, some of these egg hatcheries and chicken farms currently provide, or plan to install, backup diesel generation. Application of a 7,500 kWh, 5-hr discharge rating battery at Hollywood substation showed a benefit-to-cost ratio of 1.5. This was one of the highest benefit-to-cost ratios obtained in this study.
- Whenever there is an outage on a radial line, an interruption of service occurs. If the line is inaccessible or has difficult terrain, repair of the line may be difficult and the corresponding outage may be lengthy. One such example

Table 2-5. VOS or Outage Cost for 1-hr Interruption

	\$/kWh Not Served	
	Low	High
Residential	0.05	5.00
Industrial	2.00	53.00
Commercial	2.00	35.00
Poultry and Eggs	0.12	5.68

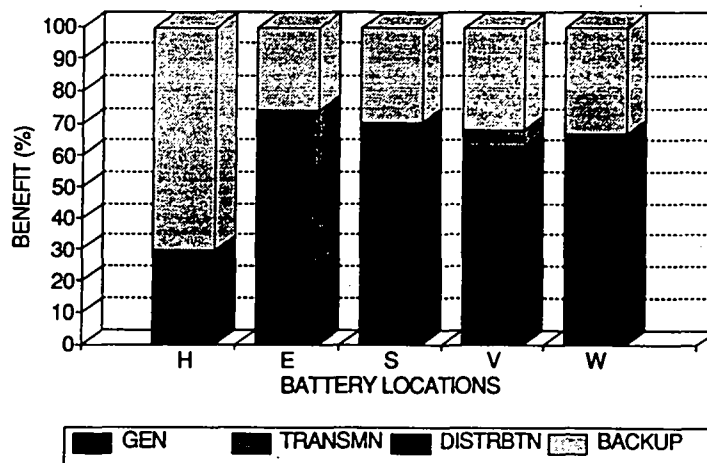


Figure 2-3. Percent of Benefits for 5 Battery Locations

selected for this study was application of a battery for backup instead of building a second transmission line. The benefit-to-cost ratio is 1.26 for this case. This substation is an attractive location (out of the five analyzed) for the battery and deferment of a second transmission line.

- A third substation was selected for evaluating the deferment of a new distribution transformer. The benefit-to-cost ratio turned out to be 0.62. The generation capacity credit was the largest, followed by the backup source credit with distribution credit being the least. No transmission deferment was used in this example. A higher backup source credit in lieu of new transmission line credit may be warranted here. The VOS has to be \$8.00/kWh for break-even of benefit-to-cost ratio as compared to \$2.61/kWh (used in the base case for the ratio of 0.62).
- Deferment of an additional 140 MVA, 220/115 kV transformer at two substations was evaluated. The benefit-to-cost ratios were 0.57 and 0.54 respectively. Because of parallel 230-kV and 115-kV lines contained by these substations, oversize battery storage capacity was needed to provide a given load reduction on the existing transformers. Hence, the battery and its cost would be about twice the required to reduce load on a radially connected transformer in which case the benefit-to-cost would be nearly break-even.

In addition to base cases, several sensitivity analyses were performed for the highest benefit-to-cost application. The sensitivity analysis included changing the following parameters, one at a time:

- Battery cost,
- Converter and balance of plant (BOP) cost,
- Battery life,
- Salvage value,
- Value of service/cost of outages,
- Extended distribution benefits.

In the first case, the battery's cost can be 60% higher than the base case, for the value of benefits to equal the cost of battery storage. In the second case, the PCS and BOP cost was doubled, and this reduced the balance-to-cost ratio from 1.49 to 1.27. These two sensitivity cases show that the battery cost has a higher

effect on the overall cost as compared to the converter and other costs.

In the third case, the battery life was reduced to 10 yr from 15 yr. This means two battery replacements are included in this case as compared to only one battery replacement in the base case. The benefit-to-cost ratio decreased from 1.49 to 1.42, which is not a substantial reduction. Thus, there may be economic advantages in improving the cycle life of lead acid batteries, but the chronological life is not significant as compared to the battery cost itself.

In the fourth case, the salvage value was doubled from 20%. Surprisingly, the benefit-to-cost ratio increased to 1.68. This may be partly explained by the escalation used in computing replacement battery cost. Essentially, the salvage part of the battery cost is escalated by 4.5% because at the end of battery life, the trade-in value of the battery is assumed to be equal to the salvage percentage of the new battery cost.

The fifth sensitivity case involved the value of service or backup source credit. As noted earlier, this item contributed most to the battery benefits. This VOS may be about 50% of the base case for the break-even cost.

In the sixth sensitivity case, the distribution benefits were extended to 30 yr. The base case showed the distribution transformer deferment for 10 yr only. Because the battery can be moved to another location, similar distribution benefits may continue to accrue. This case shows an increased benefit-to-cost ratio of 1.58. The cost of moving the battery and any change in value of service are not recognized in this case.

Recommendations

Battery energy storage at substations with radial feeds and/or serving critical customer loads may have positive benefits for OPC. OPC has approximately 24 such sites that could be candidates for further, more detailed analysis to determine the benefits of battery energy storage at these sites. A follow-on feasibility study that includes the conceptual design of site specific battery system(s) and further refines the value of the benefits at each site was recommended to OPC.

Bonneville Power Administration Puget Sound Area

In 1989, planning studies at BPA revealed that major additions to the existing transmission system across the Cascade Range might be required in the mid-

nineties. The studies indicated that 1600 MW of expected growth in the Puget Sound area peak load between 1993 and 2003 would result in voltage stability problems on the highly stressed 500-kV system across the Cascades.

BPA engineers identified 10 possible solutions to the problems. These included a new double-circuit 500-kV line across the Cascades, and up to 600 MW of combustion turbine (CT) capacity in the Puget Sound area. Some partial solutions included water heater fuel switching, time of use rates, water heater controls, low-flow shower heads, conservation, curtailment, and voltage support equipment.

SNL initiated this battery application study to determine if battery energy storage could compete with the options being considered by BPA, especially if it could defer a 500-kV transmission line or displace CT capacity.

Combustion Turbine Displacement

The daily winter load profile in the Northwest helps make battery energy storage attractive. The load profile from two days of particular concern to BPA are shown in Figure 2-4. The February 3, 1989, peak is the more difficult one for a battery because it is relatively flat. However, even on this day, the peak could be reduced 200 MW by a battery with just 1.35 hr of storage. A 400-MW peak reduction would require 2.2 hr of storage.

One of the problems with the use of CTs to address the Puget Sound voltage problem is that they cannot be started quickly enough to prevent voltage instability following loss of a major 500-kV line. Hence, they must be running when load is high. This adds sig-

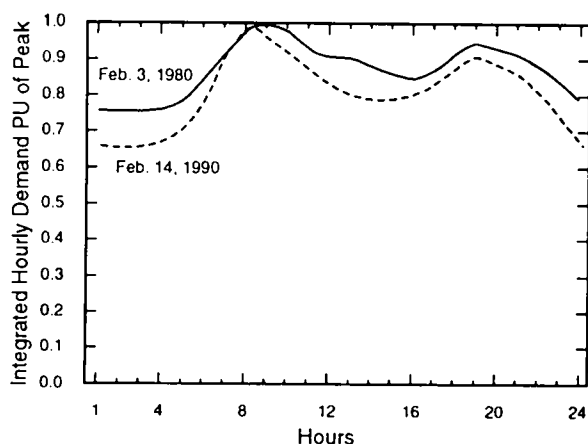


Figure 2-4. Load Shapes for High-Load Days of Concern to BPA.

nificantly to the cost of the CT option. Batteries can be switched on and brought to full power in seconds.

A benefit of CTs is that they “firm up” BPA energy commitments. That is, they allow BPA to commit to firm energy deliveries that can be served largely from hydro plants. Should water shortages occur, the CTs can be used to meet those obligations.

Based on recent SNL estimates of battery and converter costs and the instant on-off capability of batteries, batteries could provide the needed peak shaving at less cost than CTs. However, batteries cannot firm up hydro energy sales as can CTs, and thus cannot compete with this significant CT benefit.

Cross-Cascades 500-kV Line Deferral

The 500-kV line across the Cascades was the second target of the battery application study. However, continuing BPA studies revealed an opportunity to substantially boost the capacity of the existing 500-kV system by adding one 500-kV substation, a 20-mile section of 500-kV line, several large shunt capacitor banks, and two static var compensators. These additions, combined with conservation and load management, have deferred the need for combustion turbines and the new cross-Cascades 500-kV line indefinitely. Further, the cost of these options is less than 30% of the cost of the line. Further study of this option and its cost was deferred because BPA had already committed to the construction of this project.

Local Benefits of Battery Energy Storage

Batteries need not be located in high-voltage substations to provide transmission benefits. Battery energy storage can be more attractive if it is divided into small units and placed close to customer loads to reap further benefits. The potential for this in the Northwest was assessed through discussions with utilities served by BPA in the Puget Sound area. Interesting applications in which batteries might relieve the cross-Cascades transmission problem and provide local benefits are as follows:

- **Boeing Wind Tunnel** - At the time of the study Boeing was planning a 300-MW wind tunnel in the Puget Sound area. The facility would require power rising at 150 MW/min during startup and decaying at 150 MW/min during shut-down. However, utilities in the Northwest limit customer load variations to 50-MW/min. A battery could be discharged during wind tunnel startup and charged during shut-down as

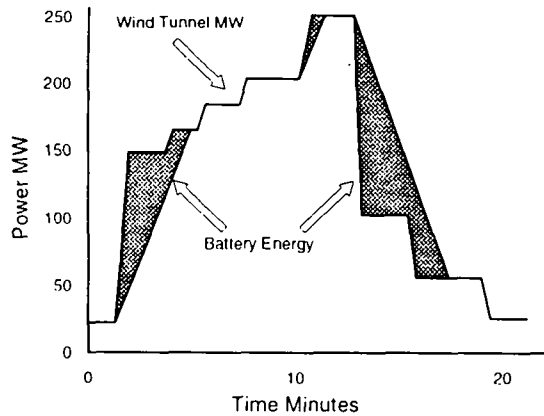


Figure 2-5. Typical Wind Tunnel Load Profile and Battery Energy Required to Limit Load Changes to 50 MW/min.

shown in Figure 2-5 to reduce load changes to 50-MW/min. A 5-min battery would suffice, though cell life may dictate a somewhat larger battery. The converter rating would be about 125 MW.

- **Aluminum Plants** - BPA serves two aluminum plants through the Seattle City Light (SCL) system. Batteries at the aluminum plants could reduce the risk of very costly aluminum cell freeze-up during power outages. A 30-min battery would prevent freeze-up. The MW level necessary to prevent freeze-up was not determined.
- **Distribution Feeder Thermal Limits** - SCL designs 26-kV feeders for a 600-A maximum capacity (27 MW) and routes them to carry 300 A during winter cold snaps. Each feeder can thus provide backup to one other feeder. However, in one area, feeders and their associated substation are reaching full capacity, and the load continues to grow. One battery, centrally located, could serve a number of feeders. The necessary battery MW rating and storage time were not determined (depends on load profile).
- **Fuel Cells** - SCL is looking at fuel cells as a possible long-term solution to the increasing load density in the city. Because fuel cells are dc devices, they might share a power converter with a battery. This would reduce battery energy storage cost, and allow energy from the fuel cell to be stored at night when the system load is low.
- **Big Six Customers** - Some of SCL's large customers have highly variable loads and thus are

subject to demand charges to cover the extra generation and transmission equipment associated with such loads. Batteries could smooth out this load. Sizes were not determined.

- **Tacoma Public Utilities** - Load is largely commercial and residential; however, an industrial pocket in the tide flats includes Occidental Petroleum (90 MW), Penwalt (60 MW), and others. As much as 400 MW of cogeneration may be developed in the tide flats area, along with 250 MW in the Fredrichsen area. Voltage regulation is an increasing problem in the area, but may be solved by cogeneration. Batteries may provide reliability, load smoothing, and voltage regulation benefits in this area.
- **Whidbey Island** - The island load is largely residential, and is growing. It is fed by two 115-kV lines at the north tip. The 115-kV lines are long and subject to occasional failure. A 28-MW diesel-driven generator is run to regulate voltage when one line is out and supply some of the island load when both lines are out. Rotating blackouts are used to share the diesel among all customers. The diesel cannot be fully loaded because of feeder "cold load pickup." A 230-kV line extending onto Whidbey Island will help after 1995, but reliability will still be low by Puget Power standards. The best solution, a cable tie between Whidby Island and the Seattle area, would cost about \$10 million. A battery could supply the 10 to 20 min "cold load" portion of the last feeders to be picked up, thus increasing the load the diesel can serve. It could then smooth the load to further increase diesel loading. A 5 to 10 MW 1-hr battery would be needed.
- **Power Plant Black Start** - Puget Power has some power plants that could be restarted more rapidly after a blackout if a nearby source of power were available.

Generation Benefits of Battery Energy Storage in the Northwest

Discussions were also held with BPA and Puget Sound area utilities to identify generation benefits of battery energy storage. All of the utilities have hydro plants that provide highly flexible scheduling to maximize economy and impose few generation constraints on operation.

Conclusions

There are limited opportunities at present for battery energy storage plants to capture large benefits in the Puget Sound area by deferring major transmission and CT investment because less costly alternatives have been identified. Also, the usual generation benefits of energy storage are not available in the Northwest.

Battery energy storage may, however, still have a place in the study area at the subtransmission and distribution level. It could be attractive by providing distribution system benefits and displacing some of the more costly alternatives that will be used to defer major transmission and CT investment.

Battery energy storage may also provide a hedge against failure of some of the less well-proven alterna-

tives to major transmission and CT investment. For instance, if conservation, fuel switching, or load management do not limit peak load growth as expected, batteries could be installed quickly and on short notice to serve peak load.

Evaluating the cost effectiveness of battery energy storage in an environment where there are no large benefits is difficult. It requires careful scrutiny of the many possible benefits that can be derived from battery attributes (see Table 2-6). This, in turn, requires close cooperation of all persons or organizations that may recognize a benefit from the installation. In the Puget Sound area, this would include at least several departments within BPA, several from one of BPA's client utilities, and, perhaps, one or more from an industrial customer.

Table 2-6. Battery Attributes

No-Cost Start/Stop
Fast Response (kW and kvar)
Four Quadrant Operation (simultaneous
kW and kvar)
Unmanned (Remote Control)
High Reliability/Availability
Low Maintenance
Short Lead Time Installation
Low environmental impact (siting flexibility)
Limited space requirement (siting flexibility)

3. Battery Systems Engineering

The Battery Systems Engineering project is aimed at developing total integrated battery energy storage systems. The objective is to develop several battery systems designs that can meet the various application requirements in the utility operating environment. Development contracts are under way at Omnion Power Engineering (AC Battery) and GNB Industrial Battery. PG&E will be the host utility to field-test the first AC Battery prototype unit and will evaluate the GNB technology as an option for distributed storage. The requirements of another host utility, PREPA, for a spinning reserve/area regulation system are included in the advanced VRLA GNB system. The specifications were provided to UMR, who will develop a model. Vent valve reliability improvements are being addressed at SNL in support of the GNB contract.

AC Battery Development - Omnion

The AC Battery is a patented, modular battery system concept proposed by Omnion Power Engineering. The concept embodies several of the design features that are desirable for utility operations. It offers redundancy at several levels, ease of maintenance, portability, and unattended remote operation. It also relies on mass manufacturing production techniques to realize the maximum potential of reducing the cost of battery energy systems. Upon completion of a successful development phase, the AC Battery will be able to meet application requirements in the 500-kW to 3-MW size ranges.

In its present conceptual form, the AC Battery is a 500-kW/500-kWh battery energy storage system packaged in multiple, transportable containers. Each container houses several "modules" that contain the batteries as well as an on-board power conversion system. This enables the modules to accept ac power and convert it to dc to charge the batteries. In the discharge mode, the dc output of the batteries is converted to ac power that is aggregated from all the modules to equal the rated power capacity of the container.

At present, the AC Battery is at a concept stage and an ~12-mo effort is needed to complete the detailed design and engineering to transform the concept into a working system. Although the concept is simple and relies on proven battery and power conversion technology, it still combines these technologies in a manner that

has not been attempted previously and places the battery in a potentially stressful environment that makes it difficult to predict performance. This uncertainty underscores the need to demonstrate the concept with a prototype unit under field conditions. Thus, the objectives of this task are to complete the detailed engineering design and to build the first prototype unit for testing at PG&E for a 12-mo test period.

Tasks/Milestones

The tasks in the AC Battery prototype development contract are described below:

1. PCS Design and Development—Includes the design and control software development of the PCS, design and test of a prototype unit, and design of a production board.
2. Module Design and Development—Includes the design of the module that will house the battery and the PCS boards. Includes the fabrication of a prototype module that will be replicated for the 36 modules of the AC Battery container.
3. Container Development—Includes the structural and thermal design of the container to house the modules and meet all the transportability and operating requirements.
4. Production Cost Estimate—A study to estimate the cost of producing the commercial design of the AC Battery assuming various rates of production. Also identifies changes in design that might be necessary for economic manufacturability at higher production rates.
5. AC Battery Testing—Includes the field test of the prototype unit at PG&E. It is expected that the unit will initially be tested in a laboratory setting, and moved to a substation site upon satisfactory check-out.

Container Development

The container (Figure 3-1) serves as a relatively compact and lightweight envelope and support for the modules with a size and shape suitable for easy transportation, yet possessing sufficient strength and rigidity. It provides tamper-proof protection for batteries and

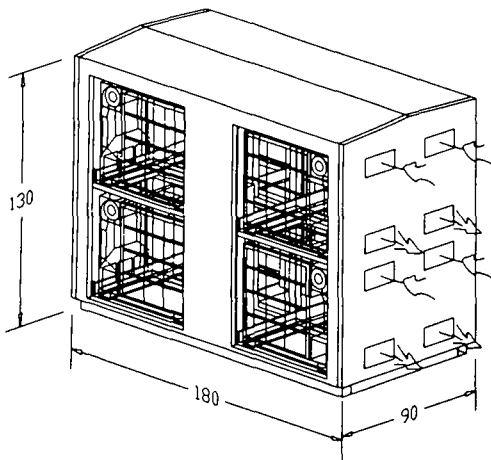


Figure 3-1. AC Battery Container Configuration (all dimensions are in inches).

electrical gear, while allowing easy access to all internal components. It features a 30-yr design life with low maintenance requirements.

The container is insulated to minimize the required heating and cooling for the batteries. It must provide ventilation for exhausting waste heat from the PCS and batteries, and any gases given off by the batteries.

The original system concept called for a single container housing 36 modules, each of which contained 21 batteries (756 batteries total). This concept called for half the modules to be field installed due to trucking weight limitations. As the development proceeded, it became apparent that some changes and improvements would be in order.

One change was the downsizing of the container, which offers the following advantages:

1. Easier transport and mobility on site.
2. All modules come pre-installed in the container for reduced site work and faster setup.
3. The cooling system can utilize a shorter, simpler ducting system. This eases the task of assuring temperature uniformity among batteries and modules.

Another feature added is the ability to load and unload modules from either side of the container. This minimizes the needed site improvements and allows the fitting of more modules in a given land area, greatly increasing the overall power and energy density.

Figure 3-1 shows the container. It is approximately 11 ft tall, 15 ft long, and 8 ft wide. The container houses

eight modules stacked two high. Individual modules contain 48 batteries with power/energy ratings of 32 kW/21 kWh, respectively. With the eight modules, the container power/energy rating is ~250 kW/167 kWh. The weight of the container with eight modules and all auxiliaries is estimated to be 40,000 lbs. Containers can be placed end to end with minimal space between them. Access to all components of the container can be accomplished from the sides of the container.

Connections to the container consist of a 250-KVA, 480-VAC three-phase service drop and connections to a SCADA system. Where multiple containers exist at a site, the SCADA system is connected to the first container only. The additional containers are then controlled by the first container. This makes the first container a master and the additional containers slaves. All containers have the capability of being masters or slaves as desired.

Another change occurred in module sizing. By incorporating more batteries per module (48 vs 21), the PCS capacity and efficiency could be increased. Additionally, only eight PCSes are needed, resulting in a potential cost savings.

Battery configuration was changed from a single layer of 21 batteries to a stacked orientation comprised of four layers of 12 batteries. This allows a stronger module. To circumvent potential complications in production and serviceability, a novel structural design incorporates layers of battery trays, which can be pre-assembled, wired, and stacked to form a rigid unit.

Figure 3-2 shows the module configuration. Each module is 58 in. wide, 51 in. high, and 40 in. deep and is rated at 32 kW.

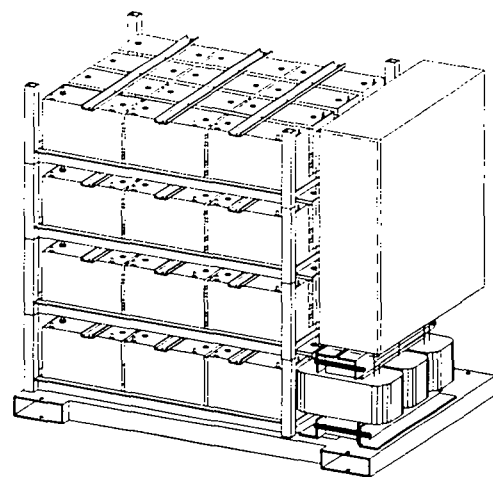


Figure 3-2. AC Battery Module.

PCS Design and Development

PCS Waveform Control

The 250-kW AC Battery is comprised of eight modules in which each module has its own converter. Skewing is a technique wherein the phasing of each module is staggered, or skewed, by 1/8th of the switching period. When all waveforms from the eight modules in the container are combined, the high frequency components created from switching tend to cancel, while the 60-Hz line frequency component remains. By utilizing skewing, lower frequency switching is possible, resulting in lower switching losses and lower cost reactors.

The skewing of bridge outputs was modeled to find out what effect various parameters would have on the output waveform both at the output of a single module and at the output of the container. The goal was to keep the total harmonic distortion (THD) of the current output of the container under 5%.

What is different here is that while in the past the second through fiftieth-integer harmonics of 60 Hz were looked at, for this development all harmonics were used. Since the IGBT converters have typically run at a switching frequency of 7680 Hz, looking at frequencies over 3000 Hz is more demanding.

Figure 3-3 shows the typical waveform that has been used in the past. The computer model used to simulate this waveform assumes a 660-VDC bus voltage, 750 μ H reactors, and a 7680-Hz switching frequency. While the individual switching cycles are hard to

make out, the width of the switching band is readily seen.

Figure 3-4 shows what skewing is hoped to accomplish. The bottom two curves are two output waveforms that have been skewed 180° apart using the computer model developed by Omnion. The top curve is the sum of the two bridges and shows the reduction in ripple current possible when bridges are skewed. This allows the reader to visualize the reduction by comparing the magnitude of single bridge ripple currents with the magnitude of the summed current. If the bridges were operating without skewing, the top wave current ripple would have the same magnitude as the bottom two waveforms. The reduction in ripple is not 100% because the ripple current is a sawtooth shape rather than a triangular waveform. If the ripple current was a perfect "V" shape, the ripple current would cancel completely.

Several options exist to look at the impact of skewing. The easiest option is to mathematically shift and sum several ideal constant frequency current waveforms. While this demonstrates the concept, it may be an oversimplification. Instead, a model of the bridge control circuit was built. This model does not operate to give a constant frequency output; rather it uses the variables that the real circuit will use and processes the data just like the real circuit. As a side benefit, the model allows tuning of the real circuit prior to building it. By looking at variables in the model, the effect of feedback and feed forward on the circuit can be seen. When several bridges are modeled, each bridge has its own model and runs independently of the other bridges. This fairly well simulates actual operating conditions.

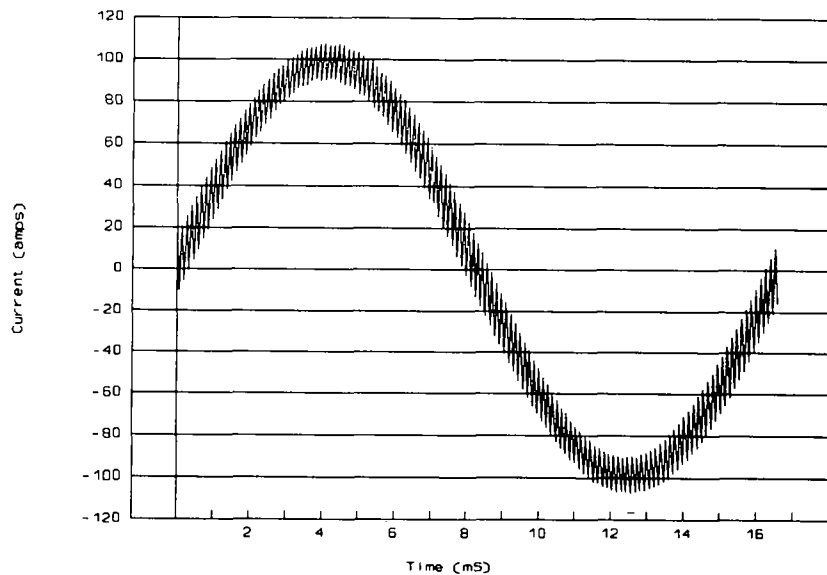


Figure 3-3. Typical AC Waveform without Skewing.

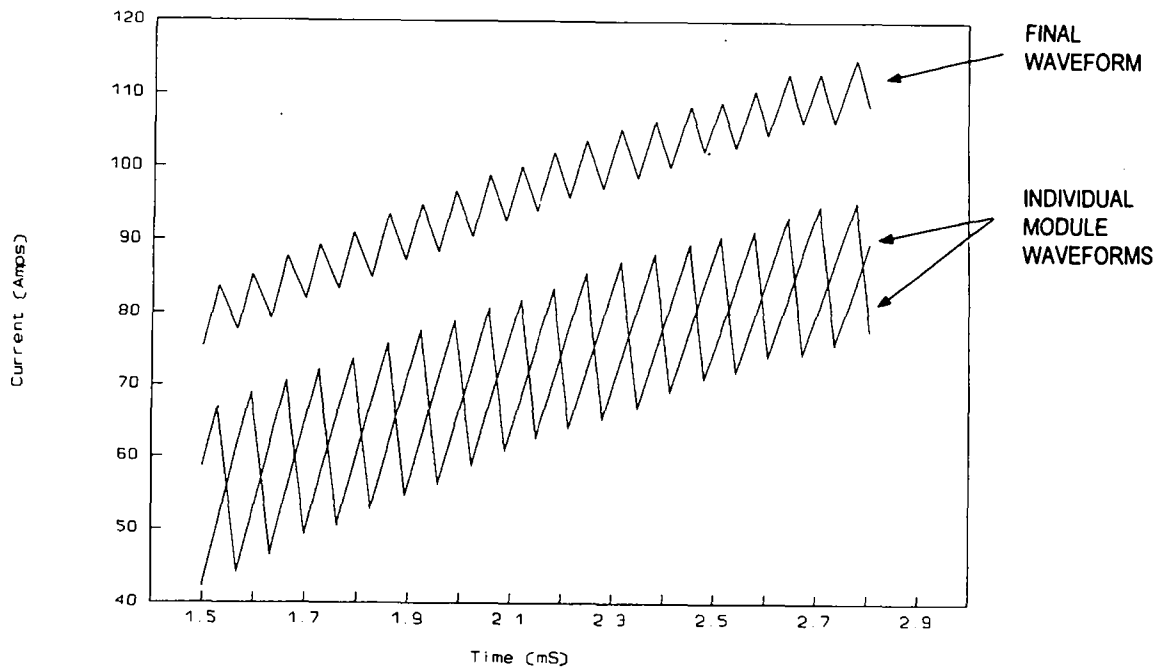


Figure 3-4. Two Modules with Skewing and Resultant Waveform.

With the model in place, the first step was to reduce frequency and reactor inductance. Reducing frequency has two benefits. The first benefit was to allow the use of more conventional cores in the reactor. Today reactors are typically used with a .002-in.-thick steel lamination. By reducing the frequency, the hope is that a thicker (and less expensive) core material can be used. Additionally, reducing the frequency of operation results in higher PCS efficiency due to the reduction in switching losses.

By reducing the inductance, the cost of the reactor should be reduced proportionately. The baseline case for all the figures that follow is 3000-Hz operation, 200 μH of inductance in skewing positions, and a dt of 4.17 μs . The dt is how often the model is updated. As dt gets larger, the model operates less accurately.

Figure 3-5 shows the impact of the number of skewed module locations on THD. Two curves are shown. In each case, the model was configured for 3000 Hz operation, 200 μH of inductance and a dt of 4.17 μs . The curves correspond to the maximum container voltage of 816 V dc (17 V/battery). A single bridge has a THD of 123% at 17 V/battery and 62% at 10.5 V/battery, which is not shown in Figure 3-5. Adding two more modules reduces the THD between 9 and 15% as shown in the figure. Thus, the number of skewing locations has the most effect between 2 and 6.

Modeling has shown that both inductance and operating frequency can be reduced while keeping the current THD below 5%. For the AC Battery PCS, the

minimum configuration of the magnetics in terms of inductance and frequency is 200 μH per phase of inductance and 3000-Hz operating frequency. This will require a 200 A IGBT. If the inductance is increased to 400 μH and the frequency to 4000 Hz, a 150-A IGBT would be sufficient.

Table 3-1 shows the current from sampled waveforms with different reactors at 60 Hz and at harmonics of the operating frequency. In the first line, the third harmonic is shown as 7.2 A. This means that a bridge operating at 3000 Hz with 200 μH of inductance has 7.2 A of current at 9000 Hz. These data were used to design the reactor.

Integrated Transformer and Reactor Design

Another area for potential weight, size, and cost savings is the magnetics. Past PCSes have used separate reactors for each phase. The outputs of each of the phases were then sent to a three-phase transformer to provide isolation and voltage matching.

Re-examination presents three options with regard to the reactor:

1. The first option is to build three separate reactors as we have done in the past.
2. Second, three reactors could be combined to make a three-phase reactor. This reduces the parts count.
3. Finally, the reactors could become leakage inductance in a transformer.

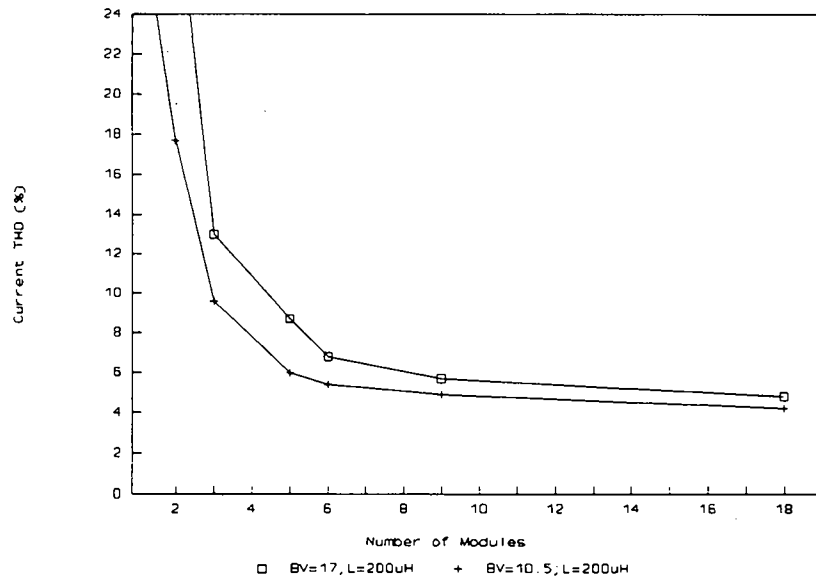


Figure 3-5. Current THD vs Number of Skewed Modules

Table 3-1. Current from Sampled Waveforms

Operating Frequency	Induct μ H	Harmonic Current (A)									
		60 Hz	1st	2nd	3rd	4th	5th	6th	7th	8th	9th
3000	200	70.8	82.5	19.9	7.2	4.0	3.2	2.2	1.5	1.3	1.1
4000	200	68.7	62.7	14.7	5.3	3.0	2.4	1.9	1.4		
6000	200	69.8	41.5	10.0	3.5	2.3					
8000	200	70.7	31.0	7.8	3.1						
3000	300	71.0	55.1	13.6	4.8	2.6	2.1	1.6	1.1	0.9	0.8
3000	400	68.6	41.7	10.2	3.9	2.3	1.9	1.4	1.1	1.0	1.0
3000	600	69.4	20.9	5.5	2.3	1.2	0.7	0.7	0.5	0.5	0.4
3000	800	71.5	15.3	4.2	1.7	0.8	0.5	0.4	0.3	0.3	0.3

The transformer would ideally be an isolation transformer with a 480-V output. This option reduces the balance-of-system cost. Cost reductions are possible by the elimination of a transformer for the container and in lower currents inside the container.

As configured, the converter output voltage is 255 V line to line. The maximum current is 70 A ac. This requires 100-A-rated equipment. By going to 480 V, the maximum current is ± 37 A ac. This is almost a 2:1 reduction and results in lower costs for disconnects, wire, and circuit breakers. By implementing this third approach, it is hoped that much of the extra cost, size, and weight will be eliminated compared to a discrete reactor/transformer design.

Software Control

Compared to previous Omnion designs, the new PCS hardware design is greatly simplified. By integrating much of the control and protection logic onto a FPGA chip, component count (and cost) drops, while reliability should increase. By utilizing a programmable chip, changes that formerly required extensive board modifications can now be done via software. A new phase-locked, loop hysteresis current regulator has been developed using extensive computer modeling and simulation. Its implementation results in a reduction in parts count and circuit complexity. A fiber-optic communications link interconnects the modules to the module control computer.

Many higher level control functions have been moved from the PCS control to the container control computer. These computation-intensive yet less time-critical tasks can be done in a centralized location, allowing greater PCS simplicity. It has the additional advantage of making it simple to tailor the AC Battery to a wide variety of applications.

The graphical user interface allows multilevel control, while clearly displaying parameters of interest. The display emulates eight module control panels and a main system panel. Status targets and digital readouts show at a glance the operating conditions for each of the modules. An X-Y display will show the four quadrant output of the container and modules. The total system display shows overall performance, while continuing to monitor the individual modules. Commands may be issued in kW, kVAR, kVA, power factor, phase angle, and dc Amperes. The computer makes all the necessary conversions.

A built-in program language interpreter, complete with on-line editor, facilitates programmable AC Battery operation. Data logging functions track and save operating information for review and analysis.

Container Thermal Management

An important consideration in a battery energy storage system is dealing with the heat generated by the batteries and PCS. The following test was conducted on a scaled-down battery array. The results have helped to confirm the differing cooling requirements for the batteries and the PCS. Batteries have a much greater thermal mass, yet have a stricter requirement for optimal temperature range. By developing separate cooling systems for each, fewer compromises are required, and overall cooling efficiency can be increased.

The power bridges will use exclusively outside air, which needs little conditioning except for some coarse filtration. The batteries and the remainder of PCS will use recirculated indoor air almost exclusively. This air will be heated and cooled as necessary to maintain the 60-100°F optimal temperature range.

Test Summary

The purpose of this test was to determine room temperature ambient airflow required to prevent overheating of the batteries under the worst-case loading conditions. Worst case is expected to occur when using the AC Battery for frequency stabilization because this subjects the battery to repetitive charging and discharging at a fairly high duty cycle.

For this test, a battery was discharged from 100% state of charge (SOC) to 80% SOC and then cycled in the following manner: 8 min discharge at 28 kW dc using a string of 47 batteries followed by 1 min rest, 8 min charge at 28 kW dc followed by 1 min rest repeated for 8 hr. This routine maintained the battery at approximately an 80% SOC. Battery voltages were monitored to ensure that the battery was not being discharged or charged on a cumulative basis.

To conduct the test, three of the 47 batteries in series were mounted in an insulated box of two-in.-thick styrofoam with 8 x 12 in. inside dimensions. The box was 48 in. long and built to represent the expected module geometry for airflow. Figure 3-6 shows the configuration of the test.

Ambient air was blown past the batteries by a variable speed fan. Air velocity was measured at the discharge. Temperature probes were installed at the inlet, outlet, and battery post and between batteries to measure the heat dissipation and battery temperature. The "between" battery measurement was taken between batteries that were touching each other to attempt to get battery internal temperature. Battery string voltage and temperatures were recorded at 9-min intervals during normal working hours. Each night the batteries were brought to full charge at constant 25 A until reaching 16 V/battery, then constant voltage to 100% SOC. The batteries were discharged to 80% SOC prior to the start of the next test the following morning.

Three levels of airflow were evaluated over 5 to 6-hr each. The air velocity was measured through a 3-in. diameter tube in order to obtain a reasonable velocity for the instrumentation and converted to cfm past the batteries. Heat extracted from the batteries was calculated by the formula $Q = \text{cfm} \cdot C_p \cdot (t_2 - t_1)$ in BTU/min considering standard air at 68°F where $C_p = 0.0181 \text{ BTU/ft}^3/\text{°F}$. The results are shown in Table 3-2.

Some of the test observations are as follows: the battery temperature did not stabilize with 4.86 cfm airflow, barely stabilized with 9.72 cfm and stabilized after about 4 hr at 19.44 cfm airflow and then tracked the ambient temperature. In each case, the battery temperature as indicated by the probe located between batteries reached about 42°C and recovered to about 38°C while on the overnight charge with no ventilation. The charge/discharge cycle used here of 5 to 6 hr operation with slow recharge is considered to be more severe than anticipated in commercial use.

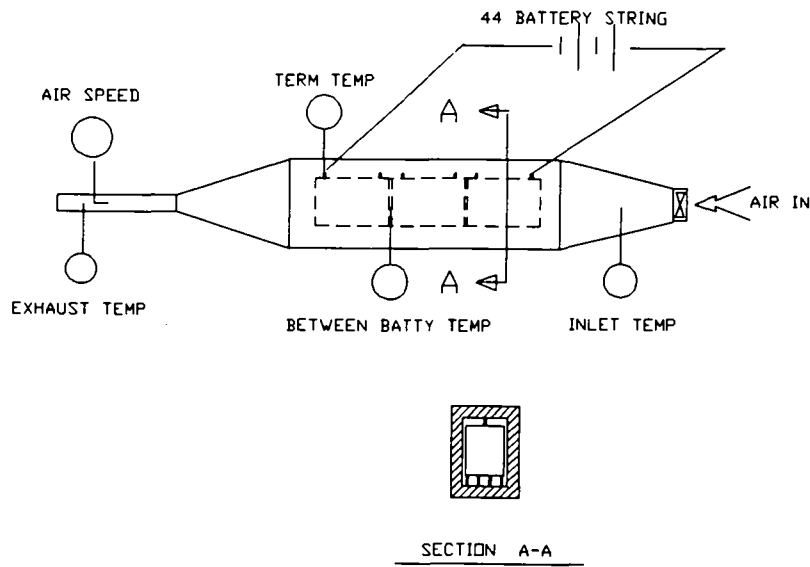


Figure 3-6. Experimental Setup for Thermal Test of AC Battery.

Table 3-2. Battery Thermal Test Results

Air Velocity (FPM)	100	200	400
Airflow (cfm)	4.86	9.72	19.44
Q (BTU/min)	0.87	2.28	3.17
Q (W/3 batts)	15	40	55.7
Q (W/module)	240	640	891

The test yielded the following conclusions:

The total battery contribution to heating within the container is ~24,000 BTU/hr (891 W*8 modules*3600/1.055) for a period of 5 to 6 hr for a daily average of 1013 BTU/hr. Considering the narrow range of ambient to discharge air temperature, it appears that a cooling capacity of about 12,000 BTU/hr should be adequate to maintain the ambient temperature within acceptable limits.

Additional testing of one module will be performed at SNL during FY93 to verify these results. Further testing at the system level to verify the thermal management scheme will be performed after fabrication of the first container at Omnion.

Technology Development - GNB

The 3-yr, \$2.83M development effort with GNB Industrial Battery Company was initiated specifically to improve VRLA battery designs to meet utility applica-

tions requirements in the mid- to late-1990s. Current VRLA battery designs are geared to meet the needs of portable equipment and emergency power backup applications and are not optimized for utility applications, which include energy reserve, power regulation, and peak load shaving. The intent of the GNB effort is to develop an advanced VRLA battery designed to meet utility needs. To ensure that these needs are understood, the statement-of-work and the make-up of the project team was specially defined so that GNB could obtain first-hand input from utilities about battery storage requirements in their network. Recognizing the near-term market potential, GNB is cost-sharing the contract at 46%; both of the host utilities PG&E and PREPA, are also cost-sharing their participation in this effort, which is indicative of the interest of the utility industry in battery energy storage systems. The requirements of PREPA for a spinning reserve/area regulation system are the driving force in the definition of the advanced VRLA being developed under this contract.

The GNB effort in this contract is comprised of three tasks. Task 1 is a two-phase activity that is in-

tended to improve the performance of VRLA batteries through changes in battery design, materials and manufacturing processes. The objectives of Tasks 2 and 3 are to define battery system requirements and to conduct economic evaluations that require extensive participation by the host utilities.

Task 1 is divided into two phases. The first phase is improving current VRLA battery designs to match or exceed the performance and costs of flooded lead-acid batteries without sacrificing the inherent advantages of the VRLA technology. The technical approach for this first phase is focusing on performance issues such as vent valve reliability, thermal management, charging profiles, positive plate behavior, and ground fault prevention, which have been perceived by the utility industry as barriers to the widespread implementation of VRLA battery systems. The studies and improvements being conducted in this phase will generate cell level data proving and improving the performance of GNB's ABSOLYTE technology in utility applications. An additional objective is to improve the consistency of cell performance by manufacturing process control.

In Phase 2 of Task 1, GNB is completing the development of an advanced VRLA battery design optimized for high-power applications. The specific development efforts are investigating evolutionary and revolutionary changes in grid and active materials make-up and electrolyte immobilization technique to improve the efficiency of energy delivery and life of the VRLA battery. A key manufacturing process that will improve manufacturing consistency and control manufacturing costs is being developed and will be implemented.

Joint efforts between GNB, PG&E, one of the host utilities, and the University of Missouri-Rolla (UMR) have resulted in the development of a preliminary, modularized, standard battery/power conversion unit including the facilities required to house and support a battery energy storage system (BESS). PG&E's analysis of their distribution network has resulted in the identification of four sites that could immediately benefit from a battery energy storage system. Furthermore, PG&E has conducted simulation studies on their transformer capacity model (TCAP) and provided GNB with several discharge profiles. GNB will evaluate current, intermediate and advanced battery designs under these profiles and will provide PG&E with a database that will provide decision criteria for selecting operating alternatives. As the result of interchange meetings between the participants teamed in this contract, PG&E has indicated a marked preference for a 3- to 5-yr life battery, which is in contrast to the requirements identified in most utility battery energy storage studies.

VRLA batteries capable of high power with this life range can be incorporated as part of the utility/battery product philosophy.

Progress being made against each of the specific task items is described below.

Task 1. Phase 1: VRLA Battery Improvements

Vent Valve Reliability

VRLA batteries operate on the "oxygen cycle" wherein oxygen gas generated during charge is recombined at the negative plate. As such, some positive internal pressure must be anticipated during the operation of a VRLA battery. The containers for VRLA batteries are typically made of an acid-resistant plastic and are not capable of withstanding extremely high internal operating pressures. This is particularly true in large-capacity VRLA batteries where the large, thin-walled plastic cell jars are incapable of withstanding more than a relatively small internal pressure without deforming. For this reason, these large VRLA batteries are often assembled into stronger metal structures to prevent them from deforming even at the relatively low internal pressures at which they operate.

The pressure relief vent valve incorporated into the design of all VRLA battery designs is provided as a safety device to allow excess gases built-up during periods of high rate charging or overcharging to be vented to the ambient atmosphere. Because the VRLA battery does operate with some positive internal pressure, the vent must stay closed during normal operation. If the vent opens at too low a pressure, unnecessary quantities of oxygen and hydrogen gas will be allowed to vent from the cell, causing loss of water from the electrolyte and potentially resulting in cell "dry-out" and eventual failure. If the vent opens at too high a pressure, the plastic cell case can deform, causing stresses at seals and joints that can deteriorate and potentially develop into leaks. A further requirement for the vent valve assembly is to prevent the ingress of oxygen from the surrounding environment to the cell, which will accelerate the self-discharge of the VRLA battery by reacting with the charged negative plate.

The vent valve system incorporated into each ABSOLYTE cell has been designed with the requirements enumerated above in mind and operates reasonably well as evidenced by over 10 yr of actual operational history. However, they have been reported to have "micro" leaks and hysteresis from vent opening to reseal operation. This is a deviation from the original design

intent and needs to be corrected. In addition, vent valve operation under extended elevated temperature conditions is unknown.

The technical approach being followed to define and improve the operation of the pressure relief vent valve and to identify improved vent designs is as follows:

1. characterize the vent/reseal operations of the current pressure relief vent valve, considering the external conditions to which the vent may be exposed over its operational lifetime;
2. identify and evaluate improvements in materials and/or fabrication that can improve the consistency of operation of the current vent design; and
3. analyze and evaluate alternate pressure relief vent systems to improve consistency of performance.

ABSOLYTE pressure relief vent valve assemblies were randomly sampled from factory stock and assembled onto test cells equipped with electronic pressure transducers. The five sample vents were tested through 20 vent/reseal cycles over a 140 hr period at 25°C. Over the course of the test, each of the vent samples released within the design range for the vent operation (i.e., 3 to 9 psig), and test data correlated well with the acceptance data generated at the factory. Variation of the venting pressure among the samples and over the course of the test was small; however, a significantly wider variation of the reseal pressures was observed among samples and over the course of the test for individual samples. Experimental data indicating variability among the five vent samples are summarized in Table 3-3, and plots of pressure vs time during the

vent/reseal cycle tests for two of the samples are shown in Figures 3-7 and 3-8.

The repeatability of the pressure release point for the ABSOLYTE vent valves has been shown to be quite consistent, typically well within ± 1 psig of the average venting pressure. The reseal pressure, however, is considerably more variable, both among samples as well as between repetitive reseals of the same vent valve assembly. Although this variable vent reseal behavior is an area of improvement, it is important to note that at no time did any of the pressure release vent valves allow the internal pressure of the test cells to drop to "zero psig," and thus, the vents demonstrated their ability to prevent the ingress of oxygen to the cell, which would be more detrimental to long-term operation than fluctuations in reseal pressure.

Upon completion of this series of tests, it was noted that the pressure transducers were being attacked by the oxygen and acid-rich atmosphere within the test cells. There was concern that the resulting corrosion was affecting the calibration of the devices. The transducers were returned to the manufacturer for repairs, and the test cells were modified to isolate the transducers from the oxygen-rich gases and the acid-laden vapors.

While the test equipment is being repaired and modified, alternate valve materials and designs are being obtained. Modifications to the surface of the rubber cylinder used in the GNB pressure relief vent design were investigated by SNL materials scientists, specialists, and staff, and samples of cylinders prepared by precision cutting of a rubber extrusion have been obtained and are awaiting fabrication into pressure relief vents. Additional pressure transducers and equipment to fit an oil trap onto each of the test cells have

Table 3-3. ABSOLYTE Vent Baseline Characterization

Vent Valve	Opening Pressure (psig)		Closing Pressure (psig)		Factory Acceptance Pressure (psig)
	Mean	Std. Dev.	Mean	Std. Dev.	
1	6.663	0.181	5.549	0.612	6.4
21	5.030	0.332	2.541	1.082	5.6
23	6.395	0.207	3.957	0.952	6.4
2	4.298	0.135	1.673	0.558	4.0
6	5.365	0.340	2.273	1.061	4.9

Randomly selected factory-assembled pressure relief valves were tested on cells through 20 vent/reseal operations over a 140-hr period at 24°C. Vent opening pressures were consistent throughout the test; reseal pressure was more variable, but still resealed above "zero" psig preventing oxygen ingress to the cell.

PRESSURE VENT BASELINE TEST VENT #1

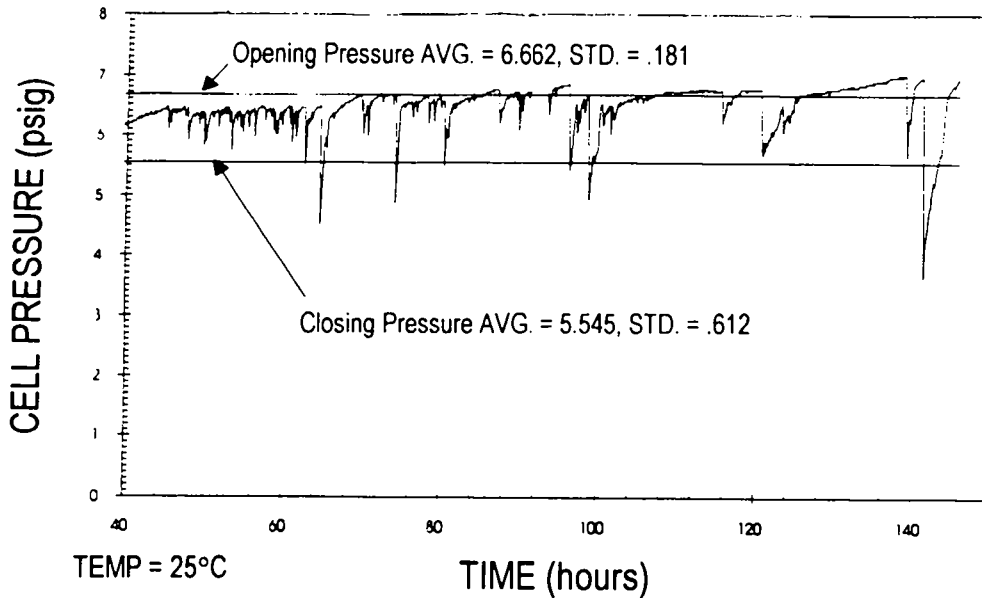


Figure 3-7. Operation of a Production ABSOLYTE Pressure Relief Vent Valve on a Cell at Constant Overcharge. The data show the vent opening repeatedly in the range of 6 to 7 psig and resealing in the range of 5 to 6 psig.

PRESSURE VENT BASELINE TEST VENT #6

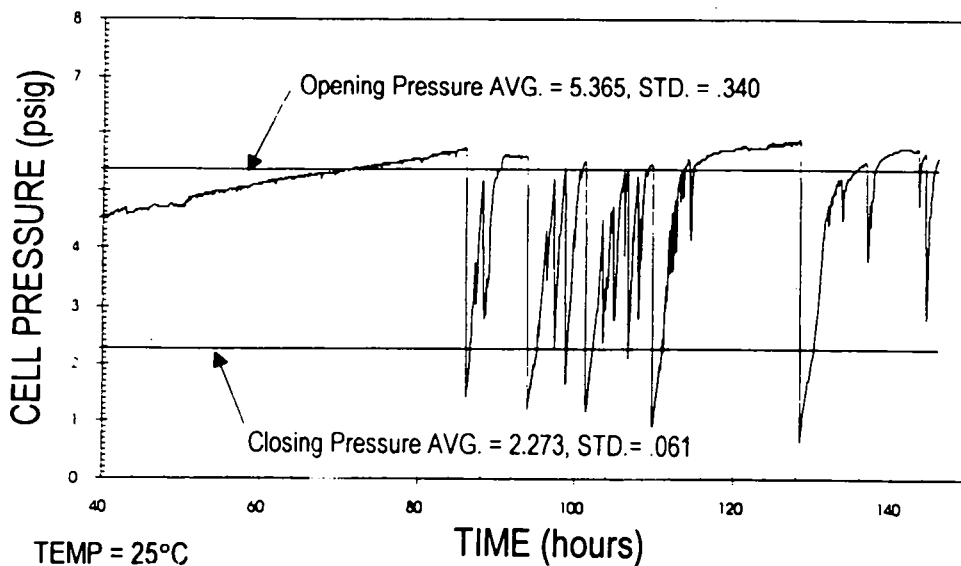


Figure 3-8. Operation of Another Randomly Selected ABSOLYTE Pressure Relief Vent Valve on a Cell at Constant Overcharge. This shows repeatable vent opening in the range of 4 to 6 psig but more variable reseal operation. The intent of this project task is to improve the consistency of operation of the ABSOLYTE vent. Despite the variation in reseal operation, the vent reseal maintained the cell at a positive internal pressure, which is essential to prevent oxygen ingress and accelerated self-discharge.

been ordered and are expected to arrive to allow resumption of the vent valve tests by October 1992.

A further complication arose recently when high temperature tests (under an IR&D program) on ABSOLYTE product showed evidence that the rubber seal washer (used when mounting the vent valve body in the cell cover) was suffering thermal degradation. This observation has led to an added task to evaluate alternate sealing washer materials with better thermal stability.

Positive Plate Growth

The normal wearout mechanism anticipated in any lead-acid battery is the anodic corrosion of the positive grid structure. The product of this anodic corrosion reaction of the grid lead with sulfuric acid is lead dioxide (PbO_2). The density of lead dioxide is roughly 80% that of the lead metal from which the lead dioxide is formed during the corrosion process. As a result of this density change, the grid structure deforms and commonly undergoes what is referred to in the battery industry as "plate growth." The plate will attempt to grow in the direction of least mechanical resistance; in the battery, this is typically along the grid frame opposite the side where the plate lug is connected to the terminal strap. The extent of growth is dependent on the actual length of the grid, and as battery size (both physical and electrical capacity) increases, plate growth becomes a significant potential failure mode.

Grid growth can result in the loss of electrical contact between the positive active material and the grid, and/or cell shorting of the positive plate to the underside of the negative plate strap. The amount of positive plate growth is a function of the grid alloy and the mechanism of corrosion, cell operating environment including ambient temperature and charging conditions, and the cell design itself.

GNB's ABSOLYTE II cells use the patented MFX alloy for the positive grid. This lead alloy has excellent corrosion resistance and GNB's R&D efforts have determined the annualized corrosion rate for the MFX alloy when maintained at 25°C and at a float charge voltage of 2.25 V/cell to be 1.84 mils/yr. That is, under these charging conditions the positive grid will corrode .00184 in. of its cross-sectional radius each year. The mechanism of corrosion for the MFX alloy is a surface reaction that evenly corrodes the lead grid structure. This type of corrosion results in the least amount of corrosion influenced grid growth; intergranular penetration corrosion results in the greatest amount of corrosion derived grid growth. Life test data from cells tested at 50°C by Argonne National Laboratory (ANL) showed only 4.7% growth of the plate's initial area after 15 mo.

of testing. Using the widely accepted Arrhenius relationship for temperature acceleration of corrosion reactions, the ANL test period equates to the equivalent of 7 yr of service at 25°C. Plate growth of 8% or greater is usually considered to be unacceptable, and deterioration of battery performance can be expected at that level of plate growth.

Although the MFX alloy affords a good deal of resistance to plate growth, other concepts can be incorporated into the cell design to provide additional protection against the deleterious effects of positive plate growth.

GNB installs a plastic "boot" on the bottom of each positive plate in its ABSOLYTE cell to protect against shorting by contact with negative active material sediment that accumulates in the bottom of the cell jar during assembly of the cell element into the jar. This boot currently is a snug fit to the positive grid. GNB is evaluating a collapsible boot that would provide space for the positive plate to grow into as the cell ages and the positive grid grows, thus preventing the build up of stress forces on the cell seals. The collapsible boot design will be evaluated on the improved ABSOLYTE design, and detailed drawings for this cell including the molded collapsible boot are being completed.

An additional approach is to design the grid so that as the grid grows, the various grid members collapse or bend in such a way as to actually increase the contact pressure between the grid and the active materials. This

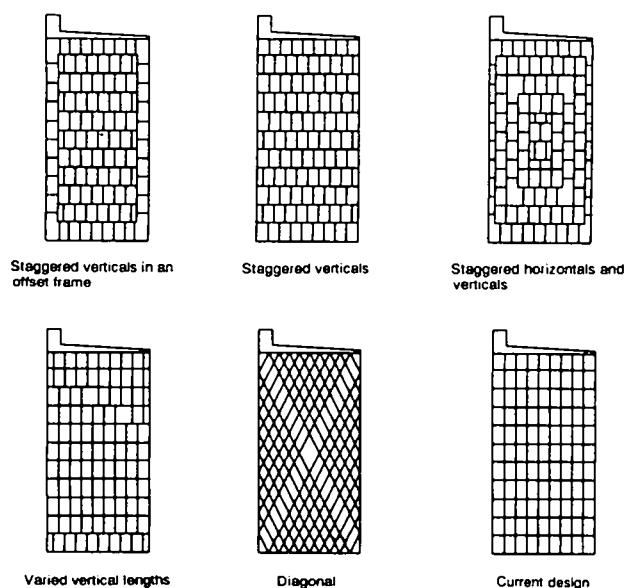


Figure 3-9. Various Positive Grid Configurations. These have been proposed to minimize growth resulting from corrosion of the grid. The advantages and disadvantages of each are enumerated in Table 3-4.

concept was used in the development and design of the AT&T/Bell Labs round cell. GNB has considered several grid design approaches to maintain active material contact during plate growth in a prismatic grid configuration. Some of these concepts are shown in Figure 3-9; the advantages and disadvantages of each of these design concepts are enumerated in Table 3-4. Because the MFX alloy does not exhibit excessive positive plate growth, the approach decided was simply to make the positive grid shorter and to provide additional space in the cell to accommodate the anticipated growth. A positive grid mold to cast the shorter grid for the improved ABSOLYTE design is being manufactured. Adjustments to the manufacturing processes (including plate wrapping, cell stacking, and terminal lug welding) to accommodate the shorter positive grid are anticipated, and experimental efforts to establish appropriate processing instructions and specifications are being planned.

Thermal Management and Charging Profiles

Elevated temperature has a deleterious effect on the life of any lead-acid battery. In flooded electrolyte types, the reduction in life is due to the acceleration of positive grid corrosion. In VRLA batteries, in addition to the acceleration of the grid corrosion process, it is suspected that elevated operating temperatures may also induce failures due to accelerated loss of water by gassing and diffusion through the container material and the pressure relief vent valves (including the seal between the valve body and the cell). In addition to the heat

generation mechanisms associated with the operation of any battery including 1) the resistive heating effects caused during discharge, 2) the heat released due to the chemical and electrochemical reactions on charge coupled with the resistive heating effects during charge, and 3) miscellaneous heating effects from polarization and the grid corrosion reaction. VRLA batteries have one additional significant heat-generating source—the oxygen recombination reaction occurring at the negative plate during overcharge.

Heat dissipation in lead-acid cells occurs through the following methods:

- Conduction through the cell materials, particularly the lead in the grids, straps, and terminal posts and to a lesser degree through the electrolyte and separator materials, and the container and cover materials.
- Convection from the surface of the battery and its components to the surrounding air. The heat dissipated in this manner is highly dependent on the amount of surface area of the battery exposed to the air and can be increased using forced air systems. In a forced convection system, it is most beneficial if the air is directed to the hottest areas of the battery stack through baffling. The addition of fins to the surface of the battery aids convective cooling by increasing the area exposed. It is also believed that turbulent airflow is more effective than laminar airflow; however, the effects are more difficult to predict and control.

Table 3-4. Alternate Positive Grid Designs

Design Name	Advantages	Disadvantages
1. Staggered verticals	<ul style="list-style-type: none"> • No lengthy verticals • Castability 	<ul style="list-style-type: none"> • Increase in grid resistance • No change in horizontals
2. Diagonal	<ul style="list-style-type: none"> • Has proven castability 	<ul style="list-style-type: none"> • Unknown effectiveness
3. Staggered horizontals and verticals	<ul style="list-style-type: none"> • No lengthy verticals or horizontals 	<ul style="list-style-type: none"> • Increase in grid resistance • Castability reduced
4. Staggered verticals in an offset frame	<ul style="list-style-type: none"> • No lengthy verticals • No full-width horizontals 	<ul style="list-style-type: none"> • Increase in grid resistance • Castability reduced
5. Varied vertical lengths	<ul style="list-style-type: none"> • Resistance not increased • No full-length verticals • Castability 	<ul style="list-style-type: none"> • No change in horizontals

Several alternative positive grid designs were assessed to minimize the growth typically encountered as the positive grid corrodes.

- Radiation provides a fairly insignificant amount of heat dissipation from a battery, particularly if the temperature differential is small.
- Evaporative cooling results from gases venting from the battery, thus removing heat. In a flooded electrolyte battery, gassing provides a secondary benefit by a circulation effect in the electrolyte that adds internal convective cooling of the cell components. In VRLA batteries, evaporative cooling is basically nonexistent as gassing of the water in the electrolyte is intentionally avoided to prevent cell dry-out and premature failure.

Being an electrolyte-starved system, VRLA batteries have a lower heat capacity than flooded electrolyte equivalents, have no internal convection, and have an additional mechanism for heat generation, namely, the oxygen recombination reaction. Thermal management at both the cell and battery levels in large VRLA batteries for utility applications, therefore, is a necessary as well as challenging requirement.

Because charging is intimately associated with the heating effects experienced in the VRLA battery, GNB has decided to integrate the identification of optimized charging profiles with the thermal management task.

UES applications usually require that the batteries be recharged during off-peak hours, and usually limit available recharge times to less than eight hours. Additional charging restraints are imposed to limit the temperature rise in the cells to control grid corrosion and water loss and extend battery life and, in the extreme case, to prevent thermal runaway. The ideal recharge profile will minimize recharge time and temperature rise during charging while maintaining battery capacity. An additional objective is the identification of recharge parameters and optimum charge termination algorithms that can be programmed into the utility power control systems.

Test cells (75A15, 525 Ah) have been received and are completing initial conditioning cycling; and except for a unit to perform frequency control/spinning reserve testing, all of the equipment necessary to conduct baseline utility profile simulations on the current ABSOLYTE design is installed and operational. The test discharge profiles have been developed with input from the utility participants in this contract and include constant current, constant power, and various sinusoidal power profiles with durations ranging from 0.25 to 8 hr. The several discharge regimes are enumerated in Table 3-5.

Ground Fault Elimination

By their nature, utility-based battery energy storage systems will be large in capacity and operate at relatively high dc voltages. As such, ground faults could pose a serious safety risk to operators and utility personnel. Furthermore, they can lead to premature failure of a portion of the battery because all of the battery charging voltage could be borne by the cells between the ground fault point and the facility ground.

ABSOLYTE battery modules at present have cells contained in steel modules that have a baked-on, powdered polyester paint. To aid with thermal management and to achieve the desired compression on the cell plate-stack, the jars of the cell are placed in intimate contact with the walls of these steel modules. This design has performed very well and has resulted in modular racking configurations that save significant floor space in large battery installations. There have been instances, however, where electrolyte from a cell has leaked out and established a conductive path to the steel module, resulting in a ground fault. The occurrence of ground faults can almost always be traced to a manufacturing defect or user abuse. By preventing electrolyte leaks and reducing the effects of electrolyte leakage should they occur, the impact of ground faults in a BESS battery can be avoided.

GNB's technical approach is to develop cell sealing techniques that will drastically reduce the occurrence of electrolyte leaks, and to evaluate battery module constructions that will not allow a ground fault to arise even if an electrolyte leak should occur.

Electrolyte Fill Control

In an absorbed electrolyte VRLA cell such as ABSOLYTE, the electrolyte volume is computed to provide the desired capacity while being fully absorbed by the plates and the fiberglass mat separator system. An inadequate supply of electrolyte will reduce the cell's capacity; however, an excess supply of electrolyte will impair the efficiency of the recombination reaction and provide free liquid electrolyte that can leak from the cell.

A fill-by-weight method has been developed and implemented at one of GNB's manufacturing facilities to demonstrate the viability and reliability of such a system. The system automatically controls the amount of electrolyte added to each cell by measuring the difference in weight between the dry cell and the cell after the electrolyte has been added. The system is programmable to allow easy changeover between cell sizes and to make minor adjustments to enhance calibration accuracy. The system has been operational for several

Table 3-5. Thermal Management Product Characterization

Discharge Regime	Discharge (hr)	Recharge Profile	CV Voltage (VPC)	Days on Test
Constant Current	8,3,2,1	CI/CV/CI	2.25, 2.30, and 2.35	24
Sinusoidal Power, Pure	8,3,2,1	CI/CV/CI	2.35	20
Sinusoidal Power, Lagging	8,3,2,1	CI/CV/CI	2.35	20
Sinusoidal Power, Leading	8,3,2,1	CI/CV/CI	2.35	20
Constant Power	8,3,2,1	CI/CV/CI	2.35	20
Dual Peak Sin. Power, Pure	3,2,1	CI/CV/CI	2.35	20
Dual Peak Sin. Power, Lagging	3,2,1	CI/CV/CI	2.35	20
Dual Peak Sin. Power, Leading	3,2,1	CI/CV/CI	2.35	20
Sinusoidal Power, Pure	0.25, 0.5	CI/CV/CI	2.35	6
Sinusoidal Power, Lagging	0.25, 0.5	CI/CV/CI	2.35	6
Sinusoidal Power, Leading	0.25, 0.5	CI/CV/CI	2.35	6
Constant Power	0.25, 0.5	CI/CV/CI	2.35	6
Dual Peak Sin. Power, Pure	0.25, 0.5	CI/CV/CI	2.35	6
Dual Peak Sin. Power, Lagging	0.25, 0.5	CI/CV/CI	2.35	6
Dual Peak Sin. Power, Leading	0.25, 0.5	CI/CV/CI	2.35	6

A test plan to evaluate VRLA batteries under utility load profiles has been developed.

All tests will monitor cell voltage, float current, temperature, cell pressure, time, and power.

Notes:

- * Initial CI charge step will be at 18 A/100 Ah; finishing CI step will be at 2 A/100 Ah.
- * All discharges will be calculated to achieve 80% DOD except the second discharge for the dual discharge which will be at 50% DOD.
- * All sine wave testing will be done using a stepped power approximated waveform with 30 steps.

months, during which time factory rejects due to excess electrolyte fill have been virtually eliminated. The capability of the fill-by-weight system is shown in Table 3-6; the 6-sigma value (± 3 -sigma) for the process is less than 2.5% of the target fill weight. The process on average fills each cell to within greater than 99.5% of the target fill weight.

This effort is deemed to have been completed.

Heat Seal Improvements

The cover-to-jar seal in the ABSOLYTE design is made by a heat-sealing method that bonds the plastic cover to the thin-wall plastic jar. In the process, a bead of plastic forms at the joint between the cover and the jar. To ensure a tight fit and for cosmetic reasons, this bead was being removed by a trimming operation. This trimming process, it was discovered, sometimes ex-

posed porosity in the plastic weld bead that, in turn, gave rise to electrolyte leaks and subsequent ground faults.

A second step taken to ensure the leak-tightness of a VRLA cell to be used in a utility BESS application was to implement a bead smoothing machine that melts and smooths the heat seal bead against the cover-to-jar seal rather than cutting it away. The shape of the smoothed bead was developed as shown in Figure 3-10 to allow cells to be fitted tightly into the battery tray module without interfering either with other cells in the module or with the module wall itself. With the bead smoothing operation and using an ultra-sensitive leak detection technique (described later in this section), a leak rate of 4% for cells having the manually trimmed heat seal bead was reduced to 0% among a group of 300 sampled cells.

This effort is deemed to have been completed.

Table 3-6. Results of ABSOLYTE II Automatic Electrolyte Fill by Weight Study

Filler Number	Battery Dry Wt. (g)	Battery Filled Wt. (g)	Electrolyte Weight (g)	Var. From Target (%)
1	14480	18400	3920	0.15
2	14545	18475	3930	0.18
3	14665	18625	3960	0.19
4	14420	18365	3945	-0.02
5	14635	18590	3955	0.18
6	14580	18525	3945	0.16
7	14650	18570	3920	0.35
8	14460	18430	3970	-0.08
9	14680	18610	3930	0.34
10	14670	18645	3975	0.14
11	14510	18460	3950	0.06
12	14410	18360	3950	-0.06
13	14510	18465	3955	0.04
14	14565	18490	3925	0.23
15	14485	18435	3950	0.03
16	14855	18775	3920	0.58
17	14605	18545	3940	0.21
18	14620	18545	3925	0.29
19	14440	18375	3935	0.04
20	14430	18370	3940	0.01
21	14550	18475	3925	0.21

A fill-by-weight process was implemented to increase the accuracy and consistency of electrolyte filling. The equipment is capable of filling a VRLA cell to better than 1% of the specified value.

Leak Detection Improvements

Improved processes, such as the fill-by-weight and heat seal bead-smoothing technique, described above will improve the reliability of VRLA cells to meet the high standards for utility BESS operation; however, it is necessary to verify that these processes remain in control and continue to produce leak-tight cells. Initially the seal integrity of GNB's ABSOLYTE cells was 100% tested by applying an air pressure of 30 psi and observing pressure decay over time using an accurate pressure gauge. With time, it was determined that this method was accurate in identifying cells only with very large leaks. A more rigorous leak test method was then instituted in which each cell was subjected to the air

pressure test while submerged in water. The production operator conducting this test could identify leaks not only at the cover-to-jar seal but also at the terminal bushing seals by looking for a stream of bubbles originating from the leak site. Even with this improvement to the inspection test, cell leakage was being identified in the field after installation and operation of the battery for several years. Historical information indicates that during the first three years of operation of a battery, the identification of new cell leaks occurs at a rate of approximately 0.05%/yr and that by the fourth year of operation for a battery the incidence rate for identifying new leaks has dropped to 0.01%. Overall, we estimated that during the 20-yr lifetime of the battery, and despite having passed a rigorous air pressure

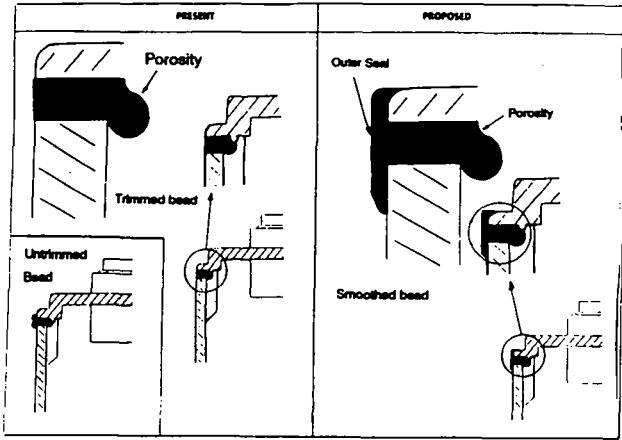


Figure 3-10. Bead Smoothing Process. This process seals porosity in the heat seal bead formed when joining the cover to the jar. The process that trimmed this bead by cutting sometimes exposed “micro” holes through which electrolyte could leak.

test during manufacture, 0.2% of the cells would develop an electrolyte leak that could create a ground fault condition.

The technical approach taken in this task assumed that the leaks that sometimes appeared several years after installation and start of operation of the VRLA battery were present during manufacture but were undetectable using the methods employed to test for leaks. These “micro” leaks existed, however, and over time the electrolyte slowly worked its way out through these leaks. A technique having a higher degree of detection capability is required to identify these “micro” leaks.

It was calculated that sulfuric acid cannot wet openings 1 micron or less in size. Furthermore, the calculated flow rate of a test gas through a 1 micron opening is 0.0001 cc/sec. A leak detection device that uses the test gas and a mass spectrometer detection system was identified as being capable. The levels of detection at-

tainable using such a device are compared to that achievable using an air pressure test in Table 3-7. Clearly such a device can detect leak rates several orders of magnitude lower than those that could result in an electrolyte leak path.

One of these leak detection systems was installed at GNB’s Fort Smith manufacturing facility and made operational. A test gas flow rate of up to 0.00001 cc/sec has been established as the acceptance rate for cells. Any cell tested that exhibits a test gas flow rate greater than this limit is subjected to an underwater pressure test to locate the leak; appropriate repairs are made and the cell retested to demonstrate compliance with the acceptance criteria.

Prior to any of the seal improvement approaches discussed in this section, the initial in-plant cell leak detection rate using the air pressure test under water was 1.2%; the detection rate increased to 7.5% with the introduction of the special gas leak detection equipment. The process improvements that were introduced as the result of this developmental task (namely, electrolyte fill-by-weight and heat seal bead smoothing) were obvious, and the current in-plant cell leak detection rate using the ultrasensitive gas flow detection system is now running at 0.35%. These improvements in process and detection have made great strides to increase system reliability of VRLA batteries in utility BESS applications.

The effort in improving the electrolyte-filling, heat-sealing, and leak-detection processes for VRLA cells has been completed.

Battery Tray Modifications

The trays that house VRLA cells in a battery installation are typically made of steel and are coated with a powdered polyester paint to provide corrosion resis-

Table 3-7. Capabilities of Leak Test Methods

Method	Detection Limit (cc/sec)
Air-Pressurized Bubble Test	2×10^{-4}
Special Gas-Pressurized Bubble Test	1×10^{-4}
Special Gas Accumulation Test	1×10^{-6}
Vacuum/Special Gas Tracer Test	1×10^{-9}

Various leak detection methods were assessed to identify a manufacturing test to assure that VRLA cells are leak-tight. Sulfuric acid cannot leak through a hole 1 micron or less in size; the flow rate of a test gas through a 1 micron hole is .001 cc/sec.

tance and to insulate the cells from the tray. This coating can be attacked if sulfuric acid should leak from the cell, leading to the development of a ground fault. In addition, tray corrosion is unsightly and undesirable. The technical approach to this task is to evaluate more protective coatings and alternative materials from which the tray could be fabricated to prevent the occurrence of ground faults.

A more stable and corrosion-resistant tray coating has been identified—an electrostatically applied epoxy coating. This “E-Coat” is superior to the present paint in salt fog tests. Coated steel coupons have been reported to survive ten times longer than painted coupons. Salt fog tests conducted on steel ABSOLYTE battery trays showed painted trays failing in less than 48 hr, whereas the E-Coated trays showed no visible signs of attack when the tests were terminated after 100 hr. The cost of this coating, however, is significantly greater than the polyester paint and goes against the overall objective to obtain a lower cost battery system for the BESS application. The E-coat finish is only available in a black color. GNB feels that the improvements made in the electrolyte filling, cell sealing and leak detection processes could reduce the importance of an improved coating to prevent ground faults.

Other tray materials are being investigated not only to resist corrosion and ground faults but also to aid in thermal management and to reduce the overall weight of a BESS installation. Aluminum has 4.3 times greater thermal conductivity than steel. Despite the fact that an aluminum section must be 44% thicker to achieve the same strength as steel, the heat transfer from an aluminum tray will be approximately three times (i.e., $4.3/1.44=3$) better than from a steel tray. The weight of an aluminum tray would be only about one-third that of a steel tray. Once again, the technical benefits of installing the VRLA cells into an aluminum tray must be weighed against the added cost. Although fabrication costs for steel and aluminum are approximately equal, aluminum stock material costs about five times more than steel and could increase the cost of the battery tray by as much as 30% over the current steel assembly. Prototype aluminum trays are being fabricated so that the thermal benefits can be quantified and compared with the standard steel configuration. It is expected that fabrication and coating of these trays will be completed during October 1992.

A nonmetallic tray is also being pursued for its acid resistance and high dielectric strength (over 500 V/mil). Thermal conductivity deficiencies will have to be overcome by incorporating a suitable hole pattern in the tray walls to allow convective heat transfer. Although ground faults can be virtually eliminated using a non-

metallic tray, the tray walls will have to be nearly double in thickness to achieve the same strength as steel. Like the aluminum tray, a reinforced plastic tray will weigh only about 38% that of the steel tray. GNB is having prototype glass-reinforced, flame retardant, polyolefin trays fabricated in a proof of concept effort to evaluate the convective heat transfer and structural integrity characteristics of a nonmetallic battery tray. Prototype plastic trays are expected to be completed during October 1992.

Plate Pasting Process Control

A principal source of variability in the performance of lead-acid batteries is the thickness of active material and density in the plates used in the cell. In addition to the variation in total active material available, variations in plate thickness in VRLA cells can lead to non-uniform compression of the absorbent glass mat separator within the plate pack of the cell. Too little compression will result in high cell resistance and low capacity; too much compression will result in separator saturation, which will reduce the efficiency of the oxygen recombination cycle. Variation in cell-to-cell performance in battery systems that have a thousand or more series and/or parallel connected cells, typical in utility load/power management applications, can result in the lower capacity cells being reversed on discharge. Such reverse charge conditions can cause irreversible damage to the cell.

Plate thickness and weight control are being sought through the use of a “fixed orifice paster” (FOP). The FOPs have been in use in the manufacture of automotive batteries for several years, but have never been successfully used in the pasting of the larger and thicker industrial battery plates that would be utilized in the manufacture of VRLA batteries for utility BESS application. In the FOP, the size of the orifice determines the thickness of the pasted plate, and paste is evenly applied to both sides of the grid as it travels through the orifice.

A FOP was acquired by GNB and installed at GNB’s Fort Smith manufacturing facility, and equipment debugging was started. The initial pasting runs demonstrated the improved control of plate thickness and plate weight that the FOP provided in comparison with the standard belt type pasting equipment. These comparison data are provided in Table 3-8 and show that the FOP provides almost four times better plate thickness control and 2.5 times better weight control than the standard belt pasting system.

In spite of an intensive debugging effort by engineering and manufacturing personnel and several

**Table 3-8. Pasted Plate Improvement
Comparison of Belt Paster and FOP**

	Belt (%)	FOP (%)
A. Plate Thickness		
• Standard Dev.	3.7	1.0
• 3 Sigma Range	22.2	6.0
B. Plate Weight (DRY)		
• Standard Dev.	1.8	0.7
• 3 Sigma Range	10.8	4.2

A FOP has significantly greater control over pasted plate weight and thickness than a belt-type paster. The FOP system, however, requires greater maintenance than a belt paster, and FOP-produced plates have unacceptable levels of cracks and voids.

modifications to the equipment, the machine has not proven reliable or "user friendly" in a production environment. Irreconcilable problems with obtaining a dried pasted plate free of voids and cracks, which unfavorably impact cell high rate discharge performance, and maintenance and operational issues associated with the equipment itself have caused GNB to abandon the fixed orifice paster as a viable manufacturing process within the time frame of this project. It has been decided that subsequent active material and pasting efforts within the time frame of this contract be conducted using a belt-type pasting system.

Positive Active Material

The positive electrode active material has a significant effect in determining the life of a lead-acid battery. The positive plate in a lead-acid battery is considered to be the "workhorse" plate because the positive active material undergoes much greater crystal structure and morphology changes than the negative active materials during discharge/charge cycling. In addition, the anodic electrochemical potentials at the positive plate cause corrosion of the positive grid alloy.

The precursor lead oxide from which the lead dioxide positive active materials are formed can affect the life and capacity characteristics of the positive plate. Fine particle oxides provide high utilization/high capacity plates; coarse particle oxides provide greater lifetime, but normally with lower initial capacity. The objective of this subtask is to increase the cycle life of ABSOLYTE batteries by forming a positive plate using an alternate precursor oxide.

The starting oxide in the current ABSOLYTE designs is a red lead/lead monoxide (Pb_3O_4/PbO) mixture that reduces the energy required for plate curing and electrochemical formation, and yields post-formed cells having initial discharge capacities of greater than 90% of rating. GNB currently uses leady oxide, a lead monoxide containing approximately 25% unreacted "free" lead in some flooded lead-acid and small (less than 100 Ah) VRLA batteries. More energy intensive curing and formation processing are required for plates made with this oxide. The resultant cells, however, do achieve increased cycle lifetimes due to the stronger positive active material developed by this oxide and its processing steps. GNB's approach is to modify leady oxide paste formulations, curing profiles and formation regimes to provide a positive plate which can be used in a VRLA construction with improved cycle life capabilities. Plates will be characterized at each process step with respect to composition, crystal structure, porosimetry data, and surface area; electrical characterization will include capacity/rate determination, deep discharge cycling, float charge, Tafel overcharge relationship, open circuit storage, and cell reversal. Upon successful validation, the best combination of material formulation and processing will be incorporated into the ABSOLYTE designs to achieve the long cycle lifetimes required for utility applications.

The leady oxide positive active material development task was to utilize the improved pasting capabilities derived from the fixed-orifice pasting equipment. Start of work on this specific subtask was held up until the FOP became fully operational. Because of the difficulties encountered in the start-up of the FOP and the subsequent decision to discontinue the implementation of it within the time frame of this project, GNB will

begin the experimental work related to the development of the lead oxide positive active material using a belt-type pasting process to produce the plates. This effort will begin during October 1992.

Task 1. Phase 2: VRLA Battery Advancements

Cell Design

This subtask consists of two parts: an intermediate cell design that is evolutionary in nature and seeks to increase the 8-hr capacity of the existing ABSOLYTE cells, and an advanced design that is revolutionary in design and seeks to maximize the short power capability of VRLA cells for utility power regulation applications.

Intermediate Design (ABSOLYTE PLUS)

The 8-hr rated capacity of ABSOLYTE II cells can be increased as much as 17% by a re-optimization of the quantity of active materials provided in the cell. Although the volume of the cell remains the same and the weight actually increases slightly, the improvement in deliverable capacity still increases the overall specific energy (Wh/kg) and the energy density (Wh/l) of the cell.

A group of 30 test cells representing six different ABSOLYTE sizes containing the re-optimized active materials balance was fabricated and placed on test to determine performance improvements. A typical com-

parison of the intermediate design cell compared to the same physical size ABSOLYTE II cell at several discharge rates is provided in Table 3-9. Although the measured improvements were as much as 50% greater at specific discharge rates, the 17% capacity improvement between current and intermediate designs is a realistic estimate that allows for manufacturing variations and early life aging effects. Testing of the prototype cells is continuing to develop Peukert's plots, which compare discharge runtime as a function of the discharge rate (current).

Advanced Design (LSB)

Present ABSOLYTE batteries are designed to provide sustained long duration discharges typical of energy storage applications. These batteries do offer significant reductions in battery footprint, space, and weight when compared to conventional flooded electrolyte lead-acid batteries. Yet, with a battery optimized for high-power applications, even greater savings in battery footprint, space, and weight can be achieved for power regulation applications. The advanced design battery has this as its objective.

High-power applications require batteries that have very low internal resistance. Accordingly, the advanced design battery seeks to reduce the resistance of all cell components so that the total cell resistance is decreased. The battery components that were subject to analysis and improvement as part of the advanced battery design effort include the intercell connectors, terminals, plate straps, lugs, grids, active material, and the electrolyte-separator system. GNB completed the development of

**Table 3-9. Performance Comparison
Intermediate Design vs Current Design**

Discharge Current (A)	Cut-Off Voltage	Support Time (hr)		% Improvement
		Current Design (ABSOLYTE II) 75A-13* Rating	Intermediate Design (ABSOLYTE PLUS) 88A-13* Data	
50	1.88	8	10.00	25.0
80	1.75	6	6.75	12.5
115	1.90	2	3.00	50.0
300	1.75	0.8	1.10	37.5

The performance of the current ABSOLYTE VRLA design can be improved by a readjustment of the active materials in the cell. Preliminary data indicate that capacity delivered can be increased 12 to 17% at all discharge rates.

* Designates model number from GNB product line.

such an advanced design battery optimized for short duration, high power applications (frequency control and spinning reserve, for example) under an IR&D program. Implementation of this advanced design is being carried out under this contract with SNL.

The GNB advanced design cell uses a sleeve as the jar and two covers (one at each end of the sleeve) to form the cell container. The covers are sealed to the jar (sleeve) by a heat-sealing process. The cell terminals are at opposite ends, one through each of the two covers. Positive and negative straps are molded into their respective covers. When the jar-to-cover seal is made, the plate lugs fit into pre-made slots in the strap. The plate lugs are subsequently fused to the strap using an inert gas welding process. In the design, the bond between the plate lugs and the terminal strap is both the current conducting path and the electrolyte/gas seal.

The initial implementation efforts for this design centered on the development of the FOP to provide plates with little variation in weight and thickness. The first prototype cells fabricated delivered the predicted low-rate (C/20) discharge performance, but failed to deliver adequate run times on the high-rate constant power discharge tests. Several more pasting and formation runs were conducted to improve the high rate performance, but results, although somewhat improved, still fell short of expectations for the design. The voltage of the prototype cells when discharged under high-rate constant power conditions dropped significantly lower than that expected of the design (Figure 3-11) indicating that a high-resistance component exists

within the fabricated cell. GNB suspects that this high resistance resides in the pasted plates used in these prototype cells. Grid design modifications and further experimentation with paste formulation and the pasting process are planned for the first quarter of FY93.

Copper Negative Grid

Historically, lead has been used as the grid material for the negative plate grid. The principal considerations in the selection of a lead alloy, or for that matter any material, to be used as the negative plate grid are over-potential characteristics and strength; corrosion resistance is not a major consideration. Lead is a poor electrical conductor, and other materials, copper for example, with higher conductivities could improve the high-rate discharge performance of the lead-acid battery. Although the copper substrate would have to be coated with lead to provide chemical corrosion resistance, the lead-coated copper grid would still significantly lower the cell's internal resistance, increase energy density, improve charge acceptance, achieve a more uniform current distribution over the length of the plate, reduce polarization, and improve active material utilization.

Copper is an ideal candidate as a negative grid substrate because it is an excellent conductor, is readily available, and can be worked and fabricated into forms that can be used in a battery configuration. Copper has a specific electrical resistance 1/12 that of lead, and when compared on a per-weight basis, the electrical resistance is less than 1/16 that of lead. Thus, cells incorporating lead-plated copper negative grids should have considerably better performance, especially at high discharge rates.

One risk of incorporating copper into a lead-acid cell, however, is the possibility of contamination. Copper is a known contaminant, and the deleterious effects of copper on the performance of lead-acid batteries are well known. The rate of self-discharge of a lead-acid cell is greatly accelerated by the presence of copper in the electrolyte. A crucial technical aspect of any effort to incorporate a lead-coated copper grid in a lead-acid cell is to ensure the integrity and porosity-free nature of the lead coating. GNB is aware of two processes under development to fabricate negative grids containing a copper substrate. Hagen Batteries AG (West Germany) has a commercially available copper-stretch-metal (CSM) process that is very similar to expanded lead grids used in the manufacture of automotive batteries. GNB has licensed this technology from Hagen for use in flooded electrolyte batteries. The second process is a co-extruded wire technology that forms a dense and virtually pore-free coating of lead around the copper

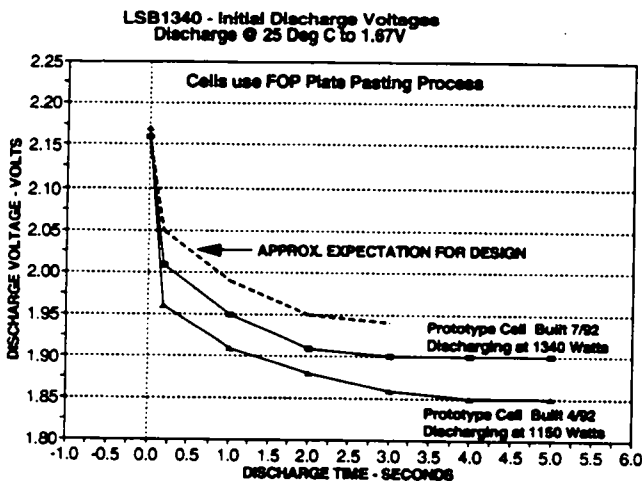


Figure 3-11. Initial High Rate Discharge Testing of the Advanced Design (LSB) VRLA. A greater than expected voltage drop was exhibited. Modifications to the grid design and improved active material to grid contact are expected to improve high-rate voltage hold up.

wire core. A grid structure then is fabricated by either weaving the wire or assembling it into a plastic or lead frame.

At this point in the contract effort, no activity has taken place on this project. It is planned, however, that GNB will evaluate these concepts to determine performance improvements as well as to assess the potential risks from contamination by the inclusion of a copper-based negative grid into a VRLA cell.

Positive Plate Design

Three of the most basic factors that limit a lead-acid cell's cycle-life and float life are positive grid corrosion, damaging changes in the positive active material (PAM) structure, and the formation of passivating films at the PAM-to-grid interface. Additionally, modifications to the positive paste to produce increased PAM utilization almost invariably cause reductions in cycle life. This project explores changes in positive grid alloy to lower positive grid corrosion, and the potential benefits of PAM additives to improve PAM stability and utilization.

Positive Grid Alloys

Selection of a positive grid alloy requires evaluation of corrosion resistance, grid growth, tensile strength, and gassing characteristics, as well as its behavior in a cell to establish cycle and float performance and oxygen recombination efficiency when used in a VRLA design. Several experimental grid alloys mentioned in the literature and conceived by GNB's technical staff are being evaluated in comparison to the MFX alloy currently used in the ABSOLYTE design. Results from the grid corrosion tests showed lower corrosion rates than the MFX alloy control, but also showed greater grid growth than the MFX alloy in three of the four experimental alloys (Figures 3-12 and 3-13). This behavior suggests that grid strength may be too low and might adversely affect processing and hence cell life. The alloys were subjected to tensile testing and a review of the data showed no correlation between ultimate tensile and grid growth as shown in Figure 3-14. Additional alloy variations were tested, but no alloy composition tested provided any significant improvement in strength.

Test cells using alloys AD-1 through AD-4 and the MFX control were placed on a float charge regime to establish appropriate recombination behavior, a critical factor for VRLA cells. Cycle and float life testing will

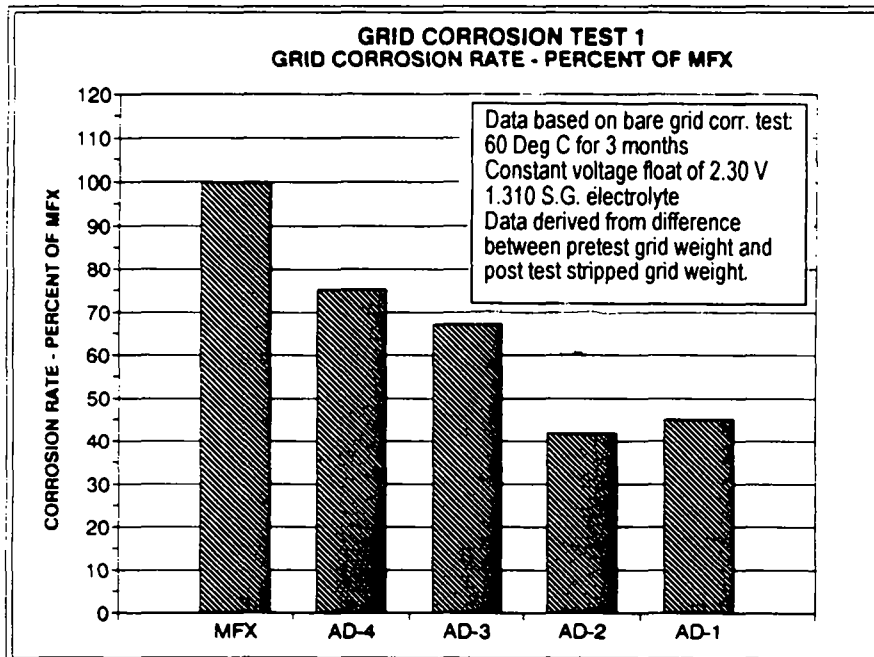


Figure 3-12. Several Grid Alloy Compositions. These compositions were tested to identify an alloy with better corrosion resistance than the MFX alloy currently used in the ABSOLYTE design. The charts show some alloys with excellent corrosion resistance.

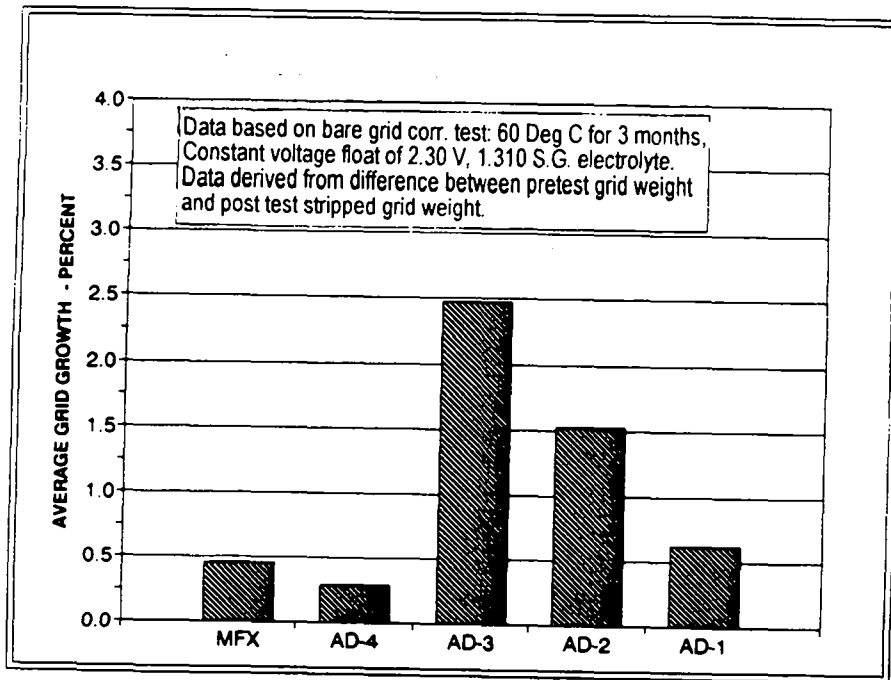


Figure 3-13. Grid Corrosion Test, Grid Growth. The same alloys that demonstrate excellent corrosion resistance either exhibit about the same or greater growth resulting from corrosion. Excessive grid growth can cause loss of capacity and case deformation.

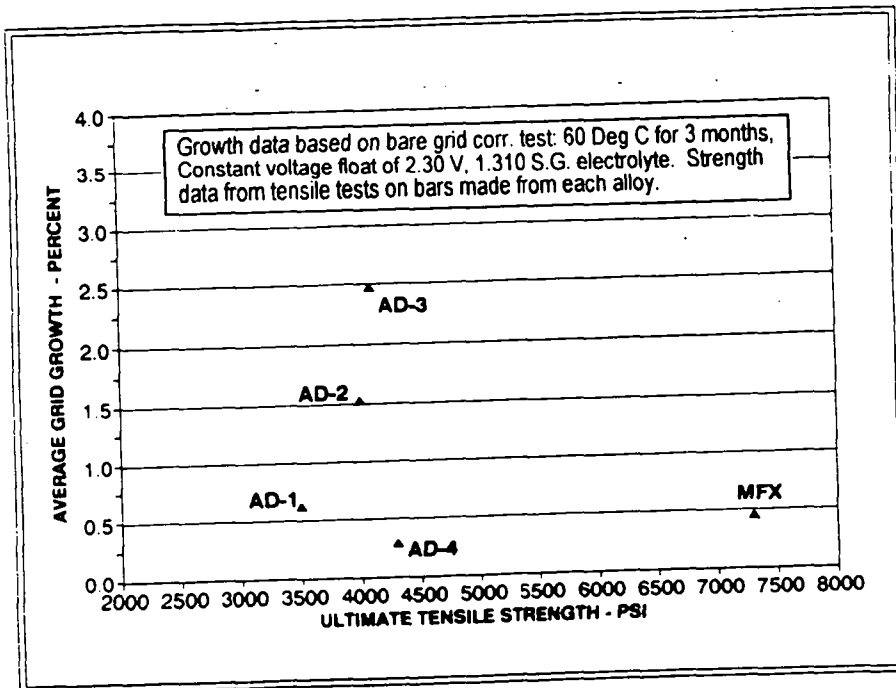


Figure 3-14. Grid Corrosion Test, Grid Growth vs Ult. Tensile Strength. Unexpectedly, there was no correlation between the observed grid growth during corrosion and the tensile strength of the alloy metal. Alloy evaluation requires both mechanical characterization and corrosion characterization.

commence once the recombination behavior has been established.

Plate Additives

The purpose of a plate additive is to help stabilize the PAM structure during cycling. A stabilized structure will allow an increase in plate porosity and, therefore, permit an increase in active material utilization without sacrificing cycle life. The approach that GNB is taking assumes that the incorporation of materials whose crystal structures are isomorphous with beta lead dioxide (i.e., identical crystal structure with similar lattice dimensions) will act as nucleating sites for lead dioxide formation during charging. In essence, the additive should behave as a beta lead dioxide particle size regulator that will help the PAM maintain surface area, porosity, and pore size. Examples of possible materials include tin, titanium, and ruthenium dioxides; additionally, one natural form of silicon dioxide has this structure. The lattice parameters for these materials are provided in Figure 3-15.

A compilation has been made of the electrical resistivities for several materials proposed as additives to

lead-acid cells (Table 3-10). This information shows that almost all potential additives should increase the electrical resistance of the fully formed PAM; however, some additives may lower the resistance of the unformed positive material, leading to higher formation efficiency. Also, some additives may help relieve mass isolation by providing conductive bridges to the current collector network and help stabilize low-rate cycling capacity. If the conductive additive is isomorphous with beta lead dioxide, it may indirectly lower the PAM's resistance by causing an increase in the particle-to-particle contact area in the PAM structure. Among conductive materials, only some conductive oxides and vitreous carbon remain stable in the PAM during charging. Carbon blacks, graphites, and unmodified "Buckminster Fullerenes" all oxidize in the positive during formation or charging. The resistivity data indicate that only ruthenium dioxide may directly help PAM conductivity, but its comparatively low oxygen overvoltage, high cost, and toxicity impair its acceptability as an additive.

Almost all organic materials eventually decompose when left in contact with the positive active material during charging. This instability limits the PAM binder

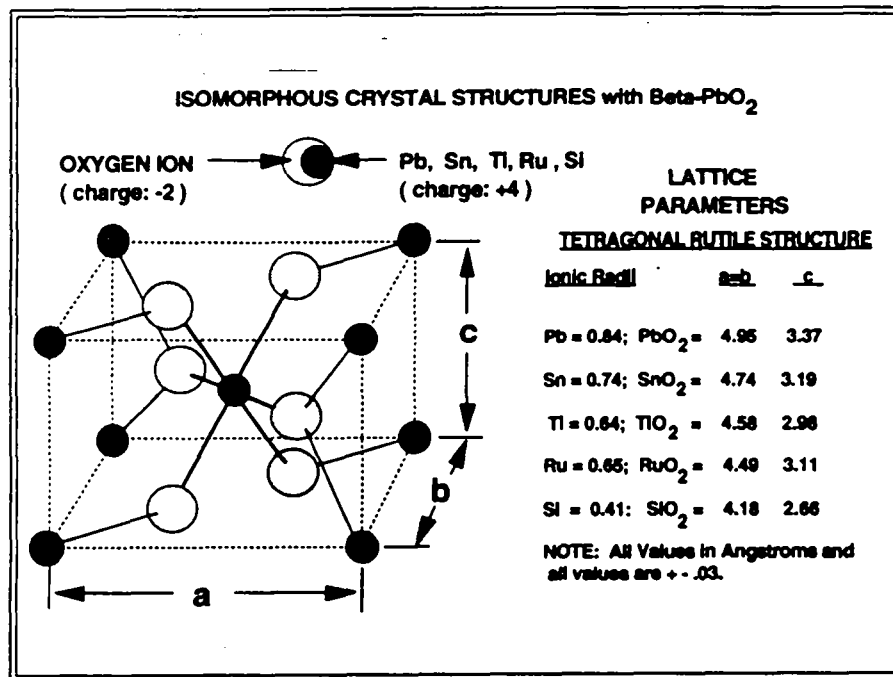


Figure 3-15. Positive Plate (Alloys/Paste Additives). Additives that may potentially stabilize the positive electrode active material structure should have a lattice structure similar to PbO₂. Examples of compounds that meet this criterion are shown.

Table 3-10. Comparison of Material Resistivities

Material		Resistivity, $\mu\Omega/\text{cm}$ (20°C)		
		Typical	Range	
Copper	Cu	1.7	1.68	1.72
Aluminum	Al	2.7	2.65	2.80
Titanium Oxide (Derivative)	TiO ₂	4.0	3	1000
Cadmium	Cd	7.2	6.8	7.6
Nickel	Ni	6.8	6.8	9.5
Tin	Sn	11	11.0	11.5
Solder (67/33)	Pb/Sn	16	NA	NA
Lead	Pb	21	20.6	22.0
Ruthenium Dioxide	RuO ₂	40	30	300
Antimony	Sb	40	39.0	41.7
316 Stainless Steel	Fe/Cr/Ni	72	NA	NA
Mercury	Hg	96	95.8	98
Lead Dioxide	PbO ₂	100	92	300
Bismuth	Bi	110	107	120
Neg. Pellet	Pb (Sponge)	183	NA	NA
Pos. Pellet	PbO ₂ (PAM)	2,130	1,000	7,400
Carbon (Graphite)	C	1,375	800	1,400
Tin Dioxide (Doped)	SnO ₂ (Doped,Sb,F)	700	500	20,000
Tin Dioxide	SnO ₂ (Natural)	Var	45,000	1E+12
Titanium Dioxide (Doped)	TiO ₂ (Doped,Ta)	100,000	NA	NA
Carbon Blacks	C	100,000	NA	NA
Sulfuric Acid (30.6%)	H ₂ SO ₄ (Aqueous)	1,300,000	NA	NA
Carbon (Diamond)	C	270,000,000	NA	NA
Titanium Dioxide	TiO ₂	Var	2,900E+6	91,000E+6
Plastics	Pe, PVC, Polystyrenes	Var	1E+13	1E+22
Lead Monoxides	PbO	Var	1E+14	1E+22
Silicon Dioxide	SiO ₂	1E+20	NA	NA
Polytetra fluoroethylene	PTFE	1E+22	NA	NA

Various materials are potential candidates as additives to a lead-acid cell. These materials and their resistivities are listed.

options. Further, the true densities of most plastics versus lead dioxide force a disproportionate volumetric displacement in the PAM. For example, a one-weight percent substitution of polyester fibers for lead dioxide in the positive pellet represents about a seven weight percent removal of lead dioxide. If porosity remains constant, the PAM utilization must increase about 2% for the plate to deliver the same Ah capacity. Since the binder adds nothing to plate conductivity and does not increase porosity, a 2% increase in PAM utilization becomes highly unlikely. Among plastics, the relatively high density of fluorocarbon materials (PTFE, PVDF) and their stability make them good candidates as a binder additive. According to the literature, the optimum PTFE paste loading is in the range from 0.05% weight percent to about 0.3 weight percent.

Preliminary selection of material types for incorporation in cell builds has been made and will include at least one cell lot of each of the following material types: tin oxides, fluorocarbons, and a titanium dioxide derivative. Determination of the additive levels and the method of their incorporation into the positive paste will be finalized in the fourth quarter, 1992.

Electrolyte Immobilization

The present ABSOLYTE design contains an absorbent glass mat that serves as a plate separator as well as the means of electrolyte immobilization. By and large, this glass mat has worked very well; however, there are some disadvantages. The most important disadvantage is material cost, which is the primary reason for the higher cost of VRLA cells. Another limitation is the wicking height of the glass mat, which limits cell height, as installed, to 24 in. or less. This task is investigating lower cost alternatives to the existing fiberglass mat separator used in VRLA cells. Also, improvements in electrolyte distribution are being sought that will improve "wicking height" and/or provide regions for oxygen recombination even when the cell element is essentially flooded with electrolyte. The investigations will involve the evaluation of vendor-supplied separator samples and performance testing of cells containing materials that pass the initial screening tests.

The approach to achieve a low cost material is to develop a composite plastic low fiberglass content material. The earliest samples provided, when assembled into test cells, failed due to electrolyte stratification that correlated with a low wicking height. Since then, only materials that exhibit acceptable wicking heights are even being considered for additional cell testing. To date, the separator supplier has completed two materials iterations, and a slight improvement in wicking height capability has been observed, but not

sufficient to compare with the current all-fiberglass material. In addition, the supplier has been requested to test the oxidation resistance of any non-glass materials to prove that the organic components will not suffer excessive degradation when the separator is in contact with the cell's positive plates. Additional samples are anticipated from the separator supplier with improved wicking capabilities.

Manufacturing Processes

Manufacturing labor (direct) constitutes less than 10% of the cost to manufacture a lead-acid cell. A major contributor to cell costs is factory overhead, which is allocated on the basis of direct labor. Overhead allocation can be reduced by reducing direct labor; but overhead itself can be decreased by increasing throughput and achieving a high degree of process efficiency and control. A critical process in the fabrication of VRLA cells is welding of the terminal post/bushing seal. Improved quality of this process is evidenced by better conductivity through the terminal weld and fewer cases of leakage paths at the burn interface as identified using the gas leak detection system discussed previously.

The approach of this task is to evaluate automated terminal welding techniques to improve quality and increase production throughput. Two methods were studied: an induction heated post terminal fusion (IHPTF) method and a tungsten inert gas (TIG) method. The studies showed that thermal control could not be maintained using the IHPTF method, and therefore, the TIG method was selected to be implemented into production. The equipment was procured in the second quarter of 1992, and process development and equipment debugging were initiated. The work identified required changes to both the equipment and the terminal parts. The adaptation of this equipment to the current ABSOLYTE product has been completed and has demonstrated improvements in both quality of the terminal bond and seal integrity.

Task 2. Baseline Design and Economics Study

In addition to the effort to improve battery performance, GNB has also teamed with PG&E and PREPA to develop the requirements for the battery system and to conduct the economic analysis of battery storage applications in utility networks using existing and advanced lead-acid battery designs.

The host utility participation is being coordinated through UMR. UMR is conducting the baseline conceptual designs of the battery systems to meet each of the

host utility application requirements. The designs developed by UMR would be used in performing the economic analysis for each host utility. PG&E intends to use the battery at substation sites, where the battery would shave the peak from the substation feeder during peak demand periods. This mode of operation extends the life of the substation transformer as well as contributing to reducing the overall utility system peak.

PREPA is interested in battery storage for system frequency regulation and spinning reserve. PREPA is currently installing the first of several 20-MW batteries that will eventually meet their network requirements. Their participation in the GNB contract as a host utility demonstrates their interest in using advanced lead-acid battery technology for subsequent battery installations.

Specifications and Design Requirements

The BESS, in particular the VRLA battery and the PCS, must be specified considering the uniqueness of each application. Specific features of the application will impact performance and design characteristics of the equipment required. In fact, the application itself may require further definition or optimization before specifying the battery equipment. The two host utilities have individual and differing battery system requirements.

PG&E's objective is to evaluate battery storage technology as an option for distributed storage. The design specification is not unique to a particular site; but rather, it is a broad specification that would be applicable, with a minimal amount of redesign, to a large number of locations within PG&E's distribution system. The BESS is planned to be a modularized, standardized design, capable of meeting storage requirements on a wide variety of distribution feeders. In order to allow the distribution planners the greatest flexibility, the design will take a modular approach with regard to both the battery and the PCS to accommodate varying power and energy needs to each site.

For the purpose of this specification, the unit battery is defined as a group of cells interconnected to provide a 544-kW dc output for 2 hr at the end of the battery's useful lifetime. The unit PCS is defined as having a nominal rating of 500 kVA. Several of the unit batteries may be paralleled on the dc side of the converter so that the nominal power rating could be achieved for a longer period of time. Using this approach, the base unit (i.e., one unit battery and one unit PCS) will have a nominal rating of 500 kVA for 2 hr.

The preliminary design analysis and specification for this modularized VRLA battery storage plant for PG&E has been prepared by, in conjunction with PG&E,

the Electrical Engineering Department of the UMR and is incorporated in this report.

The PREPA application is spinning reserve (SR) and area regulation (AR). In the case of SR, sizing of the battery is straightforward, given the required discharge time and the power level. To properly size a battery for the AR application, a typical power profile is required. The PREPA specifications for a "Rapid Reserve Battery" have been recently provided to the UMR and will be used to begin the development of a model to size a VRLA battery for this application scenario.

Baseline Conceptual Designs

To quantify the economic benefits of the ABSOLYTE battery system in selected utility applications, it is necessary to perform a conceptual level design of the entire battery facility and to develop facility costs based on that design. A lead-acid BESS is conceptually simple in its design, but requires careful attention to the major equipment interfaces, as well as proper selection of the battery and the PCS for the intended application. Standardized designs for energy storage battery systems do not exist. The major components that must be addressed in the conceptual design are the battery, the PCS, and the BOP.

The battery subsystem includes the individual ABSOLYTE battery cells, connections between the cells, cell support racks and/or module containers, instrumentation, and other accessories as required. The battery subsystem design is an iterative selection of cell size, number of cells, and the number of paralleled strings to obtain the required capacity and voltage. The discharge rate and capacity are determined by the system specification as discussed in the previous subsection. Battery voltage depends on the anticipated power level for the plant and compatibility with existing PCS equipment and dc switchgear. The voltage will be maximized and the number of parallel strings minimized to reduce cost and complexity of the dc switchgear. GNB will provide battery pricing information for the battery subsystem selected through this iterative design process. The layout of the battery subsystem will maximize energy footprint (ft²) while meeting maintenance and safety code requirements and structural constraints.

The PCS interfaces the dc battery to the ac utility system and controls the charge and discharge of the battery following a control signal that sets power level and direction of power flow. This signal can be preprogrammed in the facility control system or may be initiated by the utility system dispatcher. Suitable PCS equipment is available from a number of suppliers but

must be custom-designed for the application. Specific PCS requirements will be determined in cooperation with the utility and will consider other factors, including power quality, black start capability, response time, and efficiency and reliability. Despite being custom fabricated, reasonably accurate estimates of cost are available, since a sufficient number of orders for similar equipment have now been processed by several of these suppliers.

In a fully operational plant, the battery and the PCS are augmented by the civil, structural, mechanical, and electrical support systems making up the BOP. These include a building, thermal management systems (HVAC), instrumentation, safety systems, auxiliary power systems, and other auxiliary equipment. Experience gained in the design of battery plants for the San Diego Trolley Project and the Chino Battery Energy Storage Project will be utilized to estimate the BOP for a utility VRLA battery storage plant. The experience with the San Diego Trolley Project will be especially valuable, as this project also utilizes a VRLA battery.

Economic Analyses

The cost study of a battery energy storage plant must consider the initial capital costs, operating costs, and maintenance costs. Capital costs include the cost of the battery cells, the PCS, and the BOP. Operating costs include the cost of the energy to charge the battery, the cost of auxiliary energy consumption, and the cost of replacing battery cells at the end of their life. Maintenance costs include servicing the battery and performance monitoring, with some additional costs for other equipment and facility maintenance. The analysis will compare the conceptual design scenarios with other methods to provide the energy at the selected utility locations.

PG&E has selected the Stockton Division as an area with potential for economic battery energy storage. It has a number of planning areas that meet the criteria of high area specific marginal costs and low growth rates. Resulting from meetings between PG&E R&D personnel and the Sr. Planning Engineer in the Stockton Division and four of the Distribution Planners, two possible planning areas within their Division, Corral and Lodi, were selected for further study. Two additional planning areas in the Sierra Division (Mountain Quarries and Bear River) were recently identified and likewise will be included in the economic analyses for battery energy storage.

Further examination of the Corral and Lodi planning areas in the Stockton Division indicates that the two sites should prove to be of considerable interest

because they illustrate two different types of system loading problem. At one, a BESS would defer costly transmission upgrades, while at the other, it may defer construction of a new substation. The specific situations at these two sites are reviewed in a later section.

VRLA Battery Storage Plant Preliminary Design Specification for PG&E

Design Concept

PG&E's objective is to evaluate battery technology as an option for distributed storage. Therefore, the design specification is not unique to a particular site. Rather, it is a broad specification that would be applicable, with a minimal amount of redesign, to a large number of locations within PG&E's distribution system.

The BESS will be a modularized, standardized design, capable of meeting storage requirements on a wide variety of distribution feeders. To allow the distribution planners the greatest flexibility, the design will take a modular approach with regard to both the battery and the PCS. For the purposes of this specification, a unit battery will be defined as a group of cells interconnected to provide a 544 kW dc output for 2 hr at the end of the battery's useful life. A unit PCS is defined as having a nominal rating of 500 kVA. Several of the unit batteries may be paralleled on the dc side of the converter so that the nominal power rating could be achieved for a longer period of time. Using this approach, the smallest system (i.e., one unit battery plus one unit PCS) will have a nominal rating of 500 kVA for 2 hr.

For the baseline conceptual design, a 2-MVA plant size is required. It shall be met by the combined output of four unit batteries and four PCS units. Although a lower cost might be achieved for a single installation by specifying the design for a single converter and battery, the modularized approach is believed to result in a lower overall cost for several systems installed with differing ratings due to the standardized design.

For example, subsequent installations may contain one to four of these converter/battery units paralleled on the ac side. While most feeders may benefit best from larger battery systems, there may be several cases where 500 kVA is adequate. Also, the small unit size permits greater flexibility for distribution planners.

Market Assumptions/Cost Estimates

Costs will be estimated for both the first and second plants with no assumptions about multiplant orders or timing of orders. Thus, all the engineering costs will be

allocated to the first plant. For the second plant, only minor engineering costs for size and site-specific modifications will be included, for example, to design a modified foundation for different soil conditions.

The salvage value of all components, particularly the PCS, will be estimated after a useful life of 5 yr.

System Requirements

Duty Cycle

The battery will be operated in one basic mode during discharge: deep discharge for peak shaving applications. In this mode, the system should be capable of 60 deep cycles/yr, defined by a block load of 2 MW (500 kVA per unit battery/PCS) for 2 hr. Actual deep discharge profiles will likely be load following as shown in the example profiles, Figures 3-16 and 3-17. The system, operated in the mode described above, should have a minimum calendar life of 5 yr and a minimum cycle life of 300 cycles. Normally, the battery will be charged during the least cost periods. Super off-peak is from 1 AM to 5 AM. Off-peak is from 9:30 PM to 1 AM, and from 5 AM to 8:30 AM.

Utility Interface Requirements

The utility short-circuit MVA at the 12-kV point of connection is limited to 300 MVA for 3-phase faults. The nominal utility system voltage at the point of connection is 12.47 kV, 3-phase and 60 Hz. During normal conditions the utility grid system voltage varies as follows:

- Frequency: 59.9 to 60.1 Hz
- Line-to-Line Voltage: 12.47 kV \pm 10%

- Voltage Unbalance: \pm 2.5% of the average of the three phases

The utility's protection requirements shall be in accordance with PG&E's Power Producer's Interconnection Handbook.

PCS Performance Requirements

The PCS shall be designed in modular building blocks. The power rating of each unit PCS shall be 500-kVA ac continuous. At rated power, the PCS shall be capable of operation at a power factor of 0.95 lagging or greater above 20% rated output (charge or discharge mode). Unity power factor operation is desired. The minimum efficiency of the PCS at full load discharge shall be 92%.

The PCS shall be capable of operation in the appropriate dc voltage range so as to properly interface with the battery.

All necessary self-protective features and self-diagnostic features should be incorporated to protect the PCS and battery from damage in the event of component failure or from parameters beyond safe operating range, due to internal or external causes. Each PCS shall shut down under the following conditions:

- Utility undervoltage: PCS shutdown to occur when voltage drops below 90% of nominal voltage for 5 sec.
- Utility overvoltage: PCS shutdown to occur instantaneously when voltage rises above 110% of nominal voltage.

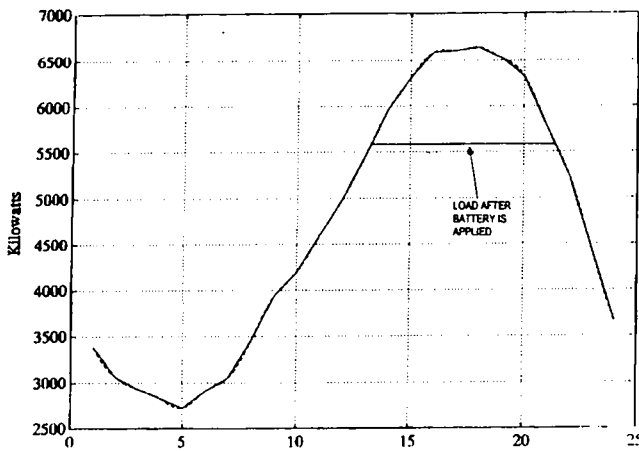


Figure 3-16. Peak Load Day Profile.

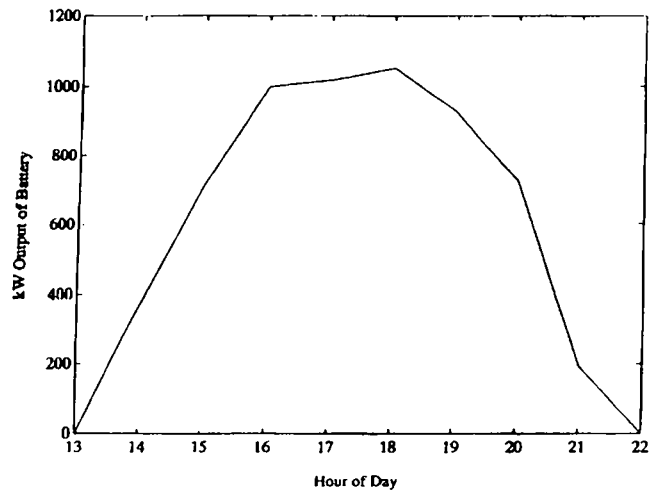


Figure 3-17. Battery Discharge Profile.

- Utility underfrequency: PCS shutdown to occur when frequency is 58.5 Hz or less for 2 sec.
- Utility overfrequency: PCS shutdown to occur when frequency is 61.0 Hz or more for 15 cycles.
- PCS overtemperature
- Smoke and/or Fire
- Loss of Control and Data Acquisition System (CDAS) power
- Control (CDAS) voltage out of range
- Islanding or Run-On: Shutdown shall occur within 1 sec of loss of utility power.

PCS-generated harmonics at the system's ac interface at rated power shall not exceed:

- a total harmonic current distortion of 5%
- a single frequency current distortion of 3%
- a total harmonic voltage distortion of 3%
- a single frequency voltage distortion of 1%.

The ac output of each PCS should be 480-V wye connected to accommodate standard transformers used to step up to the nominal distribution voltages of 12.47 and 21 kV.

VRLA Battery Requirements

The battery shall be designed in modular building blocks. Figures 3-18, 3-19, and 3-20 illustrate the PG&E unit battery concept. Each building block is called a "unit battery." One to four unit batteries may be paralleled on the dc side of the PCS to allow longer discharge durations.

The unit battery's available capacity at end of life when discharged for 2 hr to 1.75 V/cell (average) shall be $2 \text{ hr} * 544 \text{ kW} = 1088 \text{ kWh}$. The end of life is defined as the time when the unit battery can provide only 80% of its rated (new) capacity. Thus, the new unit battery shall have a rated capacity of $1088/0.8 = 1358.7 \text{ kWh}$. (To ensure that discharges of 500 kW for 2 hr can be met on the ac side for each of the 300 cycles over the 5-yr life of the batteries.)

The nominal open circuit voltage of the unit battery (at 2 V/cell) shall be 654 V dc. The unit battery shall consist of 5 parallel strings of 327 batteries in series, each battery having a nominal rating of 2 V. The maximum cell voltage (at end of charge) shall be 2.35 V dc. The unit battery's maximum voltage shall be 768.45 V

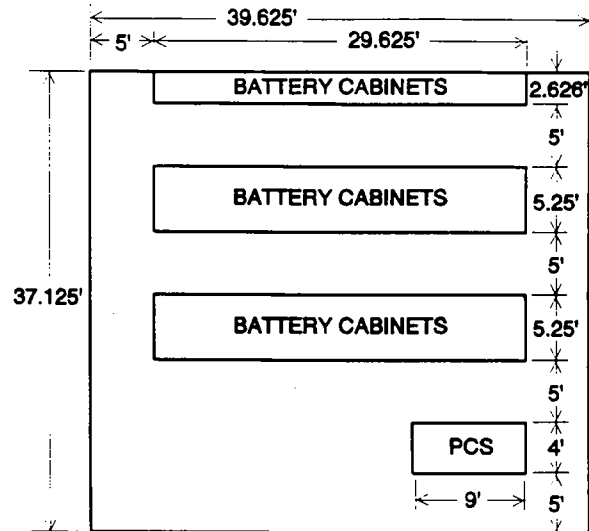


Figure 3-18. Top View of PG&E Unit Battery.

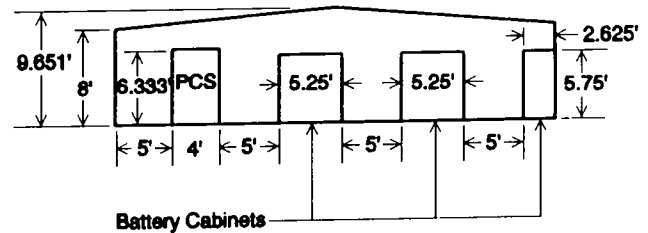


Figure 3-19. Side View of PG&E Unit Battery.

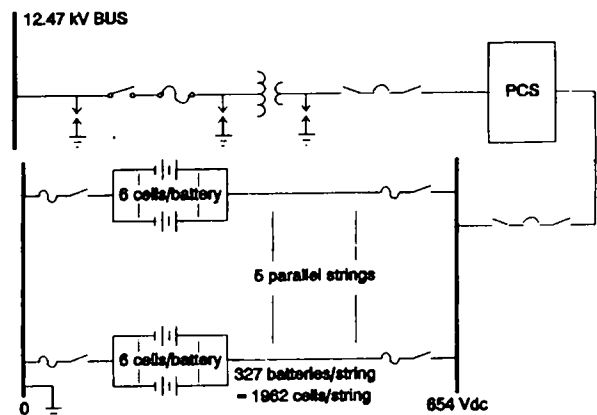


Figure 3-20. Electrical Diagram of the PG&E Unit Battery.

dc. The minimum cell voltage (at end of discharge) shall be 1.75 V dc. The unit battery's minimum voltage shall be 572.25 V dc.

The battery shall be dischargeable to a depth of approximately 80% of its rated 2-hr capacity out to its EOL to ensure that 300 cycles of 500-kW can be

delivered for 2-hr each. The round-trip energy efficiency at the dc terminals of the battery shall be not less than 80% under the proposed 24-hr duty cycle. The battery shall be capable of 300 complete discharge and charge cycles. Its minimum calendar life shall be 5 yr.

Maximum fault current of one string shall be 24,000 ADC shorted to 0 V dc or 12,858 A dc shorted to 1 V dc. Maximum fault current of the unit battery shall be 120,000 A dc shorted to 0 V dc or 64,290 A dc shorted to 1 V dc.

Balance of Plant

The BOP concept refers to the structural, mechanical, and electrical support systems (excluding the battery and PCS) required to operate the battery energy storage facility. The BOP includes the following systems and equipment:

- Battery building
- HVAC System
- Auxiliary power system
- Fire protection system
- Control and Data Acquisition System: A remote CDAS, shall be provided. It shall interface with the PG&E SCADA system.

The CDAS system shall provide for the following:

- Charging of the battery during the specified time intervals in accordance with the manufacturer's requirements.
- Discharging of the battery in accordance with the application.
- Giving complete charge and discharge control to the utility via the SCADA interface. Modes of charging and discharging should include utility defined and programmed algorithms that can accommodate time-of-day, manual overrides, and load following based on real-time (SCADA) data inputs.

The CDAS system shall monitor the following:

- battery voltage and current
- battery kWh and Ah
- ac power, energy, voltage, and current
- hydrogen levels and alarm
- fire detection and alarm
- battery ground fault detection and alarm

- room and outdoor temperature and humidity.

For selected cells, the CDAS shall monitor temperature, voltage, current, and cell internal pressure.

For ac power equipment, the plant shall include an utility pad mount 480-V Y/12-kV delta transformer, and ac switch gear and overcurrent protection equipment. Power equipment (dc) will include dc bus work, and dc switchgear and overcurrent protection equipment.

Physical Site Characteristics

Since the design must be applicable to a wide variety of sites, a specific site is not included in the specification. However, a large number of sites may prove to be promising for battery energy storage at PG&E, and these cover the spectrum of environmental conditions that exist throughout the PG&E system. They include hot, dry desert climates with cold winters and little precipitation, as well as areas in the Sierra Nevada mountains that receive hundreds of inches of snow per year. The data given below therefore represent the extremes, summer and winter, that can be found in the entire PG&E area.

- Ambient Air Temperature:
 - Design Maximum 120°F dry bulb
 - Design Minimum 12°F dry bulb
- Dust: Moderate
- Humidity: 100% maximum, 63% annual mean
- Seismic Loads: UBC Zone 4 (not simultaneous with wind loads)
- Wind Loads: ANSI A58.1, 80 mph exposure
- Rainfall: 11 in./yr
- Snowfall: 100 in./yr
- Available Space: up to 1/2 acre. (However, land costs and space availability, especially in urban settings, are primary considerations. Therefore, every effort should be made to minimize the "footprint" of the facility and keep the plant size small. PG&E has requested that the designers explore alternatives to existing battery cabinets in design tradeoffs to reduce the footprint of the system.)
- Soil Conditions are the following:
 - Bearing capacity: TBD
 - Compaction: Compacted gravel
 - Stability: TBD

Battery Sizing

To achieve a 2-hr discharge to a final voltage of 1.75 Vpc, four unit batteries will be used for the first installation to obtain the 4-MWh output. (Unit battery designed using GNB's MSB-2460 module).

$$pcseff: = 0.92 = \text{PCS one-way efficiency during discharge.}$$

$$\text{discharge:} = 2 \text{ hr} = \text{discharge time in hours}$$

$$Pac: = 500000 \text{ W} = \text{unit battery's desired output ac power for 2 hr.}$$

$$eolfactor: = 0.80 = \% \text{ capacity at end of battery's life.}$$

Let size = the necessary unit battery size for 2-hr application. Then,

$$\text{size} = \frac{pac \cdot \text{discharge}}{pcseff \cdot eolfactor} \quad \text{size} = 1.359 \cdot 10^6 \text{ Wh}$$

Now we can figure the number of cells needed to achieve the desired size.

$$avgVpc: = 1.98 = \text{Average Voltage/cell for 2-hr discharge}$$

$$Ah: = 70 = 35 \text{ A} \cdot 2 \text{ hr}$$

$$\text{celloutput:} = avgVcp \cdot Ah$$

$$\text{celloutput} = 138.6; \text{ Wh} = \text{the output of a single cell at 2-hr rate.}$$

Then the number of cells can be found by:

$$\text{numbercells:} = \frac{\text{size}}{\text{celloutput}} \quad \text{numbercells} = 9.803 \cdot 10^3$$

$$\text{numberbatteries:} = \frac{\text{numbercells}}{6} \quad \text{numberbatteries} = 1.634 \cdot 10^3$$

Since there are 40 batteries in a cabinet, the number of cabinets is:

$$\text{numbercabinets:} = \frac{\text{numberbatteries}}{40} \quad \text{numbercabinets} = 40.846$$

Thus, we need 41 cabinets for a unit battery.

Battery Siting Study - Stockton Division

The two planning areas under consideration for battery siting in the Stockton division are Lodi and Corral. The Lodi area includes seven substations and encompasses the vicinity of the city of Lodi located about 10 miles north of Stockton. Corral is a single substation area located on the outskirts of the Lodi area, directly east across the Calaveras county line.

Lodi Planning Area - Colony Substation

The Colony substation (Figure 3-21) is in the northern portion of the Lodi area, and is weakly connected to the bulk of the circuits in the southern portion. The whole of the Lodi area is forecasted to be overloaded by 1995 if no capacity is added. A new substation is due to be installed in 1993 in the North Stockton area that will solve the capacity problems for southern Lodi, but not Colony in the north. The growth around the Colony substation will require the replacement of an existing 6.5-MVA transformer bank with a new 16-MVA bank in 1995. There are a few conventional (but costly) scenarios being considered to handle the problem:

- Simple upgrade of the transformer connected to the same 60-kV transmission line (which is itself nearing capacity) to which the existing bank is tied. In this case, the division might have to support the costs for upgrades required on the 60-kV system as a result of upgrades at Colony.
- Install a 16-MVA, 115/21-kV transformer at Colony, and connect to a separate 115-kV transmission line located about three miles from the substation. This would require installing 115-kV poles and line for the three-mile distance and some upgrades to the existing 12-kV distribution feeder to accommodate 21 kV.

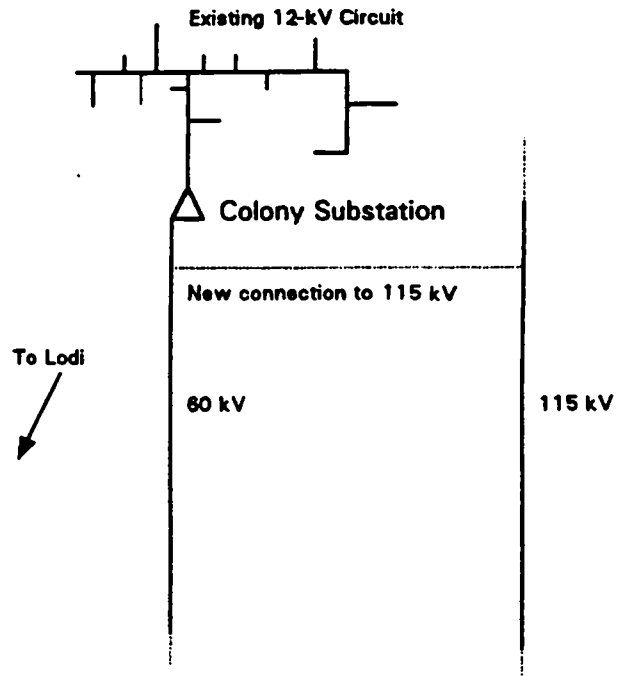


Figure 3-21. PG&E Colony Substation.

Battery Solution

As a planning alternative, a battery located near or at the substation could defer the conventional upgrades for 2 to 3 yr. The load profile on the Corral substation is not especially sharp during peak days. The profile is the primary limitation of this site as it significantly limits the length of the deferral for a given size battery. The circuits out of the substation are not very long, so there was no emphasis placed on locating the battery down the line for voltage support or reactive power compensation. The value in this case study is in the illumination of scenarios where even a relatively small transformer upgrade can require costly transmission work.

Corral Planning Area and Substation

The Corral substation (Figure 3-22) is electrically and physically distant from surrounding substations. The transformer (rated 11 MVA) load is from a single 12-kV feeder whose main circuit travels in a northeast line to North Branch substation. The two substations are isolated with one of several switches along the 12-kV line. However, the 0.75 MW/yr growth in the Corral area is being met by locating the open-switch point closer to Corral, which effectively transfers more and more load to the distant North Branch substation. By 1995, the capacity at Corral will need to be increased since the load transfers will have exhausted the capacity available from North Branch. The alternatives are as follows:

- Upgrade to 16-MVA transformer bank. This solution is again hampered by capacity constraints on the transmission (60-kV) line feeding the substation.
- The solution preferred by the planning engineer is to build a new substation at Valley Springs, about halfway between Corral and North Branch. This would be a multi-million dollar project in 1996.

Battery Solution

The battery in this case would be located between two substations but closer to the load center in the Corral vicinity. The effect of the battery would be to shift the open-switch position back towards North Branch. The open-switch position could be shifted over the 2- to 3-yr deferral period to maintain safe loading on either substation. Both substations' peak profiles are sharp and occur simultaneously. The planning engineer also said that the location of the battery may be suitable for reactive power voltage support.

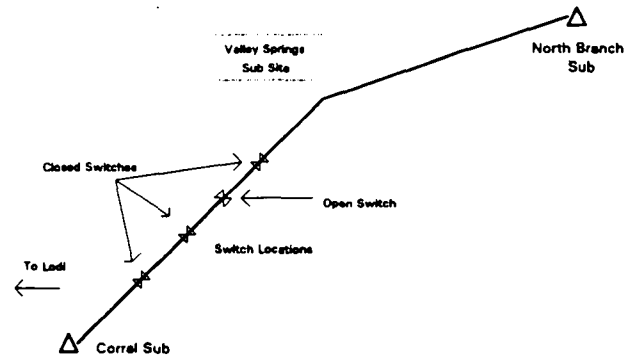


Figure 3-22. Corral Substation.

Applied Research - SNL

GNB is designing a sealed lead-acid battery to meet the short-duration, high-power discharge requirements of an electric utility. The battery's hydrogen vent assembly employs a molded ethylene-propylene-diene monomer (EPDM) rubber that compresses under a specific pressure and provides an escape path for the gas. GNB found that after storage periods of 6 mo, the rubber tended to adhere to the valve edge, causing venting pressures 60% greater than the designed relief pressure. It is believed that this problem is caused by chemical attack of the rubber by the battery electrolyte. SNL is investigating two approaches to improving the reliability of the vent. In the first instance, a plasma process has been used to both apply chemically resistive coating to the plug and to generate a plasma that may crosslink the surface of the rubber and increase its modulus. In the second instance, the use of e-beams has been investigated to crosslink the surface of the plug.

Plasma processing provides a convenient method to apply a pin-hole free, thin coating to a variety of surfaces. Three sets of plugs were supplied by GNB. The first set was coated with plasma-polymerized siloxane, the second set was coated with fluorocarbon, and the final set was exposed to a radio-frequency (RF)-generated gas plasma that was designed to crosslink the surface of the rubber. The three sets of samples were sent to GNB for environmental and performance testing.

In an attempt to crosslink and thereby harden the surface of GNB's EPDM plugs, three of these plugs were exposed to an e-beam source under vacuum at an average dose rate of 28 MRads/hr. These conditions were chosen on the basis of previous work with gamma rays in which increases in moduli of ethylene-propylene rubber (EPR) due to crosslinking were observed. While the structure of EPR is similar to that of EPDM, it should be noted that these are two distinctly different formulations; GNB's EPDM-based plugs were much softer than the EPR rubber used in the gamma ray experiments. As

shown in Figure 3-23, exposure of GNB's rubber plugs to a flux of e-beams resulted in a decrease in modulus at the surface rather than the expected increase. As the e-beam was attenuated as a function of depth, the modulus approached that of the virgin material. Apparently, under these conditions of exposure, chain scission type mechanisms predominated over crosslinking. Possible explanations for these results are 1) the GNB rubber is inherently prone to chain scission and consequently softens upon exposure to the e-beam irradiation; the tendency of GNB's plugs to undergo chain scission rather than crosslinking may be due to additives; 2) the conditions chosen were not optimum for crosslinking; the conditions used in these experiments could have been either too mild or too severe. Since replacement of GNB's rubber is not an option, SNL proposes to irradiate the rubber under mild conditions (low temperature) and severe conditions (high temperature). If possible, the effect of reducing the energy of the e-beam source may also be explored.

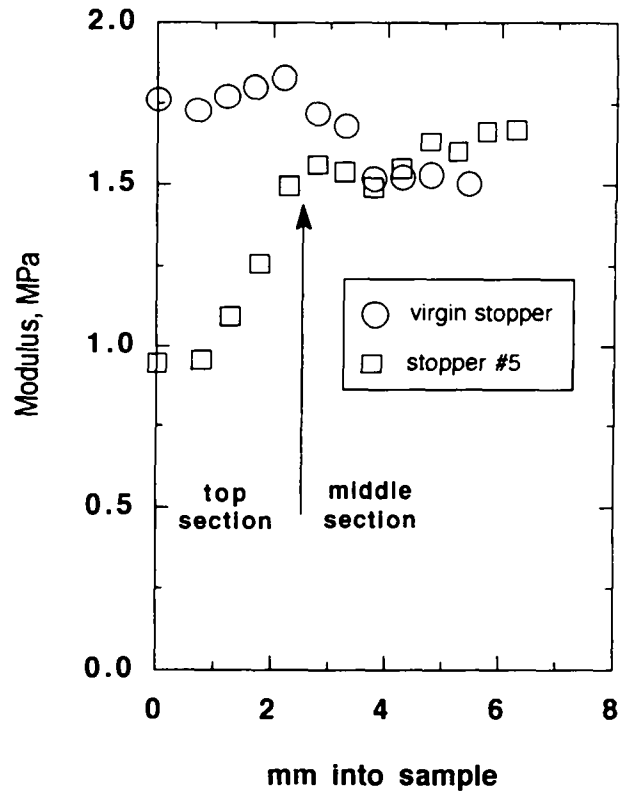


Figure 3-23. The Modulus of the Virgin Stopper and E-Beam-Treated Stopper as a Function of Distance from the Sample Surface.

4. Zinc/Bromine Project

Zinc/bromine batteries are attractive candidates for utility applications because they offer two to three times the specific energy of lead-acid batteries, have sufficient power, operate at near room temperature, are capable of being recycled, can be built at low cost, and have potentially long lifetimes. The zinc/bromine battery is composed of three parts: the cell stack, the reservoirs, and the auxiliary pumps, controls, and piping. The electrolyte solutions are continuously pumped in separate circulation systems through the anode and cathode chambers of the cell stack. During charge, zinc is plated on one side of a bipolar electrode, while bromine is formed on the other side. The bromine quickly forms a complex with quaternary ammonium ions in the electrolyte, and this complex separates, forming a second, denser phase. During discharge, the electrode reactions are reversed. The cell stack is composed of a number of bipolar electrodes and cell separators with monopolar terminal electrodes on each end. The electrodes are made from electrically conducting carbon plastic and are thermally welded into a flow frame. The flow frame contains the channels and openings used to carry the electrolyte to and from the electrodes. The flow frames are thermally welded together forming a hermetically sealed cell stack. Rigid endblocks are placed outside the terminal electrodes to minimize the deflection when electrolyte is pumped through the stack under pressure.

The objectives of the JCBGI contract are to design, fabricate, evaluate, and optimize a zinc/bromine battery system suitable for electric utilities. In Phase 1 of the program, which was completed in December 1991, the soundness of the battery technology was shown. In Phase 2, new larger cell stacks optimized for an electric utility battery will be constructed. Fortunately, zinc/bromine battery technology is readily scaled to different sizes. However, the production of a battery with different size electrodes requires a complete new set of plastic injection molds and tooling.

Engineering development tasks are on schedule. The modeling and spreadsheet work is essentially done and now can be used to size battery parts and predict performance. Work on electrodes, separators, and bromine electrode activation layers is ongoing. Success in these programs will mean improved battery performance or lower cost, but these improvements are not critical to the overall project. Laboratory battery testing is confirming the advantages of recent changes to the

welding process, and new information is being collected on cycle life, stand loss, no-strip cycles, temperature effects, zinc loading, etc. Miniature cells have been developed to facilitate investigations into zinc plating, flow rates, etc. New flow frame models are being written to study the pattern of electrolyte flow across the cells.

An 8-cell (1-kWh) SOA battery station and a twin 50-cell stack (15-kWh) improved SOA (ISOA) station were tested at SNL.

A study of the durability of carbon plastic electrodes was completed, and a project to develop new bromine complexing agents was started.

Technology Development - JCBGI

The objective of the zinc/bromine technology development is to develop and evaluate low-cost, long-life prototype modules that demonstrate the performance required for utility applications. This task is being conducted primarily through a cost-sharing contract with an industrial partner, JCBGI. The objective of the JCBGI program is to extend their technology from mobile designs to a utility design and to develop, fabricate, and evaluate a 100-kWh utility battery system. SNL is responsible for technical direction of the development contract and additionally performs evaluations of contract deliverables. The 39-mo program with JCBGI was initiated in August 1990 and is organized into two 18-mo technical phases followed by a 3-mo reporting period. Because satisfactory technical progress was made during the first phase, the second phase was initiated during the second quarter of FY92.

The major tasks of this contract are as follows:

Phase 1

1. Demonstrate leak-free battery stacks
2. Demonstrate steady long-term operation by achieving over 100 cycles with <10% drop in energy efficiency
3. Achieve energy efficiencies of ~75%
4. Demonstrate adequate performance with six consecutive, no-strip cycles

5. Verify battery cost of \$150/kWh or less
6. Address safety issues associated with the battery

Phase 2

1. Develop, design, fabricate, test, and deliver a 100-kWh Battery System

The core development program is on schedule. The modeling and spreadsheet work is essentially done and now can be used to size battery parts and predict performance. Work on electrodes, separators, and bromine electrode activation layers is ongoing. Success in these programs will mean improved battery performance or lower cost, but these improvements are not critical to the overall project. Laboratory battery testing is confirming the advantages of recent changes to the welding process, and new information is being collected on cycle life, stand loss, no-strip cycles, temperature effects, zinc loading, etc. Miniature cells have been developed to facilitate investigations into zinc plating, flow rates, etc. New flow frame models are being written to study the pattern of electrolyte flow across the cells.

An 8-cell SOA battery station was delivered at the beginning of the project. Later, a twin 50-cell stack (15 kWh) ISOA station was delivered in February 1992. This battery included most of the technology improvements and will demonstrate the capabilities of zinc/bromine batteries for electric utility operation.

Battery Fabrication and Testing

Stack and Battery Assembly

The cell stack manufacturing process has undergone continual improvement during the year. Some of these improvements include better fixturing methods (during the welding process), changes in separator cleaning, and a refinement of the thermal welding parameters. A larger fusion welding machine was installed and the welding process transferred to it. An automated data collection system that records the parameters of the assembly operation was initiated as part of long-term quality control.

A number of 8-cell and 50-cell stacks were produced during the year. Several problems that led to defective cell stacks were found and fixed. In general, the cell stacks are now reliably leak-free.

Attention has shifted to other features of the battery system. The heavy ac motors attached to the circulation pumps are being replaced by brushless dc motors. The motor rpm (revolutions per minute) is controlled by a pulse width modulator circuit that enables efficient ad-

justment of the flow rate. This simplifies the electrolyte circuit because valves are no longer needed to modulate the pump output.

Status of 8-Cell Battery Testing

A summary of the significant 8-cell battery tests follows:

V1-53 - This 8-cell battery completed 324 cycles before reaching a 10% decline in energy efficiency as shown in Figure 4-1. After 325 cycles, the performance began dropping drastically. Testing ended when the voltaic efficiency declined as the residual inefficiency increased. This resulted in a decrease in the coulombic and energy outputs. These observations were attributed to degradation of electrode activity at the cathode. The battery was torn down after cycle 346.

V1-54 - This battery was initially used for zinc loading tests with high-efficiency electrolyte, and was later switched to a more conductive electrolyte and performed baseline cycles for the remainder of the testing. After a total of 279 cycles, the efficiencies had declined beyond 10% as shown in Figure 4-2. On teardown, the zinc plating appeared smooth, with no dendrites. Several separators were blistered in local sections, which indicated possible dendrite growth into the

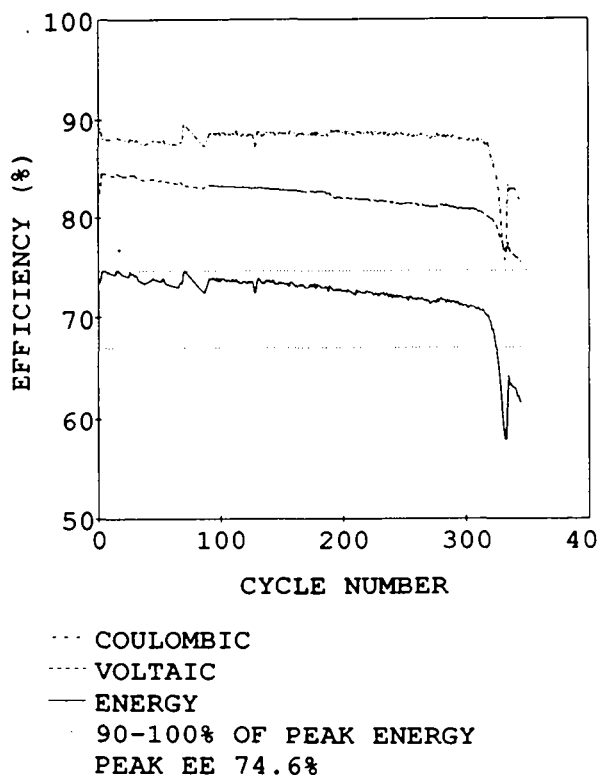


Figure 4-1. Cycle-Life Efficiencies for 8-Cell Battery V1-53.

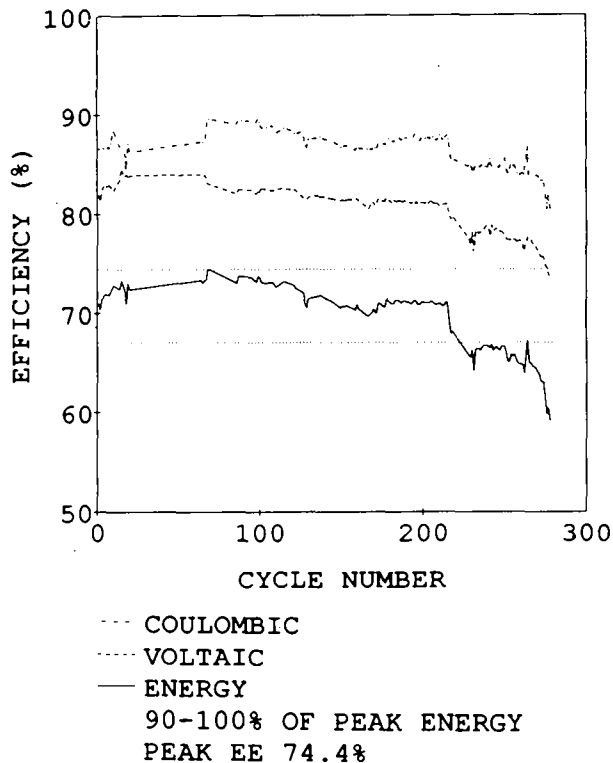


Figure 4-2. Cycle-Life Efficiencies for 8-Cell Battery V1-54.

separator. This was not surprising in view of the battery history of high zinc loading tests. Based on the tear-down observations and the battery performance, it is concluded that V1-54 failed due to degraded cathode activity.

V1-55 - This 8-cell battery maintained steady baseline cycle energy efficiencies for 365 cycles before declining. The coulombic efficiency remained virtually constant through the 365th cycle, while a steady decline in the voltaic efficiency was observed. The cycle efficiencies for V1-55 are shown in Figure 4-3.

V1-55 was dismantled at a full state of charge. The zinc plating quality was poor. However, a cracked impeller was found in one of the circulation pumps, and the electrolyte was found to be contaminated with iron, nickel, and copper ions.

Battery cell stacks V1-56 through V1-69 were used mainly to test new cathodes and assembly techniques and to qualify a new welding apparatus. Cell stack V1-57 was sent to SNL as a deliverable where it became SNL #518.

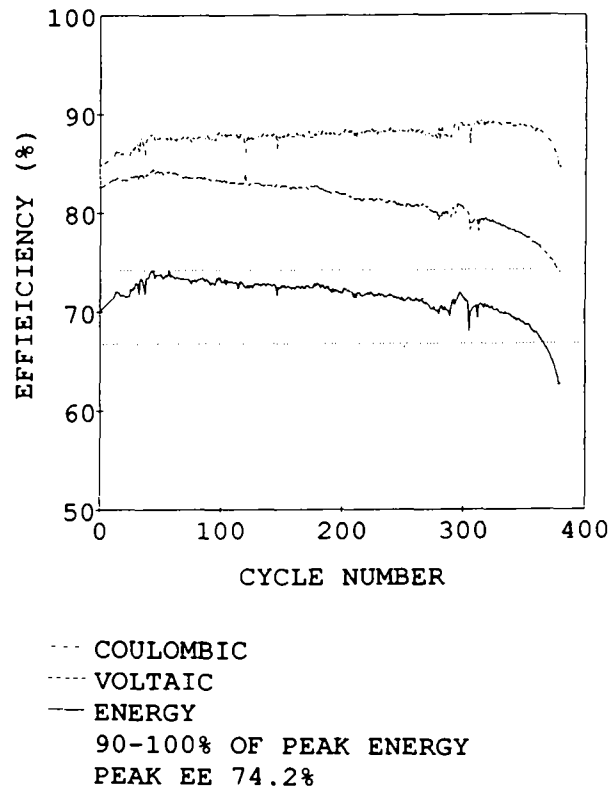


Figure 4-3. Cycle-Life Efficiencies for 8-Cell Battery V1-55.

50-Cell Battery Results

Battery Performance

The following large battery cell stacks were built with 50 cells:

VL-14 - This cell stack was torn down after 114 cycles while still operating acceptably to study the zinc distribution after a set of no-strip cycles. The observed efficiencies at cycle 114 were coulombic, 87.0%; voltaic, 82.3%; and energy, 71.6%.

VL-15 and VL-16 - These cell stacks were built to test large stack manufacturing procedures. They were operated in a parallel configuration and after 19 cycles had returned a coulombic efficiency (CE) of 90.5%, a voltaic efficiency of 86.3%, and an energy efficiency of 77.6%. They are now being tested separately.

VL-17 and VL-18 - These large cell stacks were found to have been built with defective electrodes and have been cycled only to test out cell stations.

VL-19 and VL-20 - Delivered to SNL and operated as battery SNL #526.

Effect of Orientation on Battery Performance

The results of tests of vertical vs horizontal stack orientation using VL-15(50) have shown no preference for either orientation. Multiple cycles without stripping were carried out as shown in Table 4-1. The flow was reversed periodically while the cell stack was in each orientation.

High-Voltage Cycling (50-Cell Stacks in Series)

It is often advantageous in a high-power discharge to use as high a voltage as possible to keep the current low and thus be able to use low-current leads and connections. A 15-kWh battery station (VL-17 and VL-18) was used to test the ability to charge battery stacks mounted in parallel and then to discharge them in series. For this test, the electrolyte circulation lines were connected with the cell stacks in parallel. The battery was charged with the stacks in parallel, and then the stacks were electrically reconnected in series and discharged without changing any of the plumbing connections. The battery appeared to operate normally. The voltage was doubled and the current cut in half as expected when the electrical connections were changed. There were no signs of any problems or difficulties during the test.

Minicell Battery Tests

The minicells are half-size batteries consisting of a single cell made with one terminal electrode panel instead of the double panels used in the V-design batteries. They are sealed with a gasket. These cells were specifically built to investigate different separators, electrolyte compositions, plating additives, etc. They are especially useful because the cell can be opened during a cycle and the zinc plating inspected. Then the cell can be closed and the test continued.

Current Density

The effect of charge current density on efficiencies is given in Figure 4-4 for a single cell battery. The zinc loading at each current density was kept constant at 90 mAh/cm². The CE appears to increase as the current density is raised to 40 mA/cm² and then drops off slightly. The increase is expected due to the shorter amount of time available for bromine transport at higher current densities. The decrease at current densities above 40 mA/cm² may be due to rougher zinc plating. The main effect tends to be a decrease in voltaic efficiency due to higher resistances associated with the increased current density. This also causes a corresponding drop in energy efficiency.

Separator Testing

Minicells have been used to test various separators. The standard zinc/bromine separator was coated with two different materials by two different suppliers. These coated separators are compared to the standard and to an experimental extruded separator in Table 4-2.

One of the chemical coatings (#1) appeared to slightly improve the properties of the standard separator, primarily by lowering the transport inefficiency. The other coating (#2) made the separator much worse than the original. The reason for this appeared to be that bromine severely attacked this coating as seen by the coating being partially dissolved and pulling away from the separator.

The experimental separator performed fairly well, but not as well as the standard separator material. This was expected because the bromine transport and resistance of this material were not as good as the standard;

Table 4-1. Cell Stack Orientation V1-15(50)

Cycles	CE%	Vertical Orientation (Conventional)			
		VE%	EE%	Trans%	Resid%
Baseline	86.2	84.1	72.5	6.4	7.4
Six No-Strip	90.6	84.9	77.0	7.4	2.0
Cycles	CE%	Horizontal Orientation			
		VE%	EE%	Trans%	Resid%
Baseline	86.3	84.1	72.5	7.9	5.7
Six No-Strip	90.8	84.9	77.1	7.6	1.6
Six No-Strip	90.7	84.8	76.8	8.0	1.3

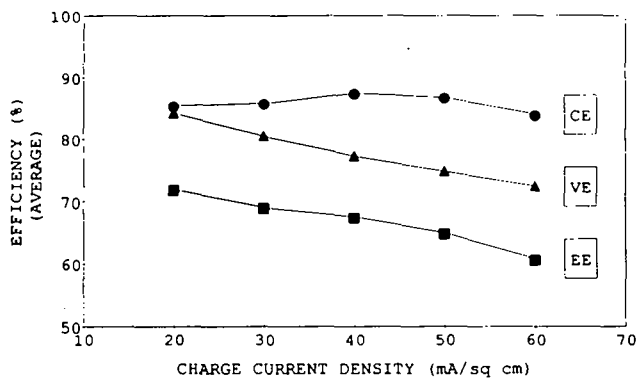


Figure 4-4. Effect of Current Density on Efficiency in the Minicell.

also, the experimental separator was not very uniform in appearance.

Results of Other Testing

In addition to standard high-efficiency duty, an electric utility battery should also be able to fit other needs. This section describes the work under way to test under another relevant discharge regime, the Simplified Frequency Regulation/Spinning Reserve (SFR/SR).

Background

The SFR/SR discharge is a simulation of electric utility, SES duty modeled from the PREPA BESS. The frequency regulation part of the SFR/SR calls for series of constant power discharge steps set at three different powers. When the SOC falls to 76%, the discharge is stopped, and the battery is given a full recharge; then the discharge is started again. The basic test lasts for 160 min and is repeated 54 times or until 6.5 days have elapsed. Then a rapid discharge is performed which simulates spinning reserve.

Zinc/Bromine Setup

New cyclers that will be fully capable of performing the SFR/SR have been ordered and received at JCBGI. Meanwhile, the controlling Simplified Federal Urban Driving Schedule (SFUDS) program in the SNL cycler was modified to apply frequency regulation steps in place of the existing steps. There is a total of 32 five-minute steps in each frequency regulation set. The frequency regulation test calls for three power levels: C1.5, C2.5, and C7.5. The three power levels were set to the values listed in Table 4-3 calculated for an 8-cell stack with high-efficiency electrolyte.

Two tests were carried out in which a fully charged battery (90 mA/cm²) was run until the battery was fully discharged. Each test lasted about 30 hr. The results

Table 4-2. Experimental Separators Tested in Minicell

Separator Type	Standard	Chemically Coated (#1)	Chemically Coated (#2)	Extruded
Coulombic %	86.4	88.4	59.8	82.1
Voltaic %	80.2	79.3	75.5	77.0
Energy %	69.3	70.1	45.1	63.3
Transport %	11.4	8.9	33.4	15.6
Residual %	2.2	2.4	6.8	2.3

Table 4-3. Constant Power Discharge Steps

Power Level	Zn/Br Battery W(kg)	8-Cell Battery (W)
C1.5	43	632
C2.5	27	396
C7.5	9	132

listed in Table 4-4 showed that the average efficiency was nearly the same as in baseline constant current cycles run before and after. The CE was slightly lower, and the voltaic efficiency was higher than in the baseline cycles. Both of these effects were probably the result of a freshly deposited layer of bromine, generated in the previous step, on the bromine electrode surface as the battery was discharged.

Recharge Added

The frequency regulation test was modified to include a periodic recharge as in the SFR/SR. After estimating that the 76% SOC would be reached after approximately three sets of steps, the controlling program was changed to add 20 Ah of constant current charge at that point. The second phase valve was set to open on discharge and to close on charge automatically.

Several frequency regulation tests were attempted using battery stacks V1-50 and V1-64. The battery voltage increased after each charge as seen in Figure 4-5, the results of one test. Due to an error in the controlling program, each charge was twice as long as it should have been and battery V1-64 was significantly overcharged. The voltage can be seen to be increasing from set to set in Figure 4-5.

Battery V1-50, with high-efficiency electrolyte, was cycled several times using the frequency regulation steps, but each cycle terminated at about 45 to 50 hr (full test = 156 hr) because of cycler malfunction. The efficiencies of two cycles, shown in Table 4-5, are not similar to the efficiencies of baseline cycles. The number 53 and 54 baseline cycles may be low in efficiency since the cycler did not maintain a set current and had to be stopped and restarted several times.

Concern

These initial trials revealed a concern that required changes in the SFR/SR test. The high power recharge pulse of $C_p/1.5$ for 5 min was too high for the battery as

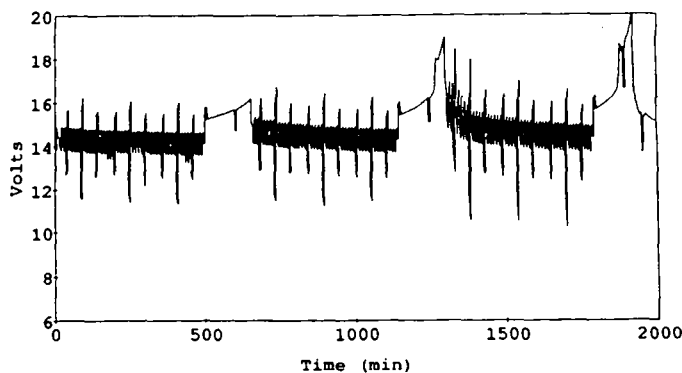


Figure 4-5. Frequency Regulation Test Using 8-Cell Battery V1-64.

it was configured. The battery voltage would often increase above the 2.1 V/cell and stop the test. The $C_p/1.5$ discharge step was not a problem for the battery. Therefore, in these tests, the recharge step was changed to $C_p/2$ for 8 min to give the same number of Ah but at a slightly lower voltage. There are other strategies to lower the voltage on charge that could be investigated in the future; a supporting salt could be added, the circulation rate could be momentarily increased, or the battery could be designed with higher power in mind by decreasing the internal resistances.

Zinc-Loading Study

The effects of increasing the Ah loading by extending the charge has shown that the coulombic, voltaic, and energy efficiency performance remained essentially unchanged between loadings of 90 to 115 mAh/cm² for battery V1-54. Tests extending the loading up to 155 mAh/cm², from the baseline cycle value of 90 mA/cm², showed a slight decline at the higher levels. The efficiencies also declined at lower zinc-loading levels of 45 mAh/cm². The efficiencies recorded during the loading study are shown in Figure 4-6.

Table 4-4. V1-64 Frequency Regulation Discharge

	CE%	VE%	EE%	Hours [†]
FR-Cycle 47	82.2	84.9	69.7	36.1
FR-Cycle 49	79.2	84.0	67.9	28.0
Average Baseline*	84.0	82.4	69.2	—

* Average of four cycles, [†] Time to 8-V cut-off, FR = Frequency Regulation

Table 4-5. V1-50 Frequency Regulation Efficiencies

	CE%	VE%	EE%	Trans%	Resid%
Cycle 47 Baseline	87.1	80.8	70.4	8.9	6.1
Cycle 51 SFRSR	77.0	84.2	64.8	17.9	5.1
Cycle 52 SFRSR	78.6	83.6	65.7	14.8	6.6
Cycle 53 Baseline	82.2	76.4	62.8	9.2	8.6
Cycle 54 Baseline	76.0	79.3	60.3	16.1	7.9

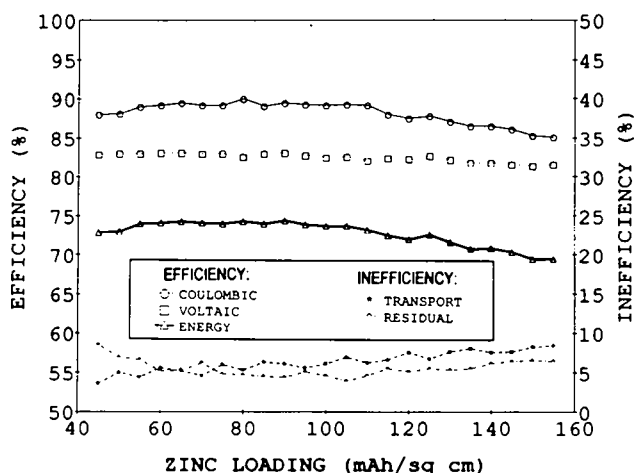


Figure 4-6. Effect of Zinc Loading on Efficiency Measured in 8-Cell Battery V1-54.

The nature of the coulombic losses varies as the loading changes. At low loading, the residual inefficiency percentage is high because the Ah remaining at the end of discharge are constant. Therefore, if fewer Ah are charged, the relative inefficiency is higher. Higher loadings were achieved by increasing the operating time. This increased the amount of bromine transport and thus the diffusion losses are higher. The energy losses are summarized by category in Table 4-6. To achieve high loadings (with 80% utilization of the electrolyte) the amount of electrolyte was increased at each loading above the baseline 90 mAh/cm².

Low-Temperature Study

In earlier studies, electrolytes based on 3.0 M ZnBr₂ and half molar each of methylethylmorpholinium bromide (MEM) and methylethylpyrrolidinium bromide (MEP) quaternary salts were evaluated for low temperature service. In those studies, it was found that an addi-

tion of 2 to 3 molar of CaCl₂ extended the freezing point well below 0°C.

The present low-temperature study was directed towards collecting information on two subjects: 1) to determine how low the battery temperature could be depressed and still allow the battery to start a cycle, 2) to measure how low temperature operation affects the battery performance.

Battery V1-50 was cycled in a cold chamber with high-efficiency electrolyte containing additional 2.0 M CaCl₂. However, the ac pump motors supplied so much heat to the battery test station that the cold chamber was unable to cool the battery while it cycled. The battery then sat in the chamber overnight with the circulating pumps turned off. The next morning, the battery temperature was -5°C when the circulation was re-started. Surprisingly, some solids were seen in the electrolyte. The temperature had risen to 10°C by the time the pumps were running smoothly enough to start the charge cycle. After an hour of charge, the voltage unexpectedly reached the high-voltage cutoff, and the cycle was terminated.

Full Discharge Without Strip

8-Cell Test Results

When a battery is continuously cycled, the Ah lost to stripping are retained in the battery, resulting in a higher coulombic efficiency when compared to a baseline cycle. The voltaic efficiency is not affected. Battery V1-60 was operated over a number of full discharge cycles without stripping following the discharge. There was an immediate gain of 2.5 to 3% in energy efficiency when the strip was omitted, but the advantage decreased as more cycles were added between strips as shown in Table 4-7. Even so, after 26 continuous cycles, the efficiencies were still higher than baseline cycle.

Table 4-6. Loading Study Efficiencies and Energy Losses

	Low Loading (45 mAh/cm ²) V1-54/Cycle 24 (%)	Baseline (90 mAh/cm ²) V1-54/Cycle 161 (%)	High Loading (150 mAh/cm ²) V1-54/Cycle 157 (%)
Efficiencies:			
Coulombic	87.8	86.6	85.6
Voltaic	83.1	81.4	81.8
Energy	73.0	70.4	70.0
Energy Loss Causes:			
Resistance Loss	48.2	46.0	44.6
Overvoltage Loss	8.1	7.7	7.5
Shunt Current Loss	0.1	0.1	0.1
Diffusion Loss	12.1	17.8	25.2
Residual Loss	31.6	28.5	11.6
Total Losses	100.0	100.0	100.0

Table 4-7. V1-60 Full-Discharge Cycles Without Strip

	CE%*	VE%*	EE%*	Trans%*	Resid%*
Baseline (#11-14)	90.1	85.9	77.4	5.9	4.0
Six cycles (#15-21)	93.2	85.6	79.8	5.1	1.7
Eight cycles (#78-86)	92.4	85.7	79.2	5.6	2.0
Eleven cycles (#43-54)	92.1	85.5	78.7	5.8	2.2
Sixteen cycles (#57-73)	91.8	85.8	78.8	6.1	2.1
Twenty-six cycles (#88-114)	91.4	85.2	77.9	7.3	1.3

* Totals

50-Cell Test Results

Several no-strip cycle sequences were performed on the 50-cell battery, VL-14. The objective was to demonstrate the feasibility of no-strip cycling a large V-design battery. As shown in the 8-cell battery tests, there is an immediate increase in battery capacity when the strip is omitted. The gain in efficiency by VL-14, however, was not as dramatic as that demonstrated by V1-60. The flow frames in the larger stack did not have the improved diverter design, which has decreased the residual zinc accumulation resultant with no-strip cycling by nearly 50%. Eight-cell stacks have had the improved diverter design since V1-59. The test results demonstrate that a 50-cell V-design stack can effective-

ly achieve 6 to 8 cycles in a no-strip test regime. The test results of the no-strip cycle study for VL-14 are summarized in Table 4-8.

At the end of the no-strip cycle study, VL-14 was torn down at a full SOC following five full cycles without strip. VL-14 was torn down while still performing well to study the zinc plating quality and distribution. It was taken down at 100% SOC. The deposited zinc was rather poor and rough. There were a number of dendrites that reached and penetrated the separator. However, there were no signs of any full short dendrites that bridged the electrodes. The poor plating may have been caused by impurities. The metal in a pump impeller was found to be fully exposed to the electrolyte.

Table 4-8. V1-14 High-Efficiency Electrolyte Full-Discharge Cycles Without Strip

	CE%*	VE%*	EE%*	Trans%*	Resid%*
Baseline (#26-28)	87.8	83.3	73.1	6.5	5.7
Six cycles (#29-34)	89.9	83.4	74.9	---	---
Six cycles (#47-52)	88.6	83.2	73.7	9.0	2.5
Eight cycles (#53-60)	88.2	83.3	73.5	---	---

* Totals

The zinc distribution was good. Upon examination, no evidence of shunt currents affecting the zinc deposited near the electrolyte ports was found.

Reverse Polarity Test

Battery V1-52 was deliberately abused by cycling with the terminals connected in reverse polarity and no apparent damage was done. The purpose of this test was to simulate both the accidental reverse installation of a battery, and to simulate battery reversal that might occur in a series string.

The battery was charged to 45 mAh/cm² loading and then discharged twice. The energy efficiencies of the two cycles were 51% and 53%. The efficiency under baseline cycling conditions was not affected. It was 64.5% before the tests and 64.7% afterwards.

Shunt Current

Measurement

In an aqueous battery system, where cells mounted in electrical series have a common electrolyte path, small currents exist through the electrolyte. These currents in the feed channels and manifolds are referred to as shunt currents and are difficult to measure directly. Usually, the currents are calculated using the known resistances of the battery components. However, it should be possible to measure the equivalent shunt current in a large stack by comparing the CE with that of a smaller battery where the shunt currents are negligible. The equivalent shunt current is defined as a manifold current which would account for the energy diverted from the major current pathway.

If all other factors are equal, the only difference between the CE of a large stack and that of a small stack is attributed to shunt currents. This difference in CE should allow the shunt current to be calculated for a cycle as shown in Table 4-9.

Table 4-9. Shunt Current Calculation for a Cycle

Measurement/Calculation	Value	Source
CE of 8-Cell Stack	90.2% sd 0.1	V1-60 cycles 8-14
CE of 8-Cell Stack	90.3% sd 0.2	V1-62 cycles 1-10
CE of 50-Cell Stack	89.3% sd 0.3	VL-15/16 cycles 1-10
Amount CE Lowered	1.0%	
Typical Charge	104.75 Ah	
1.0% of Typical Charge	1.05 Ah	
Total Cycle Time	8.352 hr	
Equivalent Shunt Current	0.126 A	

In earlier work, the total average shunt current for a 50-cell high-efficiency stack (four manifolds) was approximated by the calculation program as being 0.115 A. The JCBGI zinc/bromine model predicted 1.66-Ah loss per cycle, which is equal to 0.199-A equivalent shunt current.

Shunt Current Calculation in New Design

A calculation of the shunt currents in the new larger cell design shows that while the size of the currents would be larger, the percentage of energy lost would be about the same as in the present V-design cell stacks.

The shunt model was used to calculate the shunt currents in the manifolds of cell stacks with 40, 50, and 60 cells. These results were in turn inserted into the mass and energy balance spreadsheet to estimate the energy lost to shunt currents during a baseline cycle. The results shown in Table 4-10 indicate that the shunt currents and energy lost both increase with the number of cells in both designs.

Shunt currents also cause problems with uneven plating and possible dendrites near the channel openings. Since the shunt currents in the new design cell stack are nearly twice the size of those in the existing cells, it will be important to check for signs of dendrites and flow diversion in the tests of the early builds.

Electrolyte Utilization

Cell stack V1-62 was used to study the effect of increased zinc utilization on efficiency. By increasing the utilization, the amount of electrolyte needed could be reduced and the battery weight lowered, thus reducing cost. The zinc utilization in a baseline cycle is 65.5%. The results in Table 4-11 show that there was only a slight decline in efficiency as the zinc utilization was increased.

Stand Heating Study

A battery undergoes self-discharge whenever it is in a charged condition. This is caused by transport of

Table 4-10. Calculated Shunt Currents

		40 Cells	50 Cells	60 Cells	
V-Cell	Charge	0.0225 A*	0.0322 A	0.0482 A	
	Stand	0.0185 A	0.0286 A	0.0403 A	
	Discharge	0.0138 A	0.0214 A	0.0300 A	
New	Charge	0.0385 A	0.0598 A	0.0848 A	
	Stand	0.0345 A	0.0532 A	0.0756 A	
	Discharge	0.0283 A	0.0438 A	0.0622 A	
V-Cell		45 Wh	84 Wh	148 Wh	Energy lost
New		82 Wh	160 Wh	272 Wh	
V-Cell		1.9%	2.8%	4.1%	% of Total loss
New		1.7%	2.7%	3.8%	

* Equivalent or average current in each manifold

Table 4-11. Zinc Utilization Study V1-62

Zinc Utilization (%)	CE%	VE%	EE%	Trans%	Resid%
65.5	89.7	85.3	76.5	5.6	4.6
80.0	89.1	85.4	76.1	6.5	4.5
90.0	88.1	84.4	74.4	7.3	4.6

bromine across the separator into the zinc electrode chamber, and by shunt currents. Self-discharge continues when the battery is put into stand or open circuit because bromine transport and shunt currents continue.

The energy lost during stand, and therefore also the heat generated, can be minimized by lowering the amount of bromine compounds in the cell stack. This is done by 1) removing any bromine complex that is loose or unattached by sweeping it out with flowing electrolyte and 2) reacting the bromine that is in the cell stack. Normally, the second phase valve is closed during a stand so that fresh bromine complex is not sent to the cell stack. Since the aqueous solution also contains some dissolved bromine compounds, the electrolyte circulation should also be stopped after the free bromine complex has been swept out. Periodically, the circulation should be resumed for short periods to remove heat from the cell stack. In tests carried out in an 8-cell stack and reported last year, the minimum energy loss occurred when the second phase valve was closed and the electrolyte circulated only periodically during a stand.

A test is under way using 50-cell battery stacks to confirm the results from the 8-cell tests and to measure the heating effects as well. In this test, the effect of various electrolyte flow rates, including full stop, on the efficiency and the temperature of the battery will be examined. In an additional experiment, a small side discharge will be used to remove some of the bromine in the cell stack during a stand to see if this results in a lower overall temperature gain.

Engineering Development

Electrode Substrate Resistivity

During the past year, the carbon plastic used in the electrodes has been produced by several compounders and extruding vendors. Several carbons were used at different concentrations. In general, the resistivity decreased as the amount of carbon black in the plastic increased. This was the expected result; however, the plastic became more difficult to process as the carbon content increased. The resistivity of the carbon plastic extruded sheets has been brought down to 2-4 Ω -cm from the original standard material, which was 8.6 Ω -cm, and new techniques to extrude and weld the carbon plastic are being developed.

Cathode Activation Layer

At present, typical 8-cell and larger stacks reach end of life at around 250-300 cycles. The cause of failure is

most often a loss of activity of the porous, active carbon surface on the bromine electrode. Other cell stacks have developed a similar problem immediately following special tests. Therefore, work has been undertaken to identify 1) the nature of the problem, 2) the cause, and 3) which active surface is more susceptible. This work is being carried out with small 4-cm² electrode samples that were either cut from battery electrodes or specially prepared for the testing.

Polarization and Surface Area of Electrodes Taken from Batteries

Samples of the electrode materials taken from batteries that had been cycled showed a range of polarization and surface area values. There was little correlation between polarization and surface area with number of cycles, but there was a strong correlation between area and polarization. The samples with low surface area had high polarization.

Evaluation of Alternative Types of Cathode Activation Layers

During the past year, the feasibility and benefits of various new alternatives to the standard type cathode activation layer have been examined. Presently, a modified fabrication method is being evaluated that utilizes an environmentally friendly, aqueous-based adhesive to replace the presently used toluene-based adhesive. Heat-pressed cathode layers of both carbon paper and Teflon bound carbon powder films are being examined. The present status of each of these alternative cathode activation layers is described below.

New Aqueous Adhesive Based Layer

The first attempts at using the new aqueous-based adhesive to make porous carbon layers resulted in good initial electrode performance, but very poor accelerated cycle-life performance. Research is proceeding to find a way of stabilizing the ohmic contact of the cathode layer, which will hopefully improve its cycle life.

Carbon Paper Cathode Layer

A roll of special high-surface-area carbon paper was continuously unrolled and imbedded into a batch of full-size carbon plastic backbone material as it was coming off the extrusion line. This type of fabrication method could be extremely attractive under mass production conditions.

Terminal Electrode

Over long periods of time, the internal resistance of experimental batteries has been observed to increase.

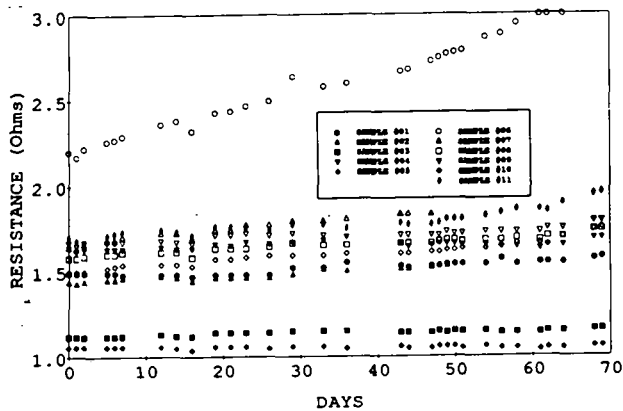


Figure 4-7. Resistances Measured in Samples of Terminal Electrode Materials (Carbon Plastic/Metal Screen) when Immersed in Brominated Electrolyte at 40°C.

This may be caused by corrosion of the interior copper metal current collecting screen. Tests were carried out to examine various carbon plastics that might reduce the amount of copper screen corrosion. The test samples consisted of two 1/2-in.-wide pieces of screen (~1/2 in.-apart) imbedded in plastic 6-in.-long and 2-1/2 in.-wide. These samples were placed in brominated high-efficiency electrolyte at 40°C. Samples No. 1 and 2 shown in Figure 4-7 represent the standard electrode materials. Most of the other samples had higher resistance initially, and nearly all show a gradual increase in resistance with time, thus eliminating them as candidates for terminal electrodes.

Separator Development

JCBGI prepared samples of porous polyethylene separator using materials somewhat different from those in the Asahi SF-600 separator. Several of these small samples showed resistance and bromine transport properties superior to those of the standard separator.

Subsequent to the laboratory trials, a series of compression-molded polyethylene compositions was prepared by a materials vendor. Results given in Table 4-12 indicate higher bromine transport than expected. In particular, JCBGI's earlier samples made with the same composition as material D in Table 4-12 had bromine transport about 80% that of the Asahi separator, and resistivity about 67% that of the Asahi separator. The reason for the discrepancies in results is now being examined.

Zinc Plating

Electrolytes from two poorly performing battery stacks, when cycled in the minicell, have yielded zinc

electrodeposits that have a poor, mossy-like appearance compared to past zinc deposits. Samples of smooth and mossy zinc deposits were analyzed by leaching in nitric acid and testing for total oxidizable carbon (TOC) and chloroform leach followed by infrared (IR) spectroscopy. The results indicated that the poor zinc deposits had higher carbon content and the presence of an oily material. The sources of these impurities are under investigation.

Electrolyte pH is considered to have an important effect on zinc plating quality and may be a factor in the mossy zinc observed recently. It has been reported that as the pH of the electrolyte approaches 4.0, mossy zinc may appear. The pH was measured for electrolytes taken from recently failed batteries, and results showed that the batteries that had mossy zinc plating also had higher pH than the standard batteries.

New Battery Design

Cell Stack Design

The final stress analysis of the new endblock using Computer Aided Engineering Design System (CAEDS) has been completed. The goal has been to minimize the thickness and weight of the parts while maintaining an acceptable level of stress and deflection under load. The drawings were changed to reflect the optimum design, and the injection mold makers are now machining the die set. The weld beads and diverters will be added as inserts to the mold after completion of the flow analysis.

Heating/Cooling Requirements

The cooling requirements of a zinc/bromine battery depend primarily on the efficiency of the battery in a particular application because all the heat generated in the battery comes directly from energy losses associated with running the battery. In this section, a background discussion of the thermodynamic efficiency will show that the practical limit of the energy efficiency is about 82%. This will be followed by some observations of the cooling function of a large battery used in laboratory testing.

Thermodynamic Efficiency

Energy losses to heat in the battery occur through processes such as ohmic heating, electrode overvoltage, and Peltier heat. The first two effects are well known, while the third is much less familiar. The Peltier heat derives from the nature of the electrochemistry and can set a limit to the overall battery efficiency.

Table 4-12. Properties of Experimental Separator Compositions

Sample Type	Thickness (mm)	R ($\Omega\text{-cm}^2$)	Thickness (mm)	Br ₂ Flux (mole/sec/cm ²)	Br ₂ Flux Adjusted to Asahi 3.3E-9
A-1	0.52	1.19	0.55	6.3E-9	6.8E-9
A-2	0.51	1.17	0.50	5.5E-9	5.8E-9
A-3	0.50	1.17			
B-1	0.51	1.24	0.53	6.5E-9	7.1E-9
B-2	0.51	1.23	0.50	6.1E-9	6.5E-9
B-3	0.51	1.23			
C-1	0.54	1.07	0.52	7.2E-9	7.8E-9
C-2	0.52	1.02	0.55	6.3E-9	6.7E-9
C-3	0.54	1.00			
D-1	0.52	0.75	0.50	7.1E-9	7.1E-9
D-2	0.52	0.81	0.49	7.0E-9	7.3E-9
D-3	0.49	0.82			
Asahi	0.58	1.21	0.58	3.05E-9	
SF600	0.58	1.18	0.58	3.11E-9	
(baseline)	0.58	1.14	0.58	3.23E-9	
	0.57	1.28			
	0.57	1.27			
	0.57	1.26			

Note: A Br₂ flux of 3.3 E-9 moles/sec/cm² is the standard value for the Asahi SF600 baseline separator.

The energy needed to drive (or that is given off by) a chemical reaction is the enthalpy (ΔH). Of this energy, only the free energy (ΔG) is available for electrochemical use. The remainder of the energy is tied to the entropy of the system (ΔS). In the following well-known relationship, the enthalpy is related to free energy by the entropy:

$$\Delta H = \Delta G - T\Delta S .$$

The $T\Delta S$ term is called the "electrochemical Peltier heat." It is defined as the energy needed to maintain a constant temperature for an electrochemical reaction. The actual energy loss mechanism results from a combination of solvation energies, electrolyte mixing, and injection of electrons into the conduction bands of the

electrode. The theoretical maximum energy efficiency is limited by the size of the $T\Delta S$ term, and is determined by the $\Delta G/\Delta H$ ratio. For zinc/bromine, the maximum energy efficiency is equal to 91%.

Independent measurement of the electrochemical Peltier heats for each electrode has been reported (*Journal of the Electrochemical Society*, 125 and 131). In a further test, the efficiency of the electrode reactions under "free discharge at steady state" were measured. In this test, the electrodes were essentially shorted except for the resistance of the ammeter in the connecting lead. The measured energy efficiency was 82%. This measurement included all three of the energy loss terms mentioned previously, but did not include any losses due to practical battery operation such as shunt

currents or separator resistance. Therefore, the 82% energy efficiency represents a reasonable ultimate goal to strive for in the laboratory.

It is well known that some batteries, such as the nickel/hydrogen battery, cool slightly when charging and that the lead acid battery does not get as hot as it could when discharging. These effects are simply the result of the electrochemical equivalent to heats of reaction. For example, when some salts are dissolved, the solution heats, and when other salts are used, the solution cools. The effect occurs for the zinc/bromine battery as well, and a first-order calculation of the heating and cooling has been done.

The electrochemical heat can be found by first looking at the thermoneutral potential, $E_t = -\Delta H/nF$ (n =moles of electrons, F =Faraday's constant). If the thermoneutral potential is below the reversible voltage, $E_r = -\Delta G/nF$, the battery will cool on discharge. If the E_t is above the reversible voltage, the battery will cool on charge. The values of the E_t and E_r for the zinc/bromine battery are 2.019 and 1.818 V respectively. The amount of heat or cooling is found by comparing the difference between the operating voltage and the E_t . If they are equal at some point, there will be no electrochemical heating or cooling. Other factors are also important. The ohmic resistance, overvoltage losses, and self-discharge reaction always generate heat in the cell. The reaction of bromine with quaternary ions generates heat reversibly. When bromine is removed from the complex, the electrolyte is cooled.

A spreadsheet calculation including each of the heats shows that the heating and cooling processes offset each other to an extent, but more heating occurs on discharge than on charge. The electrochemical cooling

process on charge is countered by the complex-formation heating. A reverse matching happens on discharge. The results of the spreadsheet calculations for a 25-A constant current cycle are shown in Table 4-13, with the heat values given in W. For comparison, the electrical power supplied to, or received from, the cell is also included.

The energy lost from the battery should be approximately equal to the heat generated. In a hypothetical 4 hr charge/3.5 hr discharge cycle, 100 Ah and 191.2 Wh will be put into the battery, and 87.5 Ah and 150.9 Wh will be taken out. These values are equivalent to 87.5% CE and 78.9% EE, a reasonable representation of actual laboratory data. The heat will be 18.64 Wh evolved during charge and 30.63 Wh evolved during discharge. Finally, 40.31 Wh of electrical energy were lost during the cycle, and 49.26 Wh of heat were calculated to have been generated. Ideally, these two numbers should be equal, but considering all of the approximations that had to be made in this first-order calculation, an 18% overestimation of the heat generated is quite reasonable.

The calculation shows that one-third of the total heat can be expected during charge, and two-thirds will come out during discharge. Therefore, the cooling system should be sized large enough to handle the higher rate of heating expected during discharge. This calculation has not included heating from parasitic losses such as the pumps and shunt currents that would need to be included to calculate the total battery cooling requirement.

Table 4-13. Calculated Heat* and Electrical Power in a Single Cell for a Constant Current Cycle at 25 A

	Charge @ -25 A	Discharge @ 25 A
Electro-Chem, W	-2.69	7.37
Self-Discharge, W	2.02	2.02
Complex Formation, W	2.98	-2.98
Ohmic, W	<u>2.34</u>	<u>2.34</u>
Total Heat, W	4.66	8.75
Electric Power, W	47.79	43.10

* Sign Convention: Negative sign shows heat absorbed by the battery.

Practical Cooling Requirements

In a test using a 30-kWh-size V-design battery, a cooling ability of about 2 kW was found to be sufficient to keep the temperature from rising in a baseline charge/discharge cycle. Data were taken from tests of a 200-cell battery made of four 50-cell stacks. All four cell stacks were connected to a single set of anolyte and catholyte reservoirs. The anolyte reservoir was cooled by water circulating through a plastic tubing heat exchanger. The cooling water was switched on whenever the anolyte temperature went above a preset temperature, typically 30°C.

The basis of the cooling calculation is simply that if the cooling is sufficient, the temperature will not rise. The total amount of heat to be removed is known from the efficiency. If the temperature is observed to rise, then the cooling rate must have been slower than the heating rate. In the three cycles used, the temperature did not rise during the charge, but did rise during two of the discharges.

The heat generated in the battery can be divided between the charge and discharge periods. It is estimated from previous calculations that about one-third of the heating occurs during charge. The heat capacity (C_p) of the battery is assumed to be about 0.9 Wh/kg-deg (the C_p of water is 1.164 Wh/kg-deg). The results listed in Table 4-15 show the calculation of the total heat in each cycle, how it was allocated to the charge and discharge portions of the cycle, and how some was taken up by the battery temperature increase. The final heating rates shown in Table 4-14 are also the effective rates of the water cooling system. There were no temperature increases observed during charge. It is clear that up to a heating rate of 2.2 kW, the cooling system was adequate

to hold the temperature constant. However, when the cooling demand was increased to 4.5 kW and higher, the battery temperature increased. The second two cycles were discharged at higher than baseline current, which explains the higher heating rates.

Therefore, the cooling system as it was installed and operated had sufficient capacity to cool 2.2 kW but not 4.5 kW or higher discharges.

Environmental Impact

A literature study has been started to predict the environmental impact of ZnBr₂ batteries. Some initial results are given here; however, this study will be continued to collect more information. The environmental effects might occur as the result of an accident while batteries or electrolyte were being transported or might be caused by a serious mishap at the electric utility station. The immediate cause of an incident would be an uncontained spill of electrolyte. The electrolyte consists of an aqueous solution of ZnBr₂, ZnCl₂, bromine, and a quaternary ammonium ion compound such as MEP bromide or MEM bromide.

Zinc Bromide

Zinc bromide is a relatively benign salt with a relatively low toxicity. The Department of Transportation hazard notification level for zinc bromide spills is 1000 lb. Once spilled, zinc bromide remains highly soluble in water and will readily be diluted and rinsed away. Therefore, it would not be expected to remain at the spill site, but would be washed away with rainwater and normal hydrological conditions.

Table 4-14. Battery Cooling

	VL24/Cycle 3	VL24/Cycle 4	VL24/Cycle 5
Energy Charged, kWh	40.9	59.8	40.9
Efficiency, %	70.8	54.0	50.2
Temperature Increase During Discharge, °C	0	27.5	21.7
Total Heat Generated, kWh	12.0	27.5	20.4
Heat Removed in Charge, kWh	3.6	8.3	6.1
Heat Removed in Discharge, kWh	8.4	7.0	4.6
Heat for Battery Warming, kWh	0	12.2	9.7
Heating Rate in Charge, kW	0.8	1.3	1.4
Heating Rate in Discharge, kW	2.2	4.5	6.9

The biological effect of zinc bromide is primarily due to the zinc ion. At high levels, it is toxic to invertebrates and fish. The EPA Acute Criteria (maximum) in soft water is 0.18 mg/l, and the Chronic Criteria (30-day average) is 0.047 mg/l. Typically, the toxic effects are decreased with increasing hardness. In a test of the effect on furoid algae, a 50% reduction in growth rate was observed at zinc levels of 5 to 10 mg/l. Zinc is already present in the runoff water from many highways and levels of from 0.16 to 22 mg/l have been measured. Since it is rapidly diluted and carried away, it has not been a serious problem in the national watershed to this point.

Bromine

Bromine is a liquid at room temperature and pressure. It is widely used in the sanitation of pools and hot spas. In the ZnBr₂ battery, it is nearly completely in the form of a chemical complex formed with the quaternary ammonium complexing agents MEPBr and MEMBr. The range of bromine dispersal is limited by the uptake of bromine. Even though the reactivity of the bromine is reduced by the complexing action, the bromine would still be expected to oxidize most organic materials that it contacts. This results in the formation of an innocuous bromide salt. Bromine also is readily absorbed into water, reacting to form soluble bromine as well as hypobromic acid (HOBr) and hydrobromic acid (HBr). Both are reactive, although less so than bromine.

Quaternary Ammonium Ion Salts

The environmental impact of the quaternary ammonium ion salts has not been directly determined. It is expected to be quite low, however. Similar compounds are used as sequestering agents in sewage treatment, and other derivatives are used in topically applied sun-blocking sun tan lotions.

Technology Evaluation - SNL

The objective of battery technology evaluation is to evaluate advanced rechargeable cells, modules, and batteries from developers working under OEM contracts. Performance and operating characteristics, as well as cycle-life data and failure modes, are determined. This information is used to improve the design and operation of all battery technologies.

The tasks being performed under this SNL activity include:

1. Evaluate 8-Cell Zinc/Bromine Battery Stack
 - 1.1 Conduct life-cycle tests and monitor performance
2. Evaluate Two 50-Cell Battery Stacks in Parallel
 - 2.1 Perform baseline life-cycle tests
 - 2.2 Perform several series of no-strip cycles

Task 1. Evaluation of 8-Cell Battery

During FY92, testing was completed on the 8-cell, 1-kWh zinc/bromine battery from the utility battery development contract with JCBGI. This battery, designated as SNL #518, featured a double-weld bead in the center of the flow frame to help prevent splitting of this internal seal. In previously tested batteries, the loss of this seal led to failures. In addition, the battery station was built such that the levels in the reservoirs were controlled by sealing the catholyte reservoir tightly after the system had stabilized at startup. The air head above the catholyte either pulled a vacuum if the level fell or built pressure if the level rose. By sealing the reservoir, the levels on both sides remained relatively constant. A photograph of this battery is shown in Figure 4-8.

Figure 4-9 is a plot of the battery efficiencies for all the charge/discharge cycles run on SNL #518. This includes a total of 26 cycles, at a zinc loading of 90 mAh/cm², which were run at JCBGI before it was shipped to SNL. These cycles were considered baseline cycles where the battery was charged for 4.5 hr at a charge current of 23.5 A. The battery was then discharged at a 24.4-A rate to an end-of-discharge voltage of 1 V/cell. The efficiency of this battery was calculated from the values obtained from the charge/discharge portion of the cycle. The battery was then completely discharged to 0 V/cell. This plot provides an overall picture of how the battery performed over the 273 cycles. During the first 150 cycles, a gradual loss in efficiencies was observed with a loss in energy efficiency of less than 3%. The results obtained on the last cycle run at JCBGI and the first few cycles run at SNL were close to each other. The CE was 88.7% while the energy efficiency was 75.1% and the voltaic efficiency was 84.7%. However, after 12 cycles had been completed at SNL, a fairly substantial decline in efficiency was observed. This decline was caused by an imbalance in the electrolyte reservoirs. The valve in the 1/4-in tie-line between the reservoirs, which is used to balance these reservoirs, was left partially open. Once the reservoirs were balanced and the valve was closed, the battery efficiencies returned to values close to the JCBGI results.

As mentioned previously, by sealing the catholyte reservoir, the levels on both the catholyte and anolyte

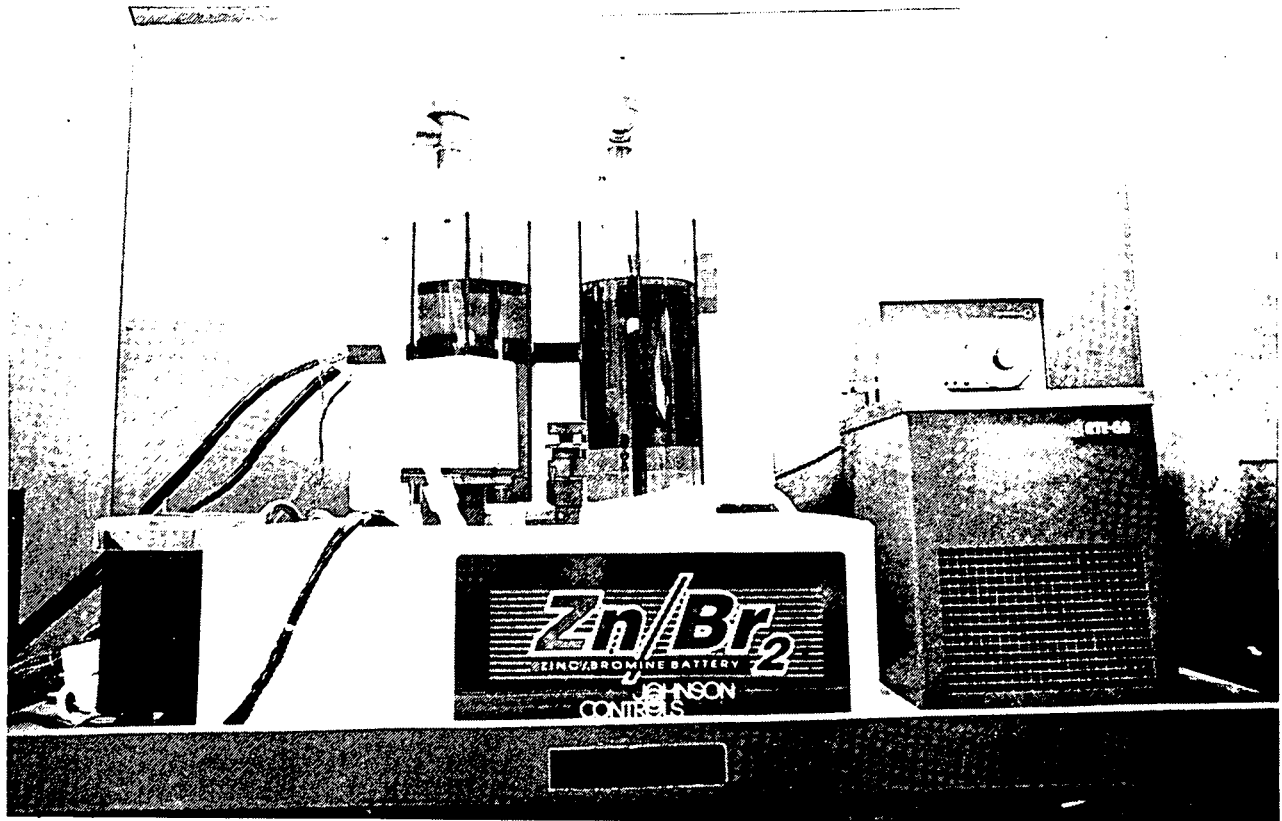


Figure 4-8. 8-Cell, 1-kWh Battery (SNL #518).

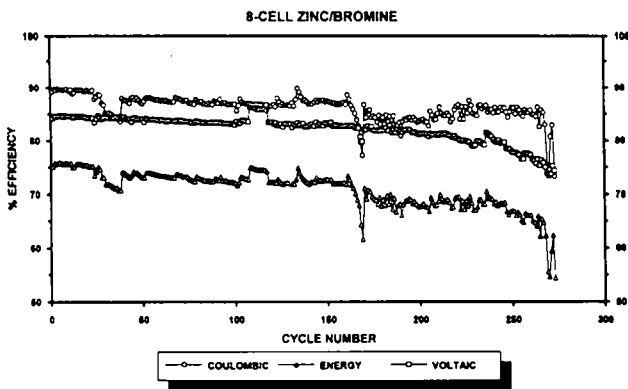


Figure 4-9. Battery Efficiencies, SNL #518.

reservoirs remained relatively even. However, a tight seal was difficult to achieve on this battery. In addition, the catholyte pump pressure tended to decrease from cycle to cycle. Because of either or both of these problems, a gradual decline in efficiency was observed over several cycles; thus, balancing procedures were required periodically to return the efficiencies to their initial values. This pattern occurred several times during the life of the battery and can be seen on the efficiency plot between cycles 50 and 100. During the first 100 cycles, the overall loss in energy efficiency

unrelated to the balancing problem was approximately 2%.

The majority of the first 150 cycles were baselines; however, two other types of cycles were also run. Between cycles 108 and 117, the discharge current was lowered from 24.2 A to 13.7 A. This produced an increase in both voltaic and energy efficiencies. The other type of test performed on the battery was a series of no-strip cycles. The first set of five no-strip cycles occurred between cycles 133 and 137. An increase in coulombic and energy efficiency occurred during the first three no-strip cycles but started to decline on subsequent no-strip cycles. A series of baseline cycles was then performed, and their efficiencies were the same as before the no-strip cycles.

Most of the cycles from 150 to 273 were also baselines. However, a second set of no-strip cycles was started on cycle 158 and inadvertently continued for an additional 15 cycles, through cycle 172. Results of the early no-strip cycles of this set were similar to what was seen on the first no-strip cycle set. However, as the no-strip cycles continued, the efficiency of the battery declined drastically, indicating an accumulation of zinc on the anodes. The concern at that point was the excessive amount of zinc that may have been deposited on the anodes and had formed dendrites that could punch holes

in the separators. Baseline cycles were immediately started to determine if the battery was damaged. Results indicated that, after the excessive no-strip cycles, the efficiency values became unstable, and a loss of approximately 6% in energy efficiency was seen. This unstable condition continued for the duration of testing on this battery. Electrolyte reservoir balancing could contribute to this unstable efficiency condition; however, it is more likely that running 15 no-strip cycles played a larger role in the unstable performance of the battery. Toward the end-of-life, a fair amount of carbon seemed to be coming from the stack, and it affected battery performance. Finally, during the last 10 cycles, a sharp decline in efficiencies was observed and the battery was removed from test when the energy efficiency dropped below 60%.

The battery was dismantled and returned to JCBGI for post-test analysis. The electrolyte was removed and tested in the minicell; the quality of the zinc deposit was good. With fresh electrolyte, the efficiencies of the cell stack improved only slightly. The average values of the last five cycles at SNL are compared to those of the five cycles run at JCBGI in Table 4-15.

After a total of 278 cycles, the cell stack was torn down at 100% SOC in the presence of visiting SNL personnel. There was a normal amount of warping in the bipolar electrodes. In one cell, on both of the electrode panels, there were a few dendrites that penetrated the separator. However, there was no indication that the dendrites had reached the anode to complete an electrical short. The zinc plating was completely absent from one corner of bipolar electrodes #6 and #7. Corresponding to this corner, the separator was severely blistered. Based on the battery performance and the evidence of the teardown, it was concluded that the cycle life was brought to a close by electrode over-voltage.

Task 2. Evaluation of Two 50-Cell Stacks in Parallel

The next deliverable from the utility battery contract with JCBGI was a 15-kWh unit that consisted of two 50-cell stacks assembled into a parallel configuration. The testing goals of this battery were to determine cycle life under baseline and no-strip conditions and to determine if the vibration welds on larger stacks hold as well as on the 8-cell units. A total of 20 charge/discharge cycles was placed on the two battery stacks prior to delivery to SNL. All of these cycles had a zinc loading of 90 mAh/cm² and were run under baseline or no-strip conditions.

On February 4, JCBGI personnel delivered and installed the two battery stacks at SNL. A photograph of the stacks, reservoirs, and plumbing is shown in Figure 4-10. The SNL number assigned to this battery was 526. A mutually agreed upon test agenda was followed for the life of the battery. The cycling formats specified in this test agenda were designated as standard baseline and no-strip regimes. The standard baseline sequence was a 4.5-hr charge at a 46.8-A rate, a 1-min rest at open circuit, an approximate 4-hr discharge at a 48-A rate to 1 V/cell, followed by a complete strip to essentially 0 V. The no-strip regime was a 6-cycle set in which cycling proceeds continuously in a format similar to a baseline, but there was no stripping until the end of the sixth cycle. A 2-min rest at open circuit was allowed between each no-strip cycle. A battery temperature of 30°C ± 1°C was maintained throughout the tests.

A technique used in the previous battery to maintain balance between catholyte and anolyte, was unsuccessful on this battery. An unbalanced condition continually occurred and prevented SNL from cycling the battery during non-working hours. On April 28, JCBGI visited SNL and installed a cross-over tube between the anolyte and catholyte reservoirs. This modification provided an

Table 4-15. Final Average Efficiencies of SNL #518

	CE%	VE%	EE%	Trans%	Resid%
Last 5 cycles at SNL	77.3	74.1	57.3	11.4	9.8
Last 5 cycles at JCBGI*	83.7	70.5	59.0	7.2	9.1

* with fresh electrolyte

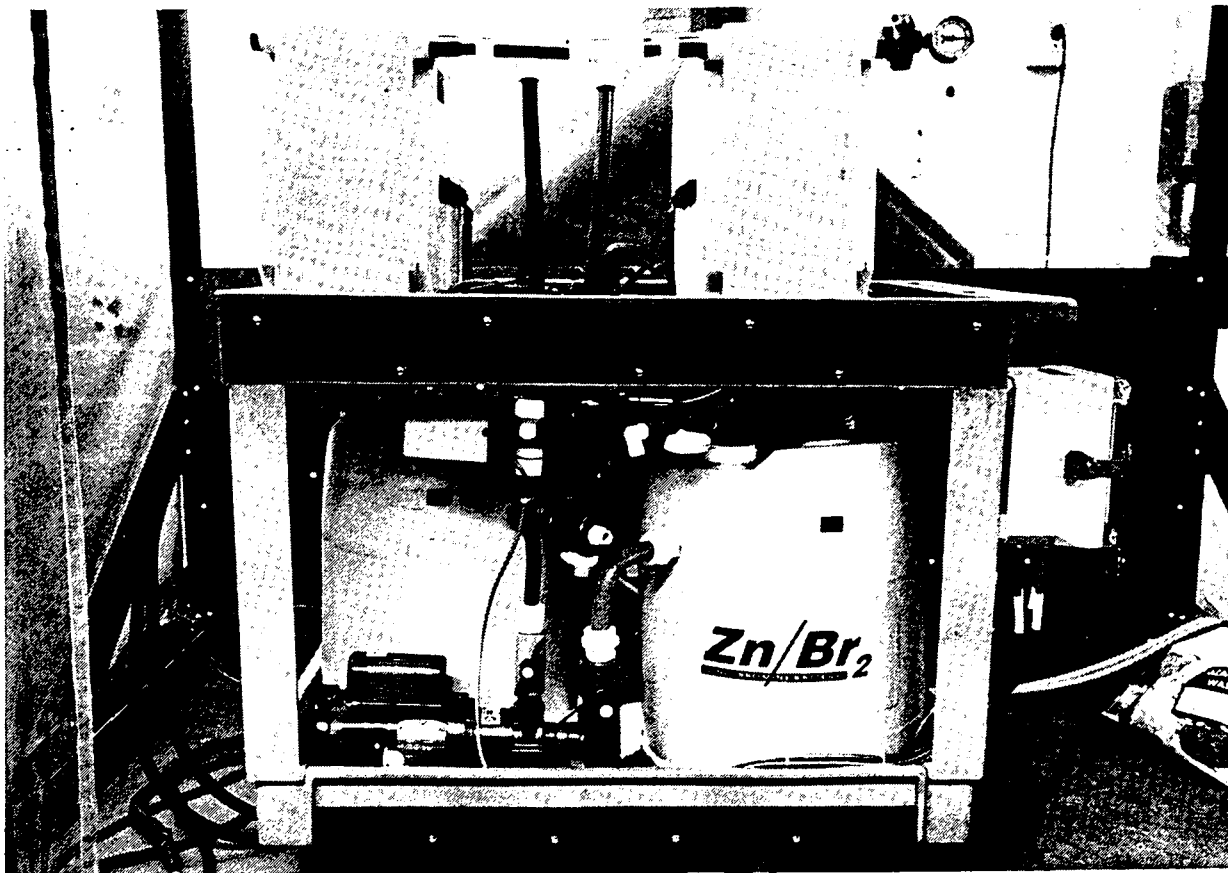


Figure 4-10. 15-kWh Unit, Consisting of Two 50-Cell Stacks in Parallel (SNL #526).

overflow path between the reservoirs if there was any imbalance. The change also eliminated a negative pressure problem in the catholyte reservoir that caused inward bowing to occur on two different occasions. With this modification in place, SNL was able to cycle the battery continuously, without concern of a potentially large electrolyte spill.

Figure 4-11 is a plot of the battery efficiencies for all the charge/discharge cycles performed on SNL #526. A total of 200 full cycles was performed on the battery, and this includes 20 cycles that were run at JCBGI before the battery was shipped to SNL. The plot indicates a very gradual decline in efficiency over the cycle range. This decline appears to be approximately the same as that seen on battery #518, the 8-cell stack. A 2.6% loss in coulombic efficiency, a 4.4% loss in energy efficiency, and a 2.6 loss in voltaic efficiency were measured between cycle 1 and 187 (the last baseline run). Running several no-strip cycles in a row does not appear to have affected the performance of the battery. The only abnormal results over the 200 cycles completed occurred on cycles 31 and 154. The cause in both cases was due to a load failure in the battery cycler that shortened the discharge length.

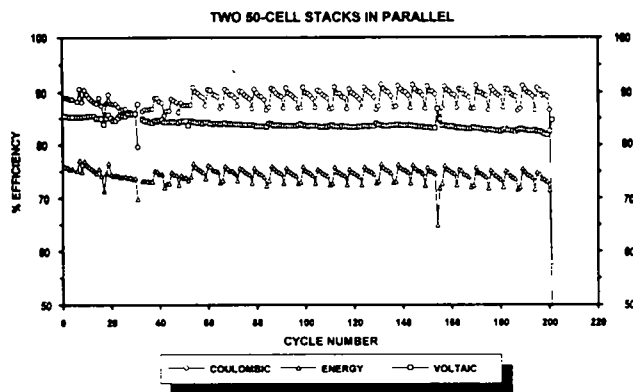


Figure 4-11. Battery Efficiencies, SNL #526.

On the morning of Thursday, August 20, a 6-cycle set of no-strip cycles was started. The first cycle of this set was completed late in the afternoon bringing the total number of cycles on the battery to 200. The voltage and current for this cycle were normal.

The second cycle completed the 4-hr and 30-min charge portion at 7:50 PM and the discharge portion was started at 7:53 PM. During the discharge, a severe lightning storm occurred in the Albuquerque area, and at 10:15 PM, a very short power outage caused the latching relay in JCBGI's control box to open. This relay removed power to both the catholyte and anolyte pump motors. However, SNL's cyclor continued to operate. To restore power to the motors, a manual reset switch must be pushed. With these pumps off, electrolyte ceased to circulate through the stacks. At 10:29 PM, the battery completed an abbreviated discharge (discharge time = 2 hr and 36 min; a normal discharge takes approximately 4 hr). At a discharge current of 47 A, a total of 122.8 Ah was removed from the battery and the discharge terminated on voltage. The nominal cutoff voltage is 1 V/cell (50 V on each stack). On this cycle, the end-of-discharge voltage was 38.15 V and the drop in voltage was rapid. Figure 4-12 is the voltage plot for cycle 201 showing when the power outage occurred and the rapid voltage decline.

During this time, both stacks heated up and probably several vibration welds, which hold the frames together, separated. There was evidence of damage to the top of both stacks. On the top of the stack over the catholyte reservoir (right reservoir in the photograph), there was a small amount of catholyte electrolyte that had leaked from a damaged weld. On the top of the stack over the anolyte reservoir (left reservoir in the photograph), there was a dark streak running diagonally across the stack. This stack also had a leak on its bottom side. No thermocouples were connected to the stacks so temperature was not recorded. Temperature was monitored in the anolyte reservoir, but with the pumps off, the electrolyte was not circulating. The maximum temperature recorded by the reservoir thermocouple was 40°C.

The battery failure was discovered the following morning, and after a cleanup period, the battery was fully discharged. Attempts were made to determine the extent of the damage to the battery through additional

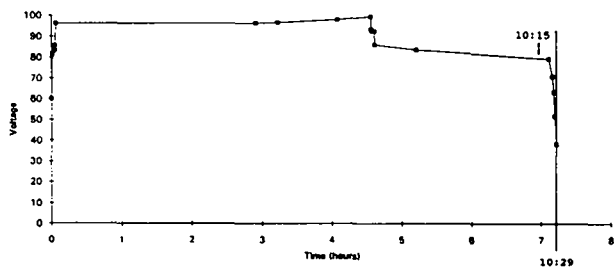


Figure 4-12. SNL #526 Voltage Plot for Cycle 201.

cycling; however, this was unsuccessful. The battery is presently being dismantled and will be returned to JCBGI for post-test analysis. SNL and JCBGI will meet to discuss the sequence of events prior to the failure, and recommendations will be made by both parties before the next deliverable is tested at SNL.

JCBGI has proven that 50-cell stacks can be constructed with no leaks in the vibration welds. SNL #526 performed extremely well while on test. Prior to the lightning storm, only two small leaks were encountered. One leak was at the heat exchanger input to the anolyte reservoir and the other at a fitting on the bottom of the anolyte reservoir. Both leaks were easily repaired and testing continued. Also, a poor connection in the thermocouple control (Dyna-sense) unit gave an erroneous temperature reading. This problem was corrected by cleaning a connector. It is estimated this battery could have performed well for an additional 50 to 100 cycles before a large loss in performance would have been expected.

Applied Research - SNL

Durability of Carbon-Plastic Electrodes for Zinc/Bromine Storage Batteries

A study to examine the effects of electrolyte on glass-filled HDPE carbon-plastic electrodes was completed. Two electrode materials, which were formulated by personnel at JCBGI, were evaluated and were designated HDPE-1 and HDPE-2. Samples were aged for six months at 40°, 50°, and 60°C as well as at ambient temperature. The electrolyte simulated the chemical composition of the electrolyte in a fully charged battery.

The samples were characterized, and HDPE-1 and HDPE-2 were found to contain 19% and 31% glass, respectively. Sorption of electrolyte by the electrode material was followed by weight gain and was found to be greater for HDPE-1 than HDPE-2. Probably this is because HDPE-1 has a higher polymer content than HDPE-2. Both samples sorb electrolyte constituents that cannot be washed away with water, and the difference between the weight gain of the two materials becomes more pronounced when the samples are washed with water and dried as opposed to simply being wiped off and dried. The data on dimensional changes are scattered, but in general changes may be less for HDPE-2 with respect to length and width and were on the order of less than 2% for both samples. The data show a dramatic increase in thickness (12-19%) of both samples at 60°C.

No evidence was found for oxidative attack of the polymer or for change in the crystallinity of the polymer due to exposure to electrolyte. The storage modulus decreased by about 10% for samples at all temperatures. This decrease in mechanical properties is attributed to sorption of the electrolyte rather than chemical decomposition, however. Exposure to electrolyte did result in increased (up to 48%) conductivity. HDPE-1 showed greater increases than did HDPE-2, perhaps because HDPE-1 has a higher polymer content and sorbed higher amounts of electrolyte.

This work is in the process of being published as a SNL report, C. A. Arnold, Jr., *Durability of Carbon-Plastic Electrodes for Zinc/Bromine Storage Batteries*, SAND92-1611.

Complexing Agents for the Zinc/Bromine Battery Electrolyte

This project was requested by JCBGI and is being carried out as a cooperative project between SNL and JCBGI. The objective is to reformulate the electrolyte for the zinc/bromine battery using bromine complexing agents that will allow further improvement in performance (CE) and safety, especially at higher tempera-

tures. Several quaternary ammonium salts have been identified as candidate complexing agents, but these compounds are not commercially available. Therefore, one task of this project is synthesis of the candidate compounds. A second task is evaluation of the candidate complexing agents. The compounds will be screened for bromine complexation and for electrochemical performance. Measurements of bromine vapor pressure will also be made.

A contract was placed in mid-September with the University of New Mexico for the synthetic work. Procedures to synthesize and purify Quat A have been developed in the laboratory, and data are being collected to confirm the structure. Once the structure has been confirmed, an initial quantity will be synthesized for delivery to SNL. Literature work is in progress to identify procedures for the synthesis of Quat B. Procedures to do screening tests for bromine complexation are being developed and tested using quaternary ammonium salts already in use as bromine complexing agents. (The specific identity of the quaternary ammonium salts is JCBGI proprietary information, which is not to be publicly disclosed. Therefore, specific quaternary ammonium salts are referred to as Quat A or Quat B.)

5. Sodium/Sulfur Project

The sodium/sulfur technology is being progressed for use in UES applications primarily because lower life-cycle costs are possible compared to conventional battery options. This potential advantage results from projected lower capital costs, less required maintenance, longer service life, and high energy efficiency. Other benefits of this technology include

- **Operating flexibility** - more applications can be accommodated with a single battery plant or battery design because of the capability to operate continuously, at all states of charge and at moderate to high rates of discharge and charge.
- **Good energy and power density** - applications with volume or footprint limitations can be satisfied.
- **Insensitivity to ambient conditions** - because an effective thermal enclosure is required, heat rejection is relatively easy and battery operation is insensitive to changes in ambient conditions.

Based on system analyses performed to date, the sodium/sulfur technology could be used in most utility battery storage applications including load leveling, peak shaving, spinning reserve, frequency control, and transmission life stability.

The objective of this project is to progress the development state of the sodium/sulfur battery technology specifically for these UES applications. This project will continue until the technology is shown to no longer be viable for these applications or it is developed to the level that a commercial product can be ensured that can replace or enhance the immediate-term markets that will be or are being served by conventional battery technologies. During FY92, advancement continued under UBS Program support. The primary development activity was performed under a contract with BPI. Additionally, the performance of the BPI technology was evaluated at SNL. A description of the project and FY92 accomplishments are contained in the remainder of this chapter.

Utility-Battery Technology Development - BPI

The advancement of the UES sodium/sulfur technology continues to follow a generalized development strategy and phased approach formulated and used by SNL. The activities that have been completed, are ongoing, or are planned (specific to sodium/sulfur) can be categorized as follows: 1) component engineering that permitted the construction of effective and safe battery modules, in turn allowing the sodium/sulfur concept to be proved (1975 - 1990); 2) preliminary battery engineering and design for a single load-leveling application that allowed the advantages of the technology to be demonstrated (1989 - 1990); 3) iteration of component engineering to resolve specific utility-battery feasibility issues and identify long-term development requirements (1991 - 1992); 4) conceptual battery engineering to provide the basis for entering into relatively expensive battery-level engineering development (1992 - 1993); 5) prototype battery engineering to qualify the production processes and final product configuration (1994 - 1995); and 6) product engineering to scale-up production to commercial levels and satisfy institutional and regulatory requirements (1996 - 2000). A very important part of the two latter phases is the comprehensive evaluation and demonstration of complete battery systems at actual utility sites.

The development of the UES sodium/sulfur technology has been continued past the component engineering and preliminary battery engineering steps because recent utility systems analyses have substantiated 1) the true need for battery storage and 2) the benefits of the sodium/sulfur technology in these applications. Based on the status of the technology, a 2.5-yr, \$3.1M contract was placed in mid-1991 with BPI to complete the activities described in Categories 3 and 4 in the previous paragraph. Approximately half of this cost-shared activity will be performed inter-divisionally at SPL. In this contract, relevant utility applications are being identified, specific cell and battery hardware developed, preliminary engineering of utility battery

modules completed, and, finally, a full-scale battery plant concept will be designed. An important part of this work is the formulation of a solid definition of battery requirements, an activity that with increased involvement of the utility industry can finally be progressed. The continued need to reduce capital (first) cost and improve service life at the battery level is the focus of the development activity because these two areas remain the key issues impeding commercialization of the technology. In addition, attention is being focused on battery configuration and maintenance strategies, effective thermal management systems, battery safety both under intended and accident situations, and ultimately on reclamation.

Of importance, development of the sodium/sulfur technology at SPL for mobile applications is proceeding along a similar, but more accelerated path. Those improvements that are applicable to both types of end-uses (e.g., manufacturing technology, some materials and components, safety features) are being incorporated in this effort. However, work under this project is focusing solely on the specific needs for UES applications.

The actual tasks that are being performed under the Beta Power contract include the following:

1. Assessment of UES applications
 - 1.1 - Utility-application identification
 - 1.2 - Utility-application evaluation and selection
 - 1.3 - Detailed battery specification preparation
2. UES Cell and Battery Component Development
 - 2.1 - Cell component development
 - 2.2 - Cell development and qualification
 - 2.3 - Battery component development
3. Preliminary Engineering of UES Modules
 - 3.1 - Module design
 - 3.2 - Module fabrication
 - 3.3 - Module evaluation
 - 3.4 - Commissioning support
4. Full-scale Battery Plant Design
 - 4.1 - Utility-battery design
 - 4.2 - Performance and cost analysis

The remainder of this section contains a description of the results obtained during FY 1992.

Results

Task 1. UES Applications Assessment

As described later under Task 2.1, a new sodium/sulfur battery system concept has been formulated that is denoted as NAS-P_{ac} (for Sodium/Sulfur ac Power). A brochure displaying this concept and summarizing some of the benefits of the sodium sulfur advanced battery was developed and printed in late 1991. It is being used as a media to communicate and assess interest in advanced batteries for UES applications. The forum for its introduction was the Utility Battery Group meeting in San Diego. Later a presentation was made in May at the Utility Battery Group meeting in Albuquerque on the status of sodium/sulfur batteries and their potential benefits. These events have served to inform the utility community, in particular, of the types of applications, in which sodium/sulfur will be attractive, and of the DOE-supported development efforts underway at BPI toward providing an advanced product.

The results from these discussions have served to reinforce the observation that, in general, utility power applications of two to three hours or less appear to be favorable for battery energy storage. These include, for example, generic transportation (such as the San Diego Trolley and the New York Power Authority) and industrial peaking applications.

Application meetings have also occurred with the New York Power Authority, Oglethorpe Corp., and the Alaskan Energy Authority to investigate their battery energy storage needs, and with PGE to assess their interest in testing a NAS-P_{ac} module. There appears to be significant interest in the proposed compact battery design offered by sodium/sulfur, provided the system cost of the system can approach the \$1000/kW target. Analysis of the manufacturing volume impact on battery price suggests that this target could be met with orders in the range of 10 to 50, 300-kW battery energy storage systems per annum, depending on whether the applications are for one or two hours, respectively. This is an encouraging result from the standpoint of willingness to invest in manufacturing to support such a market.

Task 2. UES Cell and Battery Development

The majority of the activities in this contract are performed within this task. Its primary objective is the development and qualification of a sodium/sulfur cell and associated battery hardware specifically for UES applications. Considerable effort to date has been expended on Task 2.1 to allow these development activities to be efficiently progressed.

Task 2.1 UES Battery Design Study

The design of an advanced battery energy storage system is based on the use of replaceable sodium/sulfur battery modules with a 480-V ac, three-phase, 300-kW line commutated converter. For this system, the maximum battery voltage is limited to 500 V dc. The design, however, has not been restricted to the use of this converter topology; rather, a line-commutated version was deemed to offer the lowest cost and to require the lowest dc voltage (a distinct benefit for sodium/sulfur batteries). The battery for this converter is composed of two parallel modules x 4 series, for a total of 8 NAS-P_{ac} modules. The NAS-P_{ac} modules are rated for two hr of continuous discharge at full power. The initial design life of the battery is 1500 cycles to complete discharge. No maintenance is planned up to the point of module

replacement. Thermal management has been designed to be passive and intrinsic to the battery module design. The thermal enclosure utilizes a standard, non-evacuated, thermal insulation to minimize cost and maintenance. Heat loss is anticipated to be approximately 12 W/kWh, which amounts to a 6-8% impact on system efficiency for the majority of diurnal applications. This could be halved with an evacuated enclosure, albeit a more expensive option, for applications that require longer stand times.

The battery has been designed to fit within the existing 7.5-ft-height and 7-ft-width dimensions of the preferred converter design. As shown in Figure 5-1, the total depth of the NAS-P_{ac} unit is 14-ft, which allows modules to be arranged in tandem four series high. The overall package is completely transportable by truck or seabox.

A summary of the design features of the 300-kW battery system is given in Table 5-1. The electrical and operational characteristics of the NAS-P_{ac} battery module are given in Figure 5-2 as a function of cycle (time). The twin voltage and current curves represent beginning and end of discharge conditions. Note, in particular, the flatness of the voltage profile over time. Even with 38% of the strings failed, the battery working voltage variation is less than 22% from beginning to end

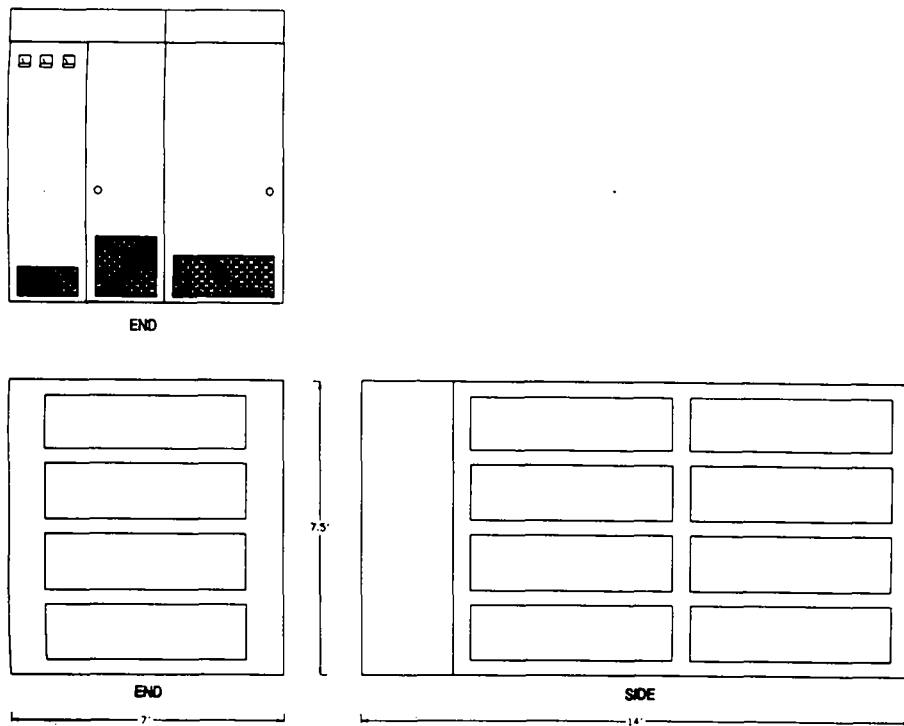


Figure 5-1. 300-kW NAS-P_{ac} Unit (2-hr Rated Duration).

Table 5-1. 300-kW x 2 hr ACUnit Battery Specification

- 300 kW Line-Commutated Converter: 480 VAC, 3 Phase
 500 - 320 VDC
 935 A (Max)
 Power Factor Correction: 430 KVAR Leading
 0.9 Lagging (Min)
- 600-kWh Rated Battery
 Composed of 8 NAS-P_{ac} Battery Modules
 Connected 2 Parallel x 4 Series
 Working Voltage Range: 464-444 (BOL); 443-374 (EOL)
- ACUnit Dimensions: 7.5 ft W x 7.0 ft H x 14 ft L
 Weight: Converter 7,200 lb
 Battery 25,000 lb
 Structure 1,500 lb
 33,700 lb (15.283 kg)
- 75-kWh Rated NAS-P_{ac} Battery Module: 125 VDC (nom)
 2 Layers of Cell Banks in Series
 6 Banks per Layer of 32 Parallel Strings
 5 Cell Series Strings
 TOTAL: 1920 Cells

Ext. Dimensions: 5.13 ft W x 4.84 ft L x 1.40 ft H
 Weight: 3125 lb (1417 kg)
 Life Expectancy: 1500 Cycles
 ($\alpha = 3500, \beta = 3.3$)

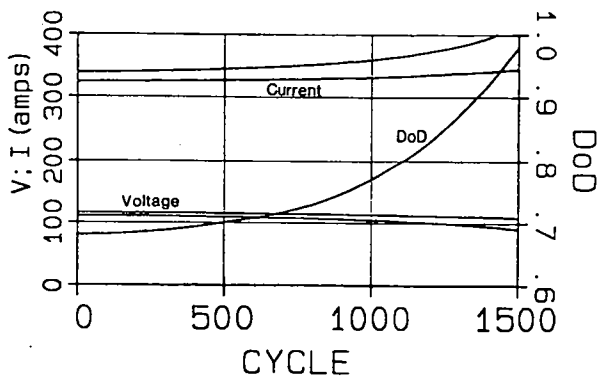


Figure 5-2. 75-kWh NAS-P_{ac} Module Performance at 2-hr Constant Power Discharge.

of life. The DOD reflects the end of discharge dynamic control in response to cell failures and cell resistance rise. Figure 5-3 shows the thermal control provided by the latent heat storage media located at cell interstitial sites within the battery module (see next two paragraphs

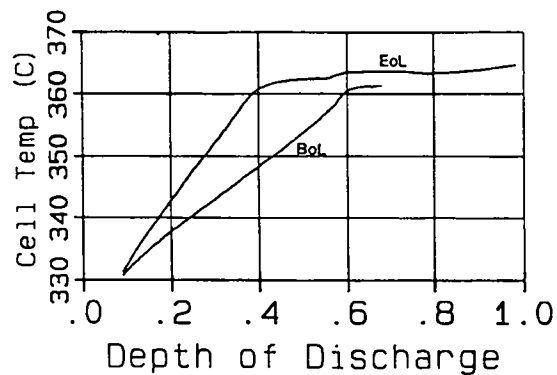


Figure 5-3. Power Discharge 75-kWh BES Module Performance, Temperature vs Depth of Discharge.

and Task 2.2.2). At the beginning of life (BOL), little, if any, of the LiCl/KCl eutectic ($m_p=355^{\circ}\text{C}$) is melted, while at the end of life (EOL), the salt is capable of maintaining cell temperatures below 365°C , while allowing the battery to deliver full power.

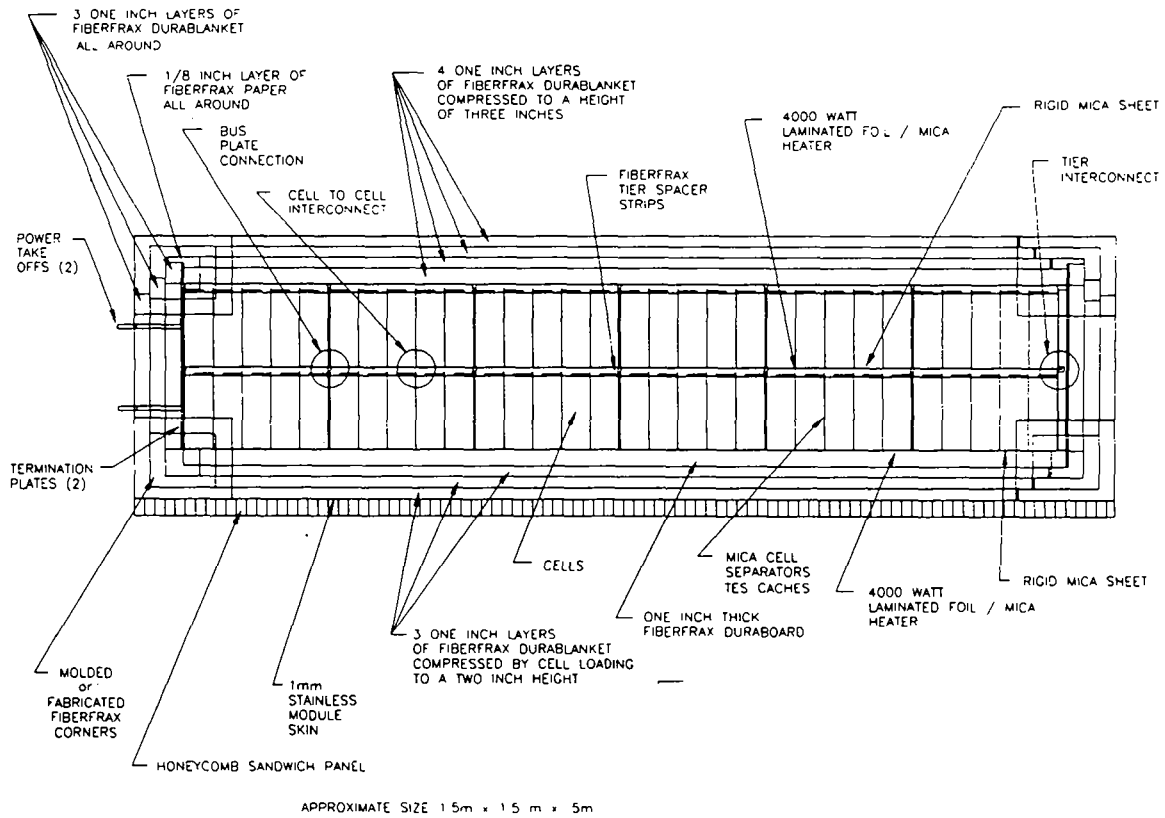


Figure 5-4. UES Battery Module, Cut-Away Side View.

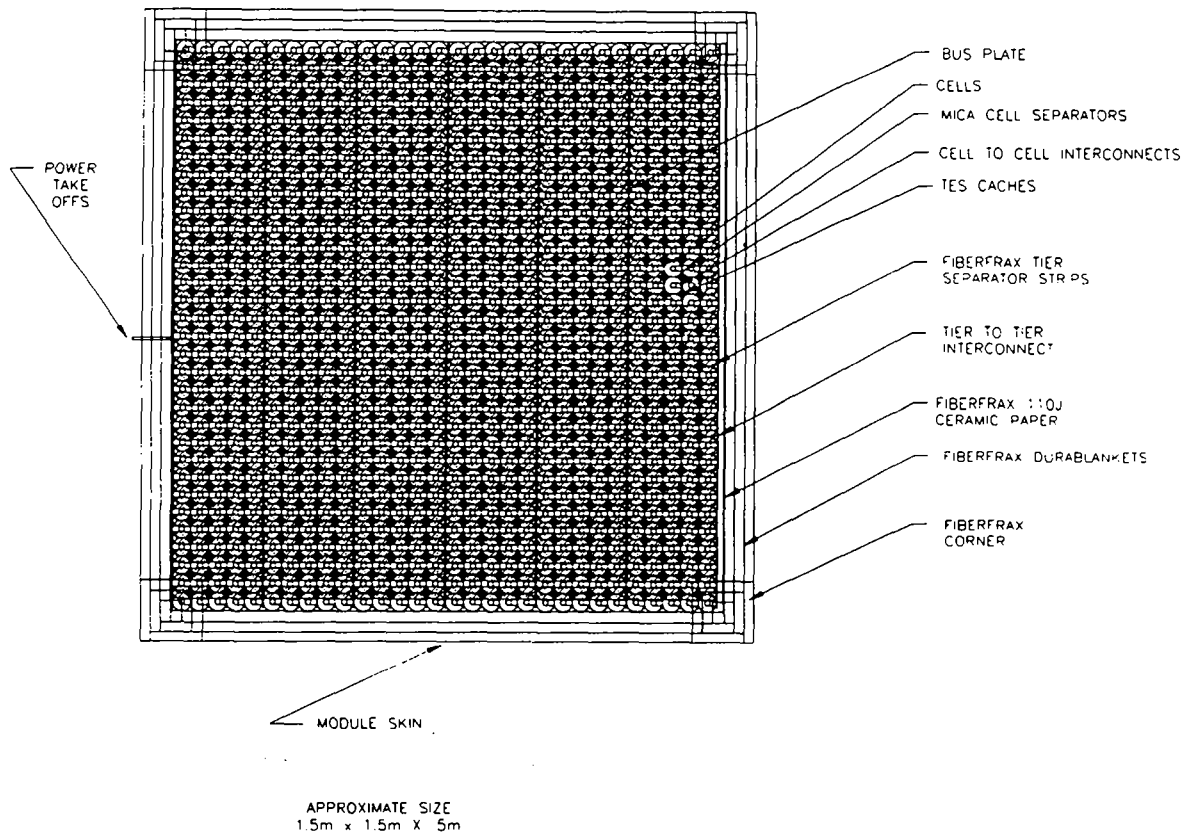


Figure 5-5. UES Battery Module, Cut-Away Top View.

Layout drawings for the NAS-P_{ac} module design are shown in Figures 5-4 and 5-5. Module height has been minimized by selection of a cell-to-cell interconnect scheme allowing in-plane series connections between cells. This approach makes voltage build-up independent of the number of vertical cells and maintains low intercell connection resistance. In a like manner, each tier (layer) of cells is connected to the tier above directly from cell top (lower tier) to cell bottom (upper tier) in order to minimize interconnect resistance. Selection of two "tiers" for this module design has been made primarily on the basis of thermal control considerations. By inspection (verified through analysis), it is apparent that in a two-tier arrangement, each tier of cells "sees" the same thermal boundary conditions. These are an essentially adiabatic center plane and five exterior walls.

Thermal control is effected, in part, through latent heat storage utilizing thermal energy storage capsules located between arrays of in-line cells. These caches of thermal salts are sized according to available interstitial space between cells, heat transfer capacity from cells to the salt and (thermal) energy storage requirements.

The module enclosure is a simple monocoque box that gains most of its stiffness through incorporation of a honeycomb sandwich panel as a base member. This design minimizes height of the enclosure and obviates the need for frame or internal support members to control deflection and cell location.

Assembly of each battery module is effected through a simple building block approach. First thermal insulation is installed in the bottom and around the sides of the single wall enclosure. (One side of the enclosure is left open for easy insertion and interconnection of cells, banks, and tiers.) Next a laminated heater is placed on the insulation. A termination plate and connecting stud are placed adjacent to the module wall with the stud extending out through an opening in the enclosure wall. Rows of cells, thermal energy storage capsules, and electrically insulating cell separators are then laid out and interconnected until a "bank" is built up. For reference, the term "bank," as applied to this module design, refers to the electrical networking of the cells into arbitrary series/ parallel arrangements that are integral to the module itself rather than to discrete blocks of cells that may be physically manipulated as such. At this point, a bank plate interconnects all of the cells in its bank in parallel. This process is repeated until the prescribed number of banks is installed for a tier and instrumentation sensors are laid in with the cells and banks. After layering of tier spacers and another heater atop a tier, the subsequent tier is built up in the same manner.

Finally, the remaining enclosure side and top are installed to complete the module assembly.

Task 2.2.1 Cell Component Development

Central Sulfur (c/S) Cell Design

The cell selected for development under this program is a c/S cell designed around the dimensions of SPL's XPB electrolyte. A c/S design was selected (over central sodium) because of the very long service life such cell configurations have exhibited to date at SPL. For example, a set of c/S cells have exhibited lives in excess of eight years under continuous cycling, and remain on test today. Thus, a c/S cell design is believed to offer the lowest risk approach to meeting the battery life requirements at an acceptable cost. Basing the cell design on the XPB electrolyte geometry was again a result of the desire to minimize the development risk. Processing for the XPB electrolyte was well established at the time the program began, and high-quality components were routinely being produced in sufficient quantities by SPL to supply the development effort. Further, since safe operation is a major goal of the contract, the XPB electrolyte size offers a conservative design basis.

A schematic diagram of the c/S cell design that is being developed is shown in Figure 5-6. Fabrication of the cell begins with the glass seal between the high purity alpha-alumina header and the beta"-alumina electrolyte. This glass bonded seal utilizes sodium resistant glasses that have been developed for this purpose under previous programs. This glazing operation is the first step in the assembly process because it is the highest temperature process. The next operation is the bonding of the safety tube and sulfur seal ring to the alpha-alumina header. Both seals are accomplished by thermocompression bonding in a single process. The sulfur seal ring is a direct aluminum to alpha-alumina bond while that between the mild steel safety tube and the alumina header is accomplished with an aluminum interlayer.

Following bonding, the mild steel outer container is welded to the safety can. At this point, an infill material is placed in the annulus between the electrolyte and the safety tube. The primary functions of the infill material are to act as a sodium wick to ensure that sodium is uniformly distributed over the surface of the electrolyte, to displace part of the sodium from the annulus limiting the amount of sodium immediately available to react with sulfur in the event of an electrolyte fracture, and to slow the flow of sodium to the reaction site in the event of an electrolyte fracture. Sodium filling is accomplished by pressure impregnating the infill. A

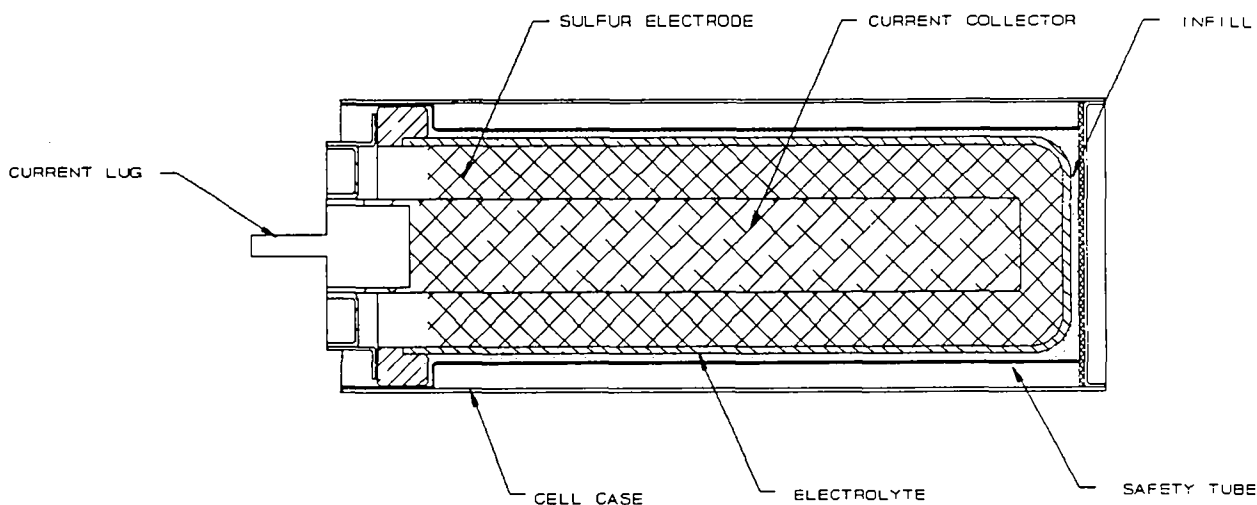


Figure 5-6. UES Central Sulfur Cell Design.

woven or expanded metal mesh is placed over the open end of the safety tube, and the end cap is inserted and welded into place.

The final assembly operations are installation of the sulfur electrode precast segments, followed by installation of the current collector assembly and welding the aluminum top cap to the sulfur seal ring forming the final cell closure.

Typical cell design characteristics and projected performance for the c/S UES cell are shown in Table 5-2.

Positive Electrode Components

The positive electrode (cathode) components have been carefully selected to minimize the potential for corrosion in sulfur and polysulfides. In addition, BPI continues to investigate alternate pole materials and coatings that might offer further corrosion resistance. Both in-cell and out-of-cell experiments are being performed in search of improved materials and processes.

Corrosion Testing. Corrosion-testing cells can provide relative life characteristics of different cathode materials in an electrochemically active melt without the added complications of other cell components.

Several electrode types have been tested, but the three described here showed the most promising results.

All samples tested were immersed in Na_2S_4 (except as noted) and heated to 330°C . Both an electrochemically active and a control electrode were exposed to the melt. The control electrode was electrically active for only one cycle per week. This procedure was followed to provide a means to distinguish degradation due to exposure and degradation due to electrochemical mechanisms. Figure 5-7 shows a schematic drawing of a typical test set-up used for these experiments. Baseline cycles consist of a 30-min anodic segment, a 30-min cathodic segment, each separated by a 15-to-30-sec open circuit period. During each half cycle segment, the potential between the reference and working electrodes is maintained at a constant level, and the working electrode current is recorded.

Chrome Plated 446 Stainless Steel – Samples 7 and 8 cycled for over 104 days, when the current densities suddenly decreased. As indicated in Figure 5-8, the change in specific current for both anodic and cathode potentials showed a mild upward trend, following the reduction in applied potential, but then turned down after about 300 Ah of charge had passed.

Table 5-2. c/S UES Cell Design Characteristics

Outside Diameter	44.0 mm
External Length	114.5 mm
Current Collector Diameter	14.0 mm
Sulfur Load	63.0 gm
Sodium Load	36.0 gm
Cell Weight	312.0 gm
Cell Volume	174.0 cm ³
Cell Resistance	14.0 mΩ
Theoretical Capacity (to Na ₂ S ₃)	35.5 Ah
Working Capacity	27.0 Ah
Power at C Rate	46.0 W
Specific Energy at C/2 Rate	155.0 Wh/kg
Energy Density at C/2 Rate	296.0 Wh/l

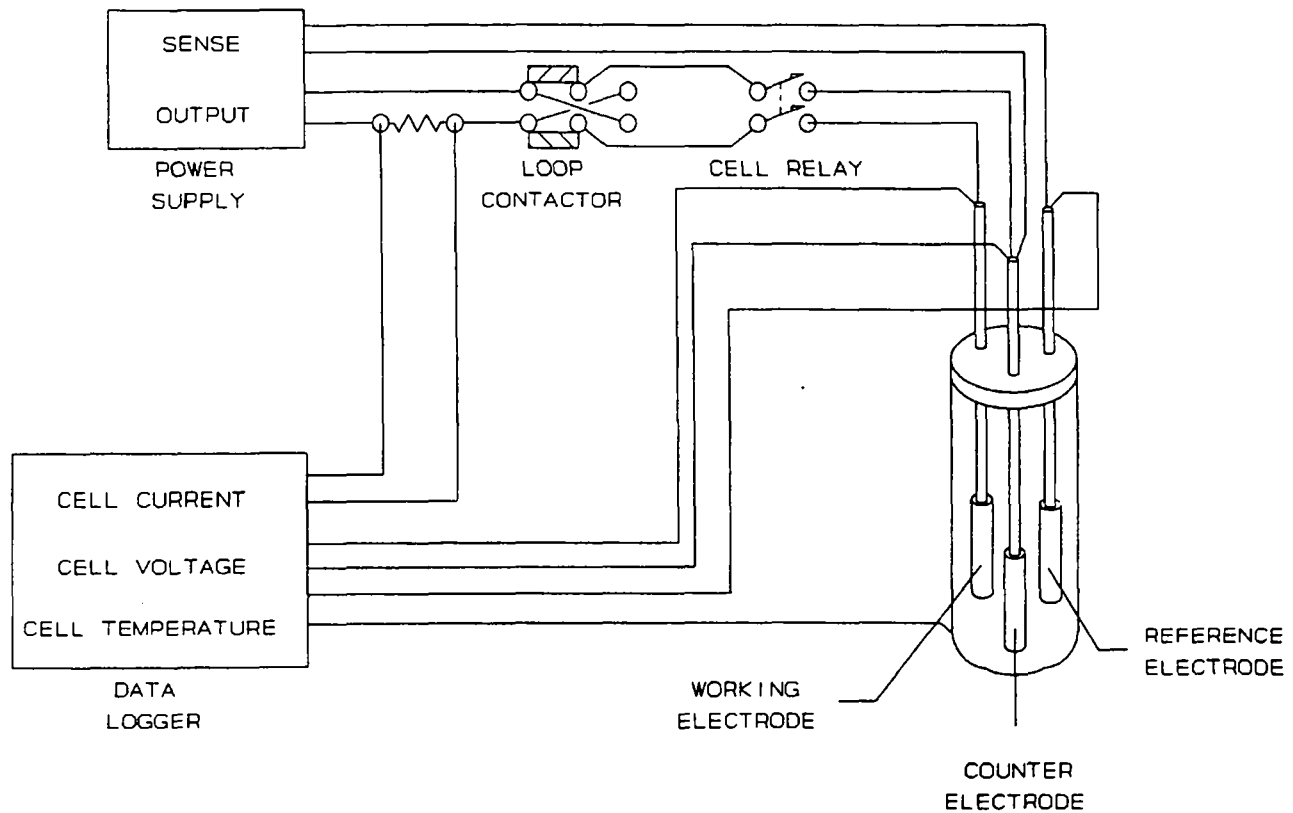


Figure 5-7. Typical Corrosion Cell Test Set-Up.

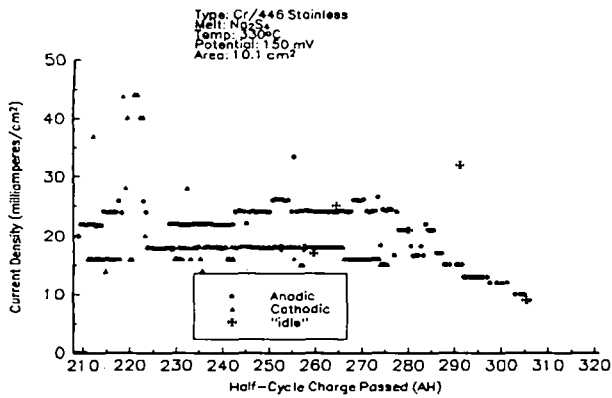


Figure 5-8. Electrical Performance for Chrome-Plated 446 Electrode Over the Life of the Experiment.

After the cell was cooled and removed from the furnace, the electrodes were removed from the test cell and examined. While the idle and active electrodes were visibly blackened (corroded), the section of the graphite counter electrode immersed in the melt had eroded to a tapered shape. The actual contact area of this working electrode to the melt was reduced, which would account for a large percentage of the observed change in current density of this sample.

The graphite reference electrode, which was exposed to the melt for the same time period as the working electrode but was subject to considerably less electrical cycling, showed relatively little erosion.

Molybdenum on Aluminum – Figure 5-9 shows a plot of the current density versus the exposure time (in days) of a molybdenum-plated sample to the melt. The upper and lower traces show the current density for the anodic and cathodic portion of the cycle to be decreasing gradually from about 34 mA/cm² (anodic) and 28 mA/cm² (cathodic) to 31 mA/cm² and 26 mA/cm² during the first 70 days, then falling more rapidly and

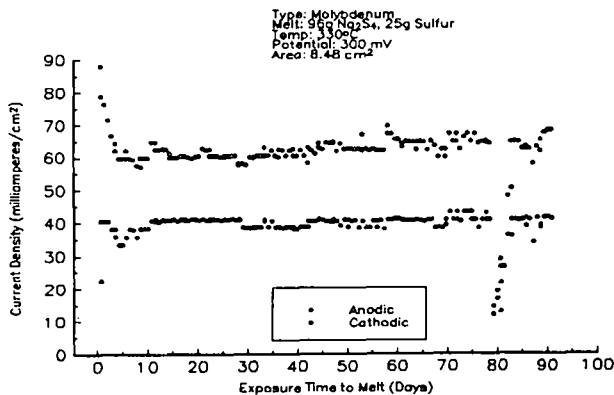


Figure 5-9. Electrical Performance for Flame-Sprayed Molybdenum on Aluminum Electrode, Over the Life of the Experiment.

eventually recovering. The cause of the decline and eventual recovery of the current density is likely a result of an unstable power supply, but this has not been verified. The current density eventually decreased and the cell was taken off test.

The color change of the sodium-polysulfide indicated that a leak to atmosphere may have been present at some time during testing. Oxidation of the polysulfide may have played a role in the decrease in current density. Both electrodes were physically examined and had a black coating (MoS₂) on the surface, but no spalling of the aluminum was seen. The electrical resistance of the samples, measured from the molybdenum surface to the aluminum current collector, was less than 0.25 Ω for both electrodes.

Pure Molybdenum in a Sulfur Saturated Melt – A flat molybdenum plate, 1 cm x 4 cm, was prepared from 0.032-cm-thick sheet stock. A 2-mm diameter molybdenum wire was welded along one long edge. The sample was then placed into a melt consisting of 96 gm of Na₂S₄ and 25 gm of sulfur. The cell was heated to 330°C and electrical cycling was started with ± 300 mV potential applied to the cell.

The initial average current density measured at the beginning of testing was approximately 85 mA/cm² and 45 mA/cm² with the sample anodic and cathodic respectively. As shown in Figure 5-10, the current density gradually decreased after 15 days of cycling to stable values of 60 mA/cm² and 40 mA/cm², for anodic and cathodic polarities, respectively. Testing was stopped after 128 days of cycling, with no change in current density.

Freeze/Thaw Durability Assessment. Freeze/thaw durability of c/S cells has long been a concern. In order to address this issue early in the program several freeze/thaw experiments were planned and executed. These

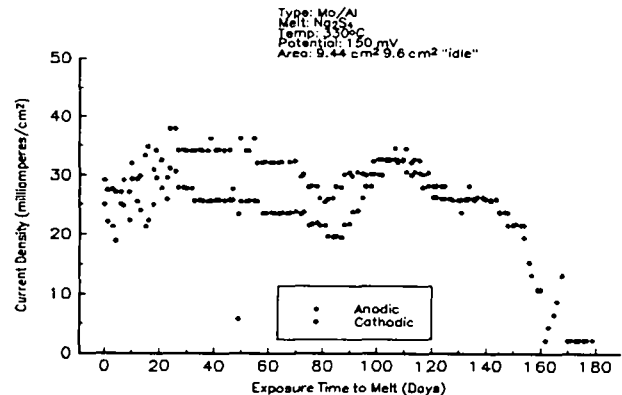


Figure 5-10. Electrical Performance for a Pure Molybdenum Electrode in a Sulfur-Saturated Melt Over Life of the Experiment.

initial experiments examined the behavior of a c/S cathode during thermal cycling.

A number of half-cell mock-ups were assembled and tested as follows. An aluminum rod acted as the current collector. Several graphite felt disks were placed over the aluminum rod to act as the graphite felt matrix of an actual cell. Sulfur was cast into the disks, and the assembly was allowed to cool. This "precast" was then inserted into an XPB type electrolyte, which was placed in a beaker of diffusion pump oil. The oil was used to ensure that the sample would be isothermal. Temperatures were recorded on an X-Y recorder as follows. The Y-axis recorded the difference between the oil temperature and the sulfur temperature, while the X-axis recorded the oil temperature. All samples were heated to 180°C. Heating rates were varied in an attempt to find an optimum heating rate to ensure cell survival.

In an attempt to determine the effect of heating rate, a sample was heated in six hours (30°C/hr), then cooled at the same rate. It survived its initial cycle, but failed during the heat-up on the second cycle. The next sample was heated in twelve hours (15°C/hr) with the same results; it survived its first cycle but failed during the heat-up on the second cycle. Both failures occurred at approximately 95°C, which corresponds to an expansive phase transformation in sulfur from the alpha to beta phase. All failures occurred at the base of the electrolyte where the sulfur density in the felt was the highest. The forces generated on the electrolyte during the expansive phase transformation caused the failures. The next experiment was an attempt to "outrun" the phase transformation. If the sulfur melts in the alpha phase, then the solid state expansion is avoided. To test this, a sample was assembled as previously described, but the heating rate was increased to 60°C/hr. The sample was cycled several times with no failures occurring.

The aluminum rod diameter was then changed to match the size of the current collector in an actual cell. The diameter increased from 0.25 in. to 0.55 in. It was planned to repeat the experiments for this larger diameter aluminum. However, at heating rates of 6, 12, and 24 hr, no electrolyte failure occurred, indicating that there is some critical current collector diameter, above which the probability of electrolyte failure is low enough for satisfactory cell durability.

The previous experiments addressed freeze/thaw durability with sulfur; however, in order to fully address the problem, a cell had to be completely assembled, electrically cycled, and then thermally cycled. This was performed with the first full cell built, which survived thermal cycling (see Section 2.2.3). Since the first cell,

several cells have been successfully thermally cycled between operating temperature and room temperature with no electrolyte failure.

SPL is providing the XPB beta"-alumina electrolyte for the c/S UES cells. The electrolyte resistivity is less than 0.5 Ω/cm^2 . In the c/S cell configuration, the electrolyte contributes approximately 40% of the overall cell impedance.

Thermocompression bonding is used to seal metal components of the two sulfur electrodes to the electrolyte header. Both seals have presented some unique problems. The sodium-side seal in a c/S configuration is a relatively large diameter seal, which requires attention to the thermal expansion mismatches between bonding surfaces. The sulfur-side closure requires the weldment of thin aluminum members. Both of these seals have required significant development trials and diagnostics to specify the process parameters required to achieve hermetic seals consistently. To date, BPI has achieved strong thermocompression bond assemblies. The negative electrode seal is still not quite hermetic, but this is due to the quality of the sealing surface of the thin safety tubes. Other tube materials and thicknesses are being tested in an effort to guarantee hermeticity.

Concurrent with the early seal trials, efforts were being made to find a suitable coating for the safety tubes, especially in the seal area. A protective coating is needed to inhibit the growth of a brittle intermetallic layer between aluminum and mild steel. Chrome plating seemed to be a likely candidate and was chosen as the coating material. Standard bright chrome was chosen for its lower cost compared to crack-free chrome. Seal samples were then assembled using chrome plated safety cans. These seals were characterized by low strength and brittleness. Through experimentation, a surface preparation of the mild steel was formulated that has enabled this combination of materials to be used. Although still not hermetic, it is now believed that the problem lies with the surface texture of the steel and not the seal.

After failure of the first chrome plated seals, a design change was initiated to make a safety tube that could withstand the environment for chromized coating. At this time, these tubes have been made and coated; however, no seals have been attempted.

Task 2.2.2 Battery Component Development

Battery component development includes the thermal management system, the cell interconnect, busplate and electrical isolation design and some fundamental studies in search of a viable failure device.

The battery module will utilize a conventional thermal insulation system using 3 in. of Fiberfrax Dura-blanket in a single skin. The tradeoff between the cost of the enclosure and the value of the heat loss yields an acceptable 4-yr payback at 3 in. thickness. The use of evacuated enclosure systems was eliminated based on cost and reliability over the design lifetime of the battery module and compounded by the large interior dimensions (4.5 ft²) of the enclosure. The module heat loss is anticipated to be 1150 W. In contrast, an evacuated system would offer 40% of this heat loss, but at a significantly higher cost. In applications that utilize the battery diurnally, the actual electrical parasitic loss associated with make-up heat is expected to be 6 to 8% of the electrical energy stored. It is recognized that there may be situations in which the need to minimize heat loss dominates the design considerations, such as long stand-by operation. In that case, an evacuated thermal enclosure will be considered, but this does not appear to be the best application for sodium/sulfur.

The module design incorporates a eutectic mixture of KCl-LiCl in separately sealed tubes located in the interstitial volume between in-line cells. Ten sample containers have been shipped to SNL for filling and final weld. Of these, seven have been returned to BPI for inclusion in cell string testing to verify the ability of the approach to arrest cell temperature rise. Assuming that the testing is successful, BPI will undertake all subsequent manufacturing of this component. The proposed additional use of this material within the central current collector of each cell will be investigated following the results of the external heat storage testing.

A design for formed separators between cells and thermal energy storage capsules has been completed. A forming tool is currently being fabricated, and trials are due to start shortly. This formed component will facilitate the assembly of the cells and thermal energy storage capsules into the module enclosure, while providing electrical isolation between these components.

A preliminary design for the cell interconnect and busplate has been completed. It was recognized that the weld resistance must be kept to a minimum, if the overall contribution of the interconnect resistances is to be limited to 6% of the cell and bank resistance, respectively. BPI will initiate weld trials between the current carrying members specified by the design in order to verify the design.

Several ideas regarding a viable open circuit failure device have been discussed and documented. In general, no single approach has surfaced that will clearly overcome the insertion losses and offer the reliability and cost needed to make it a viable concept. Neverthe-

less, a few ideas are being explored to the point of experimentation.

Task 2.2.3 Cell Design Verification

Fabrication of the first c/S UES cells was completed in April 1992. The electrical performance of the first two cells was consistent with design predictions: a resistance of 12-13 m Ω (1.20 Ωcm^2) at 330°C and a stable working capacity of 28 Ah to 90% depth of discharge (DOD). In addition, another cell was subjected to three freeze/thaw cycles demonstrating, for the first time, that this c/S cell design could survive at least a limited number of freeze/thaw cycles. This result was contrary to the previous c/S experience at SPL. The design thickness of the sulfur electrode and the improved vertical thermal conductivity of the cell are believed to be responsible for this improved durability. Although the initial c/S cell results were very positive, subsequent cells demonstrated that further improvements in the design, processing, and material selection were needed. To date, 22 cells builds have been attempted, resulting in only 13 that are suitable for testing. Improvements are already being made in two important processes—sealing and the final closure weld. However, the principal cause of the poor cell yield is believed to be the use of old beta"-alumina electrolyte tubes. New electrolytes have since been fabricated at SPL and will be available at the start of FY93. A summary of the testing of these cells is shown in Table 5-3.

Testing of the c/S, UES cell has been geared toward establishing basic electrical performance data for this type of cell. Initial attempts to perform parametric tests were hampered by premature cell failures. However, recent changes in the cell configuration have allowed testing to progress on a few cells.

Two c/S, UES cells are presently on test at the BPI facility in Salt Lake City. These cells incorporate the latest improvements to the cell design and are the first with leak tight cathode closure welds that have been tested. Therefore, these cells represent the first serious look at long-term cell performance. At 11.5 and 12 m Ω , respectively, their resistance appears to be approximately 15% lower than predictions based on cell modeling. The model, however, does include a 1-m Ω allocation for cell interconnection. The most significant cell improvement to date was to eliminate failures caused by current focusing in the electrolyte near the top of the cell. Current focusing leading to electrolyte degradation can occur when the entrance area for sodium ions is larger than the exit area during cell charging. The stresses induced in the electrolyte are further exacerbated if the electrolyte, in the area of the current focusing, is prestressed and/or has existing micro-cracks. The con-

Table 5-3. Summary of UES Cell Testing and Status

Cell Number	Resistance milli-ohms	F/T Cycles	Electrical Cycles	Comments
001	15 - 28	0	13	Faulty cathode weld. Cell breached at top.
002	13	2	4	Faulty cathode weld. Cell breached at top.
003	12 - 13	0	7	Failed during ac power loss; no data. Breached at top.
004	12 - 13	2	32	Failed during third thaw. Breached at top.
007	N/A	N/A	N/A	Failed during heatup. Cell exceeded 750°C.
008	12 - 13	1	16	Failed at top of charge. Cell breached at top.
009	12 - 13	1	25	Failed near top of charge. Melted entire top of cell. Temperature exceeded 650°C.
010	N/A	3	N/A	Dummy - No Na or Sulfur. Compression bond integrity - no leak increase.
011	18 - 45	1	41	Slow cathode leak. High resistance.
012	N/A	1	N/A	TC-Bond integrity experiments w/sulfur.
013, 014, 015	N/A	N/A	N/A	Closure weld failure.
016	N/A	N/A	N/A	No OCV. Breached during heat-up.
017	12 - 13	0	122	On test. f1 increased to over 40%.
018	N/A	0	N/A	Failed on heat-up at 280°C.
019	10 - 13	0	100	On test, cell shows stable performance at 90% DOD.
020	12 - 17	1	13	Leaking sulfur at weld.
021	N/A	0	0	Failed at 370°C during heat-up.
022	9 - 16	0	36	Showed stable performance until leaked formed in closure weld.

NOTE: Cells 3, 4, 13 through 17, and 20 utilized a flame-sprayed molybdenum as the current collector. All other cells used flame-sprayed nickel/chromium (80/20%).

Cells 7, 8, and 9 were equipped with "1/8 inch short" cathode segments. All remaining cells utilized "1/4-inch short" cathode segments to minimize current focussing at the header-electrolyte interface during recharge.

Cells 1 through 17 included a 63-gram sulfur load. All others were 53 grams.

ditions that favored current focusing existed in the early cell builds because the cathode segments extended into the glass line region of the electrolyte/header interface. Furthermore, some of the electrolytes were known to be micro-cracked at the open end prior to glassing the header to the electrolyte. Cell 017 (and subsequent cells) utilized shortened cathode segments as compared to earlier cells. This cell has been on test for more than 30 days and completed 75 electrical cycles (3000 Ah of charge passed).

The performance of three recent cells is discussed in more detail below. Two of these are the ones presently on test. The third failed early in life.

Cell 017 (Mo/Al Current Collector) – Cell resistance and unrecoverable capacity (f_1) have steadily increased from the start of testing for Cell 017. The rate of change for the resistance rise at beginning of discharge is a nearly linear increase of $62 \mu\Omega/\text{cycle}$ as indicated in Figure 5-11. This value is 25 times higher than expected. A plot of the f_1 and DOD (to fixed voltage cut-offs of 2.3 V on charge and 1.83 Voc on discharge) are shown for Cell 017 in Figure 5-12 and reveal a gradually increasing f_1 from around 9%, at the beginning of testing, to over 21% after 60 cycles, with the DOD limited to 90 percent.

Figure 5-13 shows a plot of the DOD for three different cycles for Cell 017. While the degradation in relative performance is clearly seen between each cycle, the position and slope of the single-phase region of each charge curve is nearly identical. This observation strongly suggests that the cause of the increase in cell resistance and f_1 is not due to a loss of catholyte, but some other mechanism.

One possible explanation could be that the molybdenum/aluminum interface is attacked by sodium polysulfide, passivating the aluminum, thus effectively reducing the active area of the current collector. This condition would manifest itself as an increase in cell resistance due to a loss of current collector area. The unrecoverable capacity of the cell would also tend to increase as the current density at the current collector interface increased. Another explanation for the loss of charge acceptance could be that the catalyzing agent, e.g., transition metal sulfides, allowing charge in the two-phase region is nearly depleted.

It is possible that more than one mechanism is responsible for the observed changes in this cell. If the molybdenum/aluminum interface is passivating, eventually the cell will no longer function. However, if the cause of the degradation is due to a loss of the catalyzing agent, the expectation is that f_1 would stabilize at ~60%.

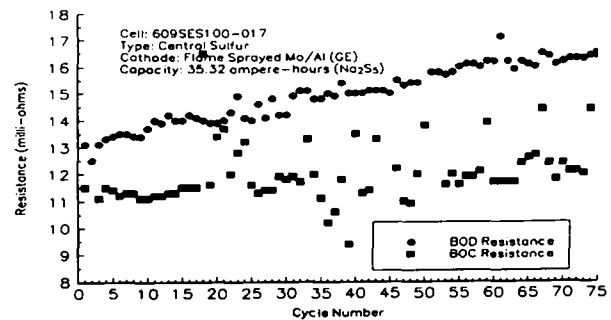


Figure 5-11. Cell Resistance at the Beginning of Discharge and Beginning of Charge vs Cycle Number for Cell 017.

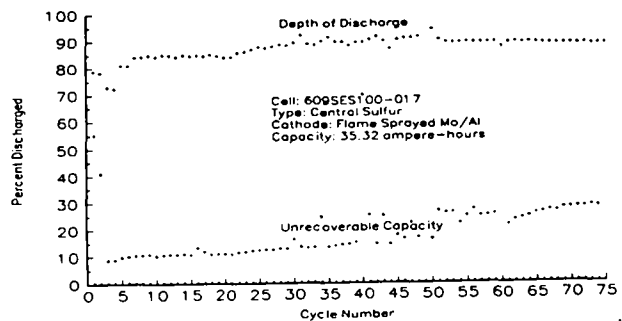


Figure 5-12. Depth of Discharge and f_1 vs Cycle Number for Cell 017.

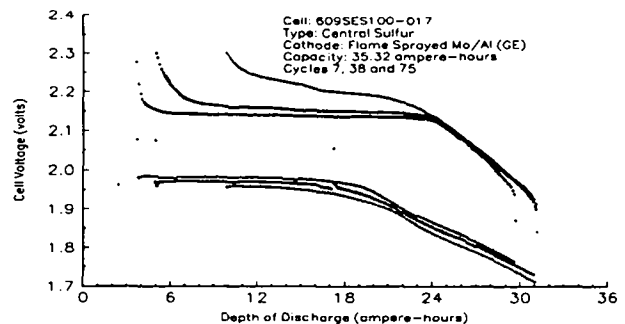


Figure 5-13. Depth of Discharge Plots of Cycles 7, 38, and 75 for Cell 017. Charge and discharge currents were 5 and 7 A, respectively.

Experiments with flame-sprayed molybdenum/aluminum electrode samples that were electrically active in sodium-polysulfide melt, suggest that failure of the current collector may occur after 160 days of exposure to the molten salt. These data would tend to support the “loss of catalyst” theory, but it is important to note that the analysis of the corrosion cell data is not complete. Also, the charge transfer mechanisms in the c/S cell and the corrosion cell are different and may

therefore lead to different failure modes of the current collector.

Cell 019 (Ni/Cr Current Collector) – Cell 019 has completed 50 electrical cycles and continues to show stable performance with respect to cell resistance, useable capacity, and charge acceptance. Cell resistance at the beginning of discharge and charge is plotted against cycle number and shown in Figure 5-14. The higher value for the beginning of discharge resistance is likely due to the formation of sulfur adjacent to the electrolyte at the end of charge, reflecting a good charge acceptance value as indicated in the plots of depth of discharge and f1 versus cycle number shown in Figure 5-15. The plot of cell resistance shows a slight upward slope, which may be due to corrosion of the Ni/Cr current collector. Consistent cell behavior is suggested in Figure 5-16, which shows four polarization plots for this cell, of cycles 6, 20, 31, and 50. The differences seen in the relative position of these curves is consistent with the slight changes in cell resistance and the expected error of the calculated data.

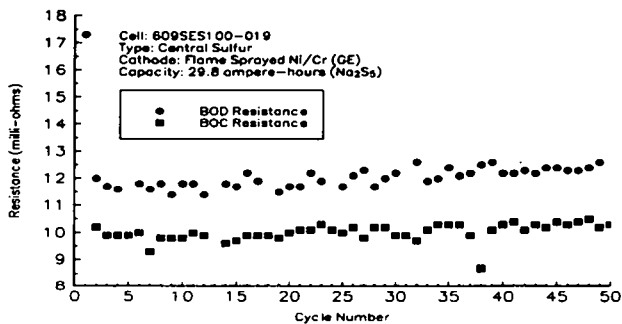


Figure 5-14. Cell Resistance vs Cycle Number for Cell 019.

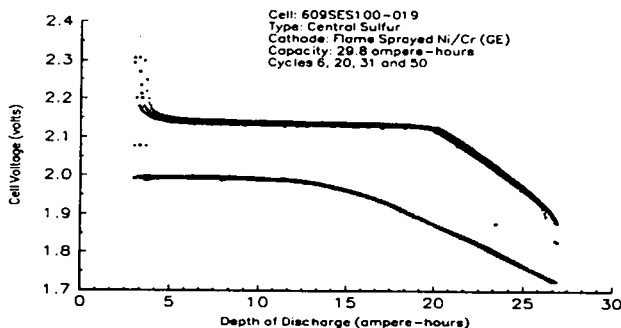


Figure 5-16. Depth of Discharge Plots of Cycles 6, 20, 31, and 50 for Cell 019. Charge and discharge currents were 5 and 7 A, respectively.

Cell 022 (Ni/Cr Current Collector) – Initially this cell showed stable resistance and f1 values. However, following cycle 25, the cell resistance and f1 gradually increased until the cell failed after cycle 35. The lower curve shown in Figure 5-17 and the resistance curves shown in Figure 5-18 show an increase in the slope following cycle 25. These changes were accompanied by a visual indications of leaks in the cathode compartment. The most likely cause of failure was a leak in the cathode compartment caused by failure of the cathode weld. This weld is difficult to make and tends to heat the cell to a point where sulfur vapor could contaminate the weld nugget. Thermal stresses induced during electrical cycling may have fatigued the weld to the point of failure, allowing catholyte to escape and react with air. The reaction products corroded the current lead on the cell anode causing complete loss of electrical contact.

Cell Development Summary

The results of testing performed to date show that the cell performance projections for the BOL can be met. Typical cell performance test results are sum-

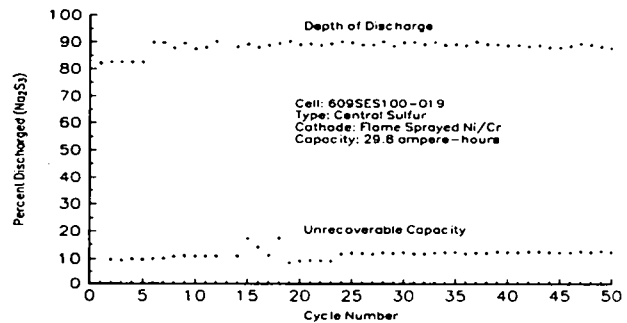


Figure 5-15. Depth of Discharge and f1 as a Function of Cycle Number for Cell 019.

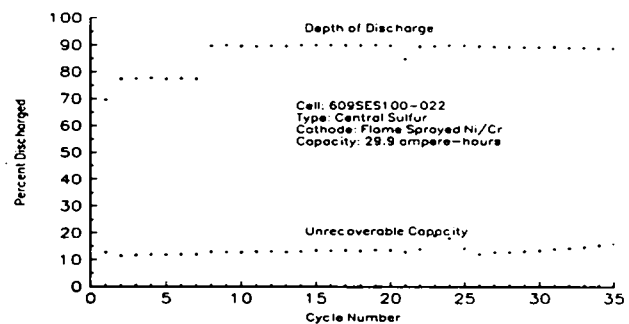


Figure 5-17. Depth of Discharge and f1 vs Cycle Number for Cell 022.

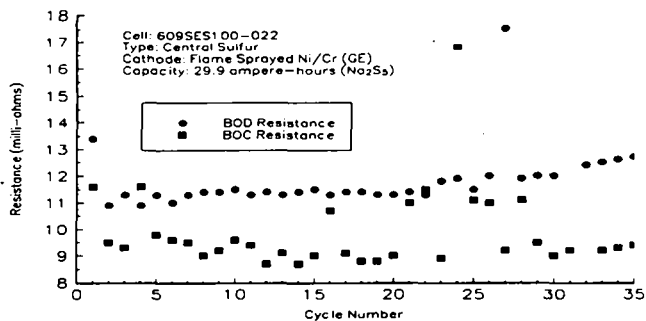


Figure 5-18. Cell Resistance vs Cycle Number for Cell 022.

marized in Table 5-4. These results are in excellent agreement with the projected cell performance.

The actual masses of cells tested are around 362 gm. Some of this extra weight is due to the use of current lugs added to the cell for testing that are different (heavier) from those that will be used on production cells. The remaining weight increase is in the safety tube, which is twice as thick as in the initial design, and in higher graphite felt density in the cathode. For utility applications, the added mass is beneficial for its effect on battery thermal management.

Because of the high incidence of early failures in the cell development effort, it is not possible at this time to speculate about the longer term cell durability and reliability. However, because two causes of early failure have been identified and cell design and fabrication procedures have been changed with a positive effect, longer term cell performance data should now be possible. Further, with the incidence of early failures minimized, statistically valid assessments of the safety and freeze/thaw durability of the present design can be made.

Task 3. Design and Fabrication of UES Module

The design of a representative UES module is scheduled to begin during the fourth quarter of FY92. The basic design of the module is already being completed in Task 2. Two modules are scheduled to be assembled. The first will be tested at BPI as a precursor to the deliverable module, which is scheduled to be shipped to Sandia at the conclusion of the program. The start of this activity is likely to slip about three months to allow additional c/S cells to be built and tested. This revised schedule is also consistent with the decreased funding rate expected in FY93.

Task 4. Full-Scale Battery Plant Design

Originally, the objective of this task was to generate an integrated battery-power conversion system design specific to a utility application selected in Task 1. Along with this, a detailed cost summary would be generated to determine the viability of the proposed design. This task was scheduled to start during the fourth quarter of FY92.

Because the proposed design has developed around a modular ac concept, the drawings and cost will have been generated in adequate detail as an output of Task 2.1 design activity. Therefore, consideration is being given to applying funding for this task to initiate an aspect of system engineering: the design and development of a battery management system. While this subject was intended for subsequent contracts, the need for a unique control system has evolved as a result of some of the studies performed under Task 2.1.

Technology Evaluation - SNL

The performance and operating characteristics, as well as cycle-life data and failure modes for candidate sodium/sulfur cells and modules are determined in this SNL activity. This information is shared with the

Table 5-4. Typical Cell Performance Test Results

Cell Resistance	12 mΩ
Working Capacity	27 Ah
Power at C Rate	45 W
Energy at C/2 Rate	51 Wh

developer to improve the design and operation of the technology.

The specific tasks that were performed include:

1. Evaluation of 40-Cell XPB Module
 - 1.1 - Perform life-cycle tests under UES test profile
2. Evaluation of Single XPB Cells
 - 2.1 - Conduct parametric tests to determine cell performance
 - 2.2 - Perform life-cycle tests

Task 1. 40-Cell XPB Module

During the summer of 1991, SNL received a 40-cell XPB sodium/sulfur module that represents a portion of a single tray of a UES battery design. This module was part of the deliverable agreement from the 5-yr Core Technology contract with SPL. Figure 5-19 is a photograph of the module showing how the cells are picked, while Figure 5-20 is a schematic diagram that represents how the unit is configured electrically. The cells used in this module were designed for utility applications and have a rated capacity of 30 Ah. Four of these cells placed in series make up an 8.28-V string, and ten 4-cell strings placed in parallel make a 300-Ah rated module. This module was instrumented with seven thermocouples (strategically located at positions selected by SPL) and a current shunt on each of the ten strings. The module was placed in a convection furnace and heated at a rate of 6°C/hr to 340°C. Battery voltage, string currents, battery temperatures, and furnace temperature were monitored.

Initial testing started in September 1991. Several break-in cycles were performed at a reduced charge/discharge rate to a shallow DOD. This was done to lower the module resistance. The initial resistance was 38 mohms; however, after 12 cycles, this value had dropped to less than 12 mohms. A plot of module capacity and resistance vs cycle number is shown in Figure 5-21. An average capacity of 257 Ah was removed from the module during the first 24 cycles. This was achieved by discharging the module at a C/3 rate to an end of discharge (EOD) open-circuit voltage of 8.0 V, approximately equivalent to 80% DOD. The module was charged at a C/9 rate to 9.1 V. Discharge cycle 25 was performed to 100% DOD, and a module capacity of 305 Ah was achieved (slightly exceeding the rated value of 300 Ah). Nine additional cycles were then run at 80% DOD. On cycle 32, string #10 experienced an open in one of the cells and the module capacity dropped to 235 Ah at 80% DOD. A cor-

responding increase in module resistance was observed. The string current profiles indicated the loss of string #10, two hours into discharge. The discharge currents on the other nine strings increased slightly to compensate for this failure.

After the loss of string #10, 22 additional cycles were placed on the module. Unstable performance during most of these cycles indicated that there were problems with a second string. Finally, on cycle 54, it was confirmed that string #5 had a cell failure when the module capacity dropped to 186 Ah at 80% DOD. Three 100% DOD cycles followed and a capacity of 230 Ah was achieved, confirming the total loss of two strings. A further decline in capacity and increase in module resistance was observed between cycles 61-75. During this time, the string current profiles indicated that string #1 was experiencing problems. The capacity on cycle 75 was 160 Ah at 80% DOD. However, this value increased to 180 Ah on cycle 76, and from that point on, a gradual decline in capacity was observed with no large fluctuations until cycle 131. Cycles 113-115 were performed at 100% DOD, and a capacity of 210 Ah was achieved.

The capacity of this module at 100% DOD declined further on cycles 141 and 142 and 154 and 155 to a value of 190 Ah; a loss of 38% from what was measured early in life. An increase of approximately 0.5 mohm in the end-of-discharge module resistance was observed each time a string failure occurred. The EOD module resistance increased from a low of 6.3 mohms to 7.7 mohms during the first 131 cycles. Between cycles 132 and 168, the EOD resistance was very erratic.

Figures 5-22 and 5-23 are string current profiles for cycles 167 and 168, the last two cycles run at 80% DOD. These profiles show that strings 5 and 10 had definitely failed and that strings 1 and 7 were close to failure.

The relatively rapid decrease in capacity of this module is not consistent with the behavior observed in earlier 40-cell modules tested at SPL, but is somewhat similar to modules built at the same time period. This inconsistent performance is a source of concern that is currently being studied at SPL.

Following cycle 168 on the 40-cell XPB module, shake-down tests on the SES test profile, developed by SNL, were performed. Most of the errors in the software were corrected before the module performance had declined to a level where it was no longer appropriate to operate. This module will be returned to SPL, and a second 40-cell module will be placed on test to characterize its performance on the SES test profile.

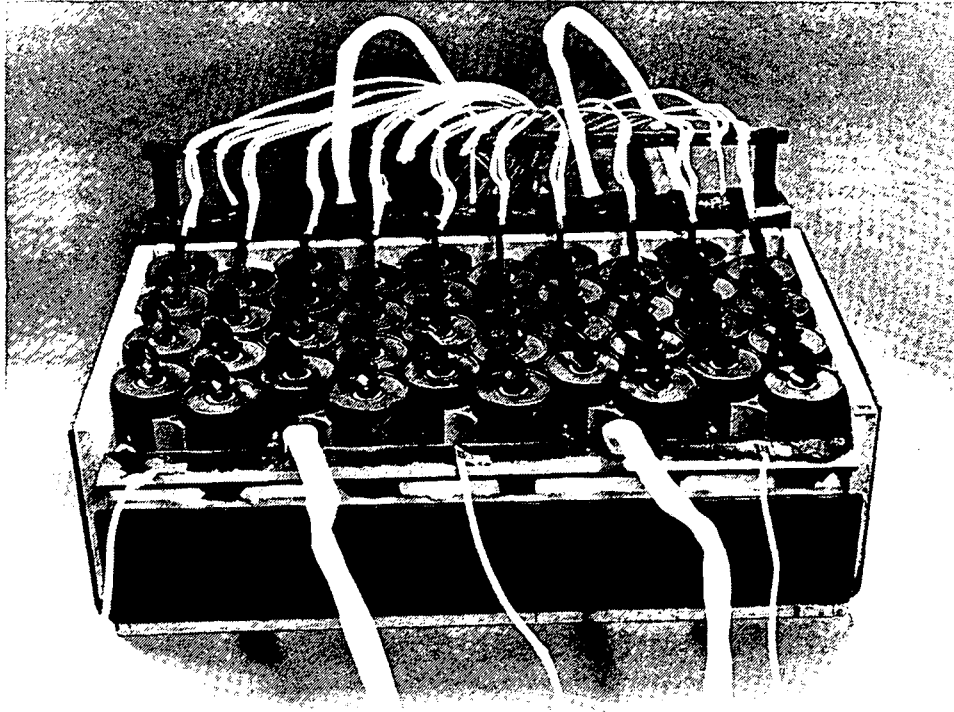


Figure 5-19. Forty-Cell XPB Sodium/Sulfur Module.

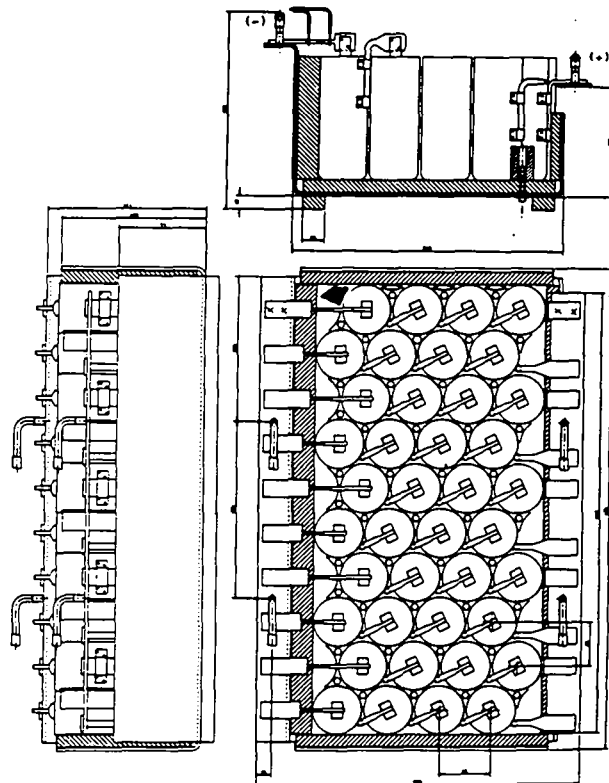


Figure 5-20. Schematic of Electrical Configuration of the 40-Cell Sodium/Sulfur Module.

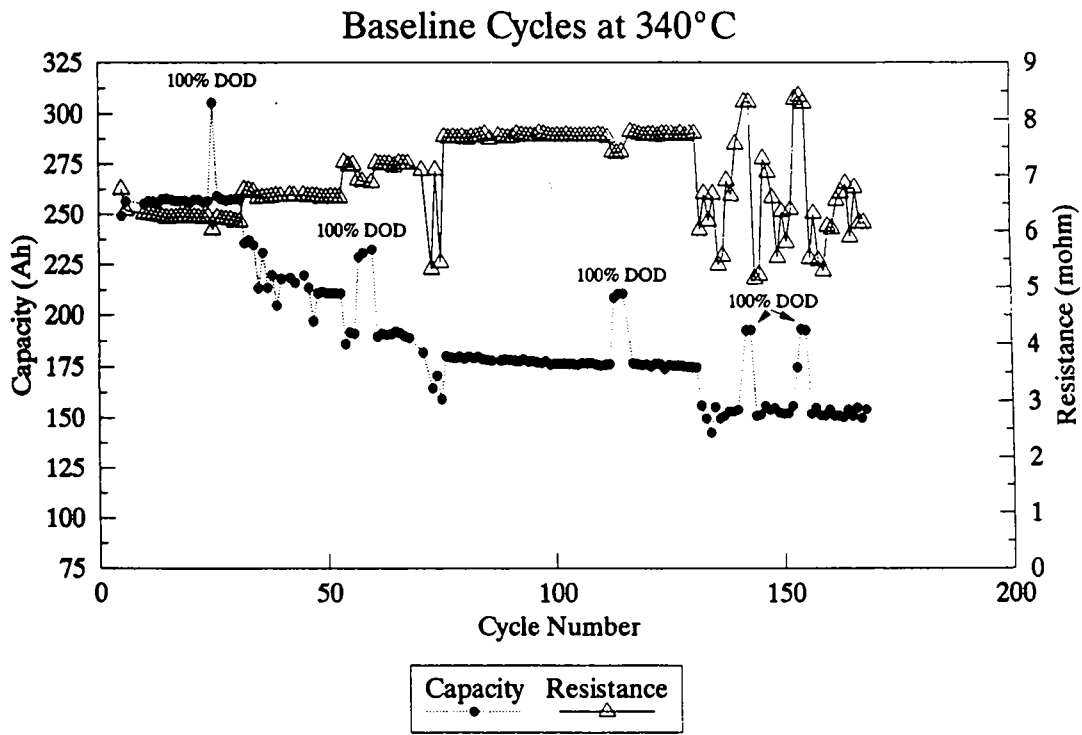


Figure 5-21. SPL 40-Cell XPB Module Test Results.

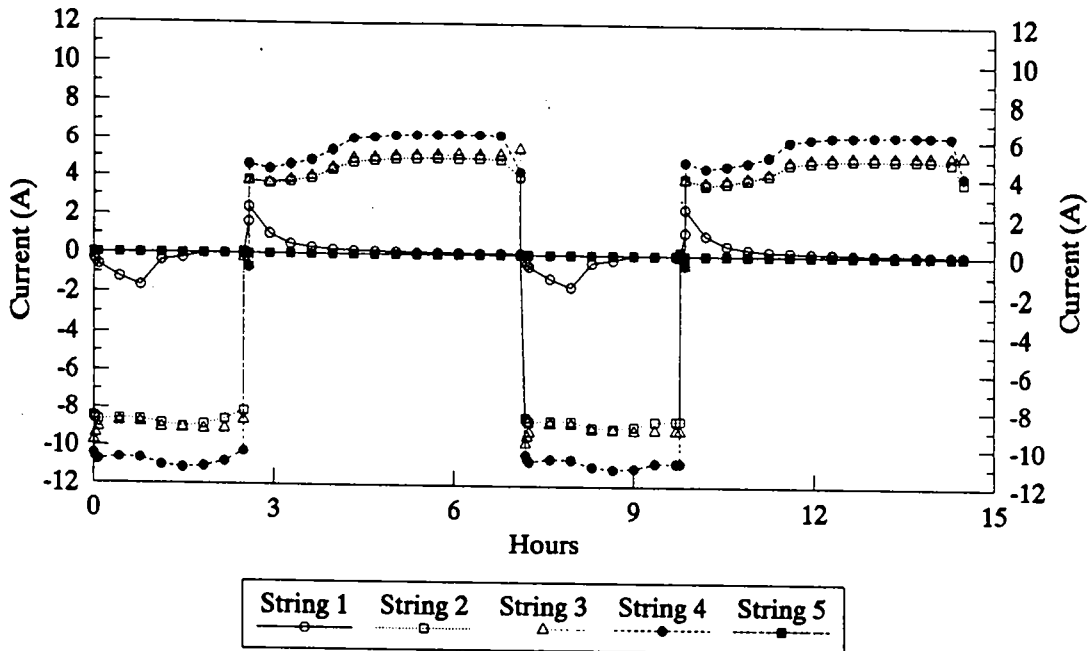


Figure 5-22. SPL 40-Cell XPB Module, Currents for Strings 1-5 (Cycles 167 and 168).

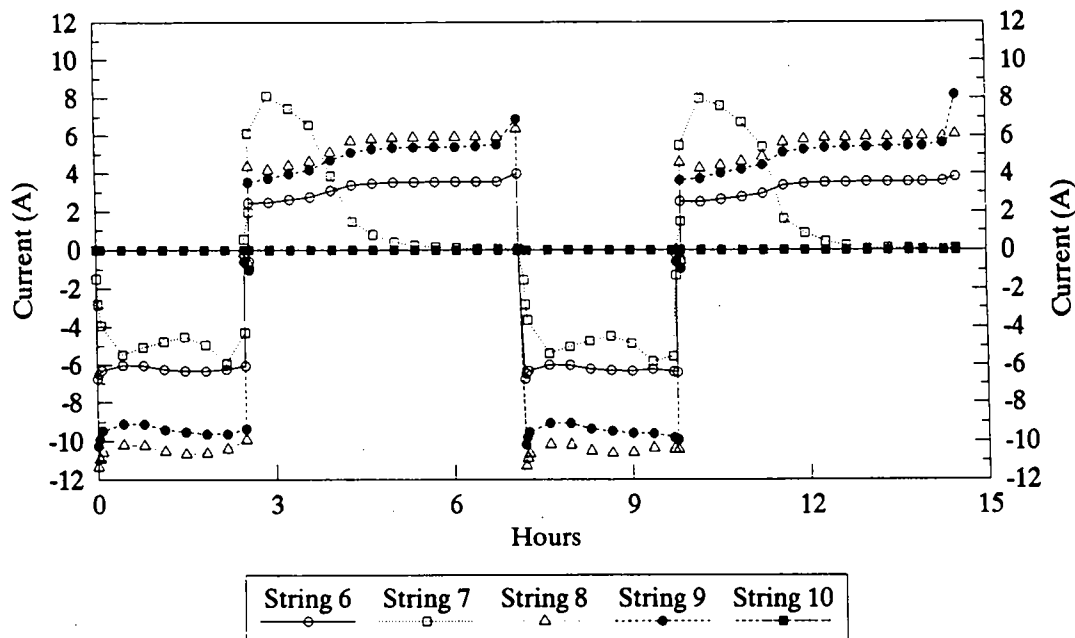


Figure 5-23. CSPL 40-Cell XPB Module, Currents for Strings 6-10 (Cycles 167 and 168).

Task 2. XPB Single Cells

Two 30-Ah XPB cells from the technology development contract with BPI were placed on test during the third quarter of FY92. These cells were designated as SNL #527 and #528. A test plan was developed that consisted of the following:

1. Commissioning that included a thermal warm-up and electrical break-in cycles until the EOD resistance ≤ 12 mohms. Once the resistance was within this range, one cell was kept at 350°C while the other was set at 330°C.
2. Baseline capacity tests in which the cell is discharged to 100% of its rated DOD (open circuit = 1.9 V) at the C/3 rate and charged at c/S.
3. Capacity tests run to determine capacity response to varying charge and discharge rates. Discharge to 100% rated DOD (open circuit = 1.9 V) with current modulated at $\pm 10\%$, or until the high-temperature limit is reached.
4. Constant power tests.
5. Peak power tests.
6. Stand tests.
7. Life-cycle tests using continuous Simplified Frequency Regulation regime to 80% DOD (open

circuit = 2.0 V) and charge at the 6-hr (5A) rate. Cycling shall be interrupted at the end of each month to run three baseline capacity tests.

Once the break-in cycles were completed, three baseline capacity tests were run. The initial capacity of both cells was very close to their rated 30-Ah value. The capacity of cell #527 at 350°C was 30.2 Ah while the capacity of cell #528, which was being cycled at 330°C, was 30.0 Ah. The EOD resistance of both cells was 8.4 mohms.

Next a series of capacity tests was performed to determine how charge and discharge rates affected capacity. These tests were conducted in a random fashion with baseline cycles run at the beginning and end. Figure 5-24 is a plot showing these data. The data points on this plot are average values for three cycles at each charge/discharge rate. The capacity of both cells followed the same trend. A loss in capacity occurred with an increase in the charge or discharge rate. As expected, for the majority of these tests, the capacity of the cell operating at 330°C was lower than that of the cell operating at 350°C. The baseline capacities of both cells at the beginning and end of these tests remained relatively constant. All of the capacity tests that were specified in the test plan were performed except for the 30-A (C/1) discharge set. Initially, high temperatures on the cells were reached before the cycles could be completed, and then problems with cycler relays were

encountered. Testing was temporarily suspended while the cyclers were repaired.

Both XPB cells were moved to a new test station, and baseline capacity tests were performed to determine if a freeze/thaw cycle the cells experienced affected performance. The capacity of Cell #527 increased from 30.2 Ah to 31.0 Ah while the capacity of Cell #528 remained the same at 30.0 Ah.

Constant power tests were run to determine the energy output at various power levels. A set of three cycles was performed at power levels of 6-W, 12-W,

25-W, and 60-W. The cells were then charged for 6 hr at a 5-A rate to an end of charge (EOC) voltage of 2.4 V. Due to over-temperature problems at the 60-W level, a set of cycles, at a reduced power level, was required. Figure 5-25 shows the results of these constant power tests. The data points are average values for the three cycles run. On a relative basis, the results presented in Figures 5-24 and 5-25 for XPB cells are consistent with those obtained previously for SPL-PB cells.

The attempts to run peak power tests were unsuccessful because of high cell resistance.

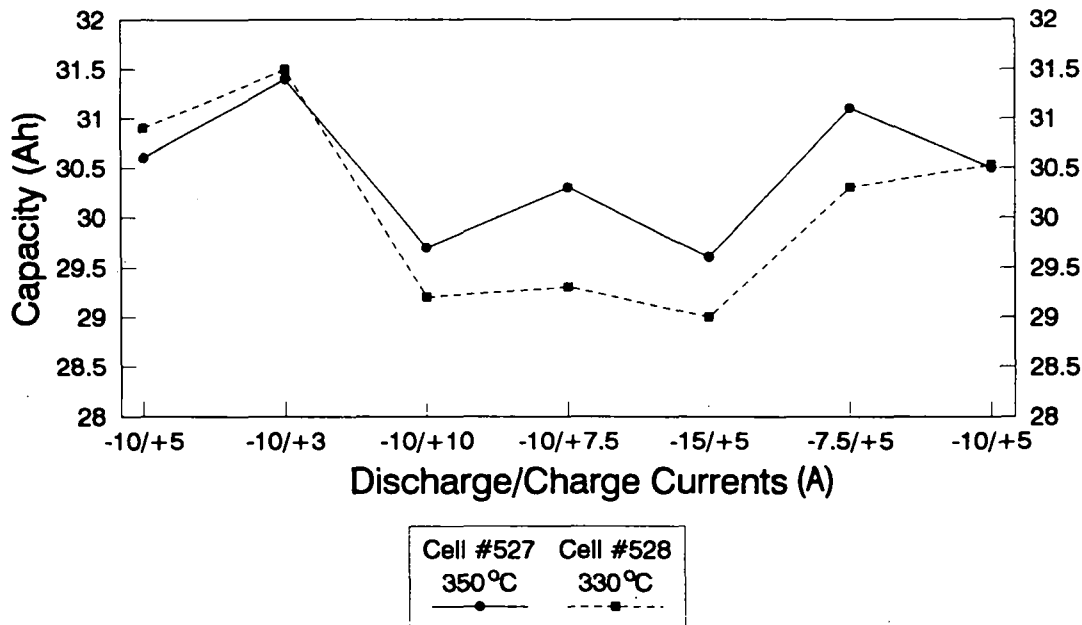


Figure 5-24. XPB Cells, Parametric Tests with Charge and Discharge Current Varied.

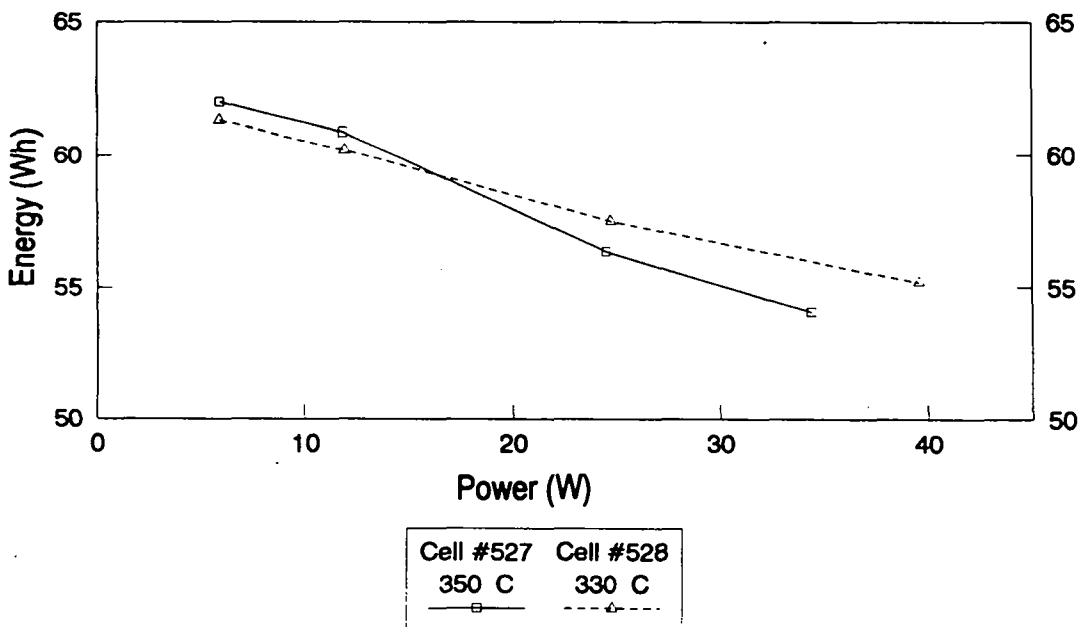


Figure 5-25. XPB Cells, Constant Power Tests.

6. Supplemental Evaluations and Field Tests

SNL Test Facilities

In preparation for the upcoming evaluations of utility battery performance at SNL, improvements to the facilities have been in progress. This activity has included procurement of 4 large power supplies, 3 load units, a computer, and a stand-alone tester. Several of the loads and power supplies were temporarily used to evaluate the 100-cell zinc/bromine battery from JCBGI and two 40-cell sodium sulfur XPB modules from BPI. The UNIX computer work station was purchased to gather test data on sodium/sulfur modules. The stand-alone tester was fabricated by Transistor Devices to evaluate large lead-acid deliverables from GNB and the PREPA/C&D lead-acid battery. An SES test profile, which will be used to evaluate the lead-acid batteries and XPB sodium/sulfur modules, has been developed by SNL. A small enclosure was built to perform controlled temperature tests on the PREPA/ C&D battery.

Nickel/Hydrogen Field Tests

JCBGI, contract #78-8203, originally provided technical support for the testing of four 2-kWh CPV nickel/hydrogen batteries, two each at the Florida Solar Energy Center (FSEC) and the Southwest Technology Development Institute (TDI), and the testing of a 7-kWh boilerplate CPV battery at JCBGI. Testing was terminated at TDI in November 1991.

FSEC Tests

In November 1991, one of the two batteries that had originally been delivered to TDI for testing was shipped to FSEC. The plan was to couple this unit in series with the remaining unit at FSEC. Independent characterization cycles were run on each of the two batteries as a routine state-of-health check before starting the series configuration tests. Battery P022, the remaining unit from FSEC, accepted 232.2 Ah before charge was terminated based on a decline of the pressure slope. It delivered 196.6 Ah, well above the 160 Ah rating. Battery coulombic efficiency was 85%. Voltage cell pair matching was excellent. Battery P005, the unit from TDI, also performed well despite being hampered by a short in one of the 10 cells. It accepted 231.8 Ah before charge was terminated based on roll-over of the pressure

slope. It delivered 185.9 Ah, also well above the 160-Ah rating. Battery coulombic efficiency was 80%.

Shortly after completing the characterization tests, a small leak was identified in battery P005, and it was removed from test and returned to JCBGI for analysis. Subsequent examination at JCBGI indicated a vessel failure at one of the adhesive-bonded end domes, similar to the mechanism that had been observed previously on the other two batteries. Testing of battery P022 continued with the photovoltaic array reconfigured for the single battery. The battery was placed on the simulated vaccine refrigeration cycle. In this profile, the battery was cycled daily to approximately 20% DOD. Plans are to terminate testing at FSEC and return the battery to JCBGI.

7-kWh Battery

The 7-kWh nickel/hydrogen battery continued to be evaluated during FY92. This battery had previously been on test for two years at SNL before being returned to JCBGI. The battery design consists of four 12-V units, wired in a series/parallel arrangement to deliver 300 Ah at 24 V and packaged in a rectangular framework (49"x 34"x 39"). Passive cooling assisted thermal management; no active cooling was provided. Electrical taps were provided on a panel to allow series testing in 12-V multiples up to 48 V with a capacity of 150 to 600 Ah. Each battery module contains 10 prismatic cells. Each cell contains nine cell-modules, a concept developed to reduce manufacturing costs and promote ease of handling. One cell-module, which is the building block of the prismatic cell, consists of two sintered and electrochemically impregnated nickel positives in a back-to-back configuration with an electrolyte absorber between them, two separators, and two negative electrodes. The components of the cell-module are bound together by two outside diffusion screens.

During the year, a series of tests examining the effects of discharge and charge rate was completed. In the discharge rate tests, a range of C/3 to C/20 was covered. The four 12-V batteries were coupled as two independent series sets for the tests. The charge consisted of a C/10 rate for 12.5 hr. Capacity was quite stable over the rate range, varying from 190 to 195 Ah for the C/4 to C/20 rates (Table 6-1). Even at the highest rate tested, C/3, the battery pairs delivered 183 and 189

Table 6-1. 7-kWh Ni/H₂ Battery Discharge Rate Tests

Cycles*	Discharge Rate	Battery Pair PV1-PV3		Battery Pair PV2-PV4	
		Amp-hour Capacity	Mid-Disch Volt/Cell	Amp-hour Capacity	Mid-Disch Volt/Cell
1-8	C/5	191.5	1.24	193.1	1.25
9-15	C/10	195.0	1.29	195.1	1.30
16-22	C/20	194.7	1.32	195.1	1.32
23-28	C/15	194.7	1.31	195.1	1.32
29-41	C/3	183.0	1.16	189.2	1.18
42-49	C/4	190.0	1.21	193.2	1.22
50-54	C/5	193.3	1.24	194.8	1.25

* For convenience, cycle numbers were reset at zero prior to initiating the parametric tests. The batteries had been cycled at JCBGI at the time of fabrication and daily at SNL over a period of ~2 yr for a total of ~800 cycles prior to the initiation of these tests.

Ah, respectively, well above the 160 Ah rating. Results of the C/5 rate tests run at the beginning and end of the series of discharge rate tests indicate stable performance over the 54 cycle test period.

A series of tests examining the effects charge rate was completed in the second quarter of FY92. The 12-V batteries remained in the same configuration as in the previous tests. Battery performance was excellent and consistent over the charge rate range of C/5 to C/20, again demonstrating the flexibility of the nickel hydrogen system (Table 6-2).

Toward the end of the second quarter, life-cycle tests were started on the four battery stacks that comprise the 7-kWh system. Presently, the batteries remain on the life-cycle test regime. The batteries are being charged for 750 min at the C/10 rate and discharged at the C/5 rate to 100% DOD (1.0 V/cell). The batteries have exceeded 1040 cycles to date, including approximately 800 cycles run at SNL prior to the initiation of the tests at JCBGI.

As can be seen in Figures 6-1 and 6-2, delivered capacity of the nominal 160-Ah batteries is steady at 195 Ah for both battery pairs, corresponding to a

coulombic efficiency of almost 98%. The scatter in the early portion of the data (cycles 1 to 80) is due to variations in charge and discharge rates that were being examined at that time.

A steady rise in pressure has been observed in the PV1-PV2 battery pair. The slight decrease in pressure at around cycle 970 resulted when the pressure reached the limit of the safety relief valve. No corresponding pressure rise has been observed in battery pair PV3-PV4. It is not clear whether this is due to a true difference in behavior between the pairs or if there is a low-level leak from the PV3-PV4 pair that could be counteracting the pressure rise. Similar increases in pressure have been observed previously in cells tested at SNL.

Cycling has been temporarily suspended due to a failure in the cyler cooling system. Tests will be resumed as soon as the problem is corrected. The batteries will remain on the two cycle/day life-test until failure, defined as a drop in capacity of 80% of the 160-Ah nominal rating. However, this effort will no longer be supported by SNL, and further testing will be sponsored by JCBGI.

Table 6-2. 7-kWh Ni/H₂ Battery Charge Rate Tests

Cycles*	Charge Rate	Battery Pair PV1-PV3		Battery Pair PV2-PV4	
		Amp-hour Capacity	Mid-Disch Voltage	Amp-hour Capacity	Mid-Disch Voltage
50-54	C/10	193.3	1.24	194.8	1.25
55-59	C/20	190.6	1.24	192.6	1.25
60-72	C/5	190.1	1.24	191.3	1.25

* For convenience, cycle numbers were reset at zero prior to initiating the parametric tests. The batteries had been cycled at JCBGI at the time of fabrication and daily at SNL over a period of ~2 yr for a total of ~800 cycles prior to the initiation of these tests.

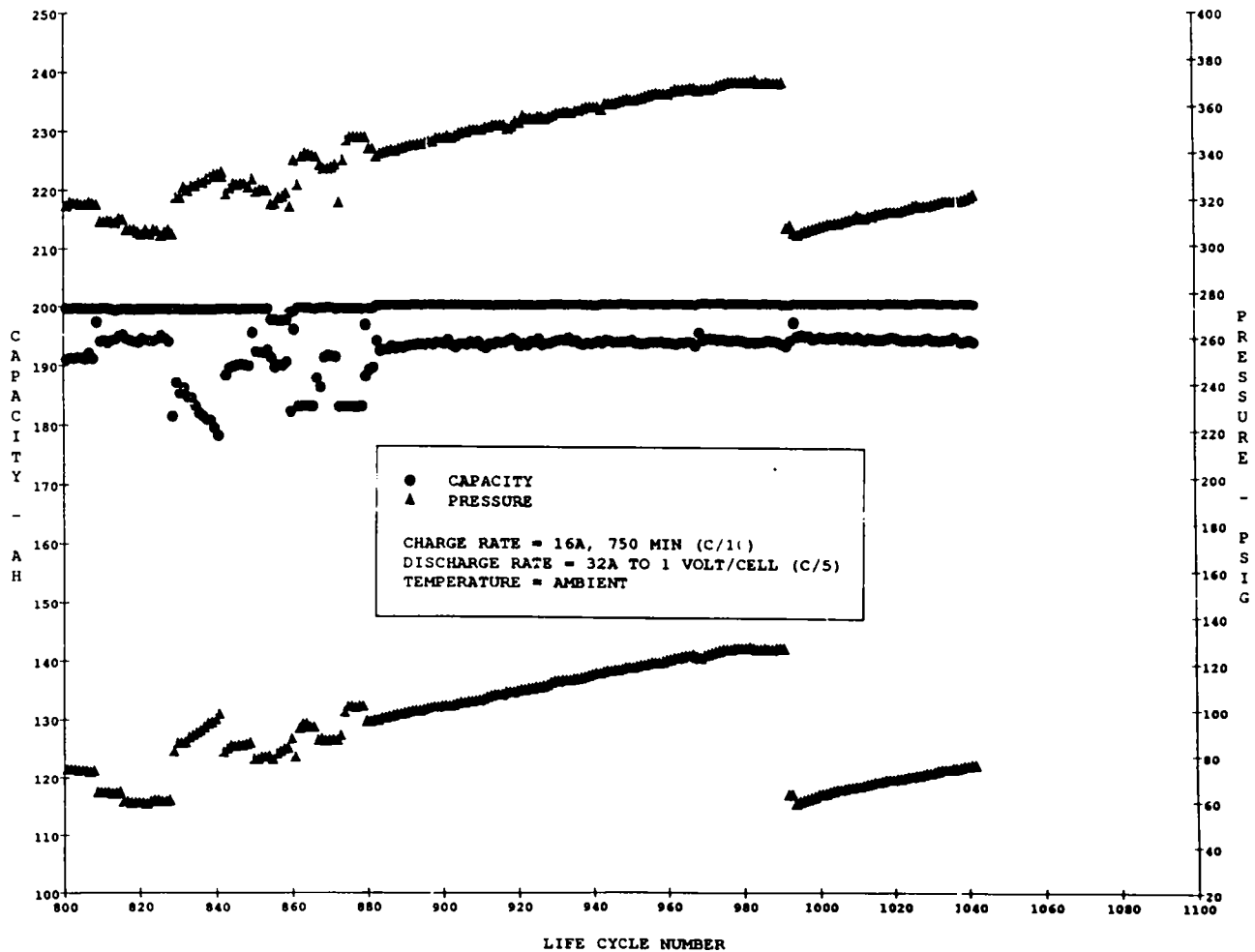


Figure 6-1. Performance Summary of Ni/H₂ Batteries PV1 and PV2 (Batteries Series-Connected).

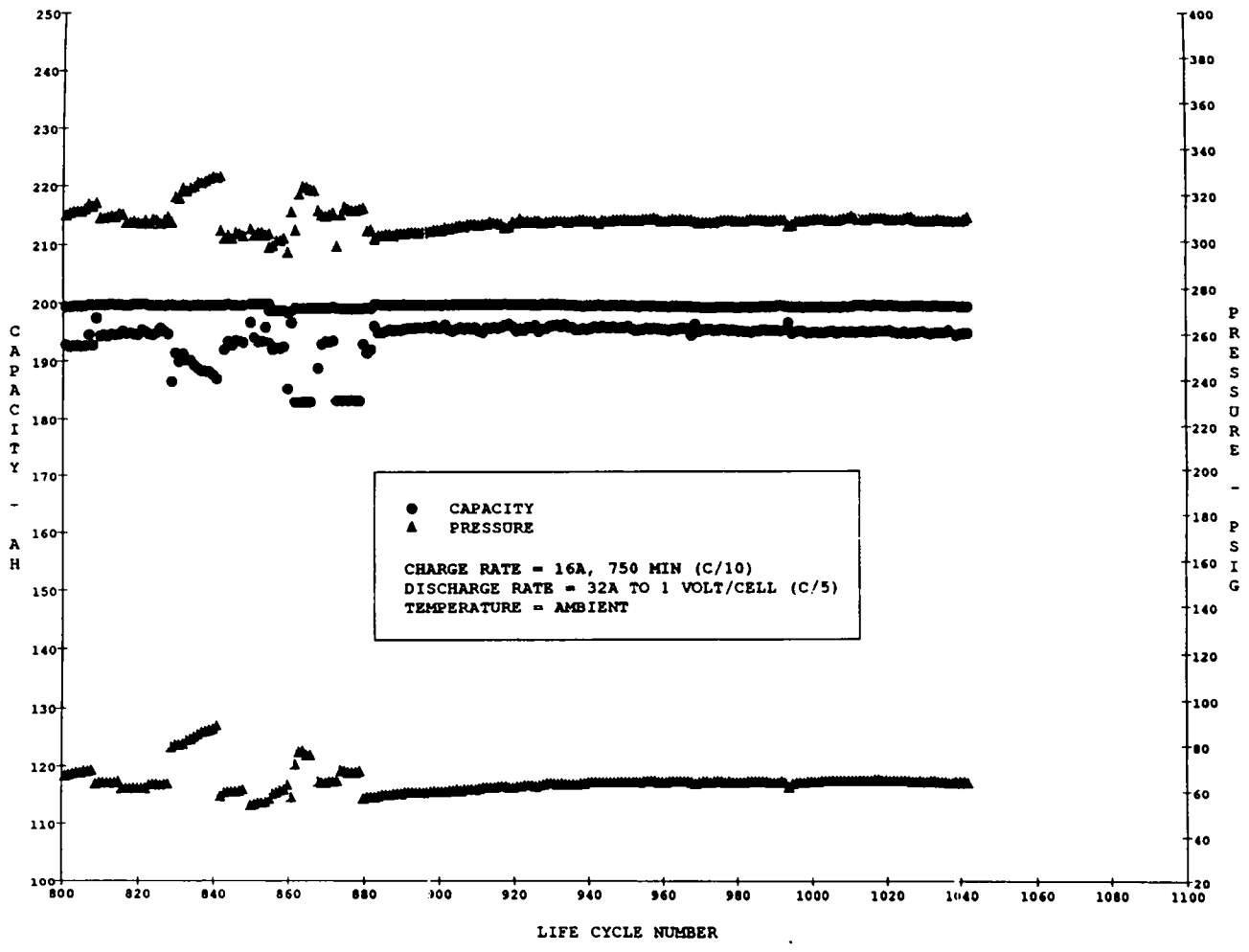


Figure 6-2. Performance Summary of Batteries PV3 and PV4 (Batteries Series-Connected).

Appendix: Presentations and Publications

Presentations

- Akhil, A. A., J. Salim, and H. Clark, "Overview and Preliminary Results of DOE System Studies," 2nd Utility Battery Group Meeting, San Diego, CA, November 1991.
- Akhil, A. A., "Utility Specific System Studies Review of Results," 3rd Utility Battery Group Meeting, Albuquerque, NM, May 1992.
- Butler, P. C., J. Hurwitch, G. Hunt, A. Akhil, "Review of Battery Benefits and Market Potential," Presentation to General Electric Management and Staff, Salem, VA, May 1992.
- Butler, P. C., "Status of Task 3: Test Procedures Working Group," 2nd Utility Battery Group Meeting, San Diego, CA, November 1991.
- Eidler, P., "Zinc-Bromine Load Leveling Battery Project Update," 3rd Utility Battery Group Meeting, Albuquerque, NM, May 1992.
- Jabbour, S., "Dispelling Two Myths," 3rd Utility Battery Group Meeting, Albuquerque, NM, May 1992.
- Koenig, A., "Status of Sodium-Sulfur R&D for Storage Applications," 3rd Utility Battery Group Meeting, Albuquerque, NM, May 1992.

Lex, P. J. and J. F. Mathews, "Recent Developments in Zinc/Bromine Technology at Johnson Controls," Presented at the 35th International Power Sources Symposium, Cherry Hill, NJ, June 22-25, 1992.

Meyer, H., "AC Battery Development Project Status," 3rd Utility Battery Group Meeting, Albuquerque, NM, May 1992.

Rider, R., "Delco Remy/AC Battery 'Concept'," 3rd Utility Battery Group Meeting, Albuquerque, NM, May 1992.

Zagrodnik, J. and K. Jones, "Nickel Hydrogen Batteries for Terrestrial Applications," 27th Intersociety Energy Conversion Engineering Conference (IECEC), San Diego, CA, August 1992.

Zagrodnik, J. and K. Jones, "Nickel Hydrogen Battery - Common Pressure Vessel," 35th International Power Sources Symposium, Cherry Hill, NJ, June 1992.

Publications

Magnani, N. J., P. C. Butler, A. A. Akhil, J. W. Braithwaite, N. H. Clark, J. M. Freese, *Utility Battery Exploratory Technology Development Program Report for FY91*. Sandia National Laboratories, SAND91-2694, December 1991.

Distribution

ABB Power T&D Co., Inc.
630 Sentry Parkway
Blue Bell, PA 19422
Attn: H. Weinrich

Alaska Energy Authority (2)
P.O. Box 190869
Anchorage, AK 99519-0869
Attn: D. Denig-Chakroff
A. Sinha

American Electric Power Service Corp.
1 Riverside Plaza
Columbus, OH 43215
Attn: C. Shih

Argonne National Laboratories (3)
CTD, Building 205
9700 South Cass Avenue
Argonne, IL 60439
Attn: C. Christianson
W. DeLuca
K. Myles

Arizona Public Service
P.O. Box 5399
Phoenix, AZ 85072
Attn: R. Hobbs

AT&T Energy Systems
3000 Skyline Drive
Mesquite, TX 75149
Attn: M. Bize

Bechtel
P.O. Box 193965
San Francisco, CA 94119-3965
Attn: W. Stolte

Best Facility
321 Sunnymeade Road
Somerville, NJ 08876
Attn: G. Grefe

Bonneville Power Administration
Routing EO
P.O. Box 3621
Portland, OR 97208
Attn: J. Ray

C&D Charter Power Systems, Inc.
3043 Walton Road
P.O. Box 239
Plymouth Meeting, PA 19462-0239
Attn: S. Misra

California State Air Resources Board
Research Division
P.O. Box 2815
Sacramento, CA 95812
Attn: J. Holmes

Charter Power Systems, Inc.
3043 Walton Road
P.O. Box 239
Plymouth Meeting, PA 19462-0239
Attn: S. Misra

Chugach Electric Association, Inc.
P.O. Box 196300
Anchorage, AK 99519-6300
Attn: T. Lovas

Consolidated Edison (2)
4 Irving Place
New York, NY 10003
Attn: M. Lebow
N. Tai

Corn Belt Electric Cooperative
P.O. Box 816
Bloomington, IL 61702
Attn: R. Stack

Decision Focus, Inc.
650 Castro Street, Suite 300
Mountain View, CA 94041
Attn: S. Jabbour

Delco-Remy
7601 East 88th Place
Indianapolis, IN 46256
Attn: R. Rider

EG&G Idaho, Inc.
Idaho National Engineering Laboratory
P. O. Box 1625
Idaho Falls, ID 83415
Attn: G. Hunt

Eagle-Picher Industries
C & Porter Street
Joplin, MO 64802
Attn: J. DeGruson

East Penn Manufacturing Co., Inc.
Deka Road
Lyon Station, PA 19536
Attn: M. Stanton

Electric Power Research Institute (4)
3412 Hillview Avenue
P. O. Box 10412
Palo Alto, CA 94303
Attn: S. Eckroad
R. Schainker
P. Symons
R. Weaver

Electrotek Concepts, Inc.
P.O. Box 16548
Chattanooga, TN 37416
Attn: H. Barnett

Eltech Research Corporation
625 East Street
Fairport Harbor, OH 44077
Attn: E. Rudd

Energetics, Inc. (3)
7164 Columbia Gateway Drive
Columbia, MD 21046
Attn: J. Hurwitch
D. Baker
C. Matzdorf

Energy Systems Consulting
41 Springbrook Road
Livingston, NJ 07039
Attn: A. Pivec

Exxon Research Company
P.O. Box 536
1900 East Linden Avenue
Linden, NJ 07036
Attn: P. Grimes

Firing Circuits, Inc.
P.O. Box 2007
Norwalk, CT 06852-2007
Attn: J. Mills

General Electric Company (2)
Building 2, Room 605,
1 River Road
Schenectady, NY 12345
Attn: D. Swann
E. Larson

General Electric Drive Systems
1501 Roanoke Blvd.
Salem, VA 24153
Attn: C. Romeo

General Motors
Tech. Ctr. Engineering West, W3-EVP
30200 Mound Road
P. O. Box 9010
Warren, MI 48090-9010
Attn: M. Eskra

Giner, Inc.
14 Spring Street
Waltham, MA 02254-9147
Attn: A. LaConti

GNB Industrial Battery Company (3)
Woodlake Corporate Park
829 Parkview Blvd.
Lombard, IL 60148-3249
Attn: S. Deshpande'
G. Hunt
J. Szyborski

Hawaii Electric Light Co.
P.O. Box 1027
Hilo, HI 96720
Attn: C. Nagata

Hughes Aircraft Company
P.O. Box 2999
Torrance, CA 90509-2999
Attn: R. Taenaka

Integrated Power Corp. (2)
7524 Standish Place
Rockville, MD 20855
Attn: T. Blumenstock
D. Danley

ILZRO (2)
P.O. Box 12036
Research Triangle
Park, NC 27709
Attn: J. Sharpe III
R. Nelson

Johnson Controls Battery Group, Inc. (4)
5757 N. Green Bay Avenue
P. O. Box 591
Milwaukee, WI 53201
Attn: P. Eidler
R. Miles
T. Ruhlmann
W. Tiedeman

Johnson Controls Battery Group, Inc.
12500 W. Silver Spring Drive
P. O. Box 591
Milwaukee, WI 53201-0591
Attn: J. Zagrodnik

Lawrence Berkeley Laboratory (3)
University of California
One Cyclotron Road
Berkeley, CA 94720
Attn: E. Cairns
K. Kinoshita
F. McLarnon

N.E.T.S.
P.O. Box 32584
Juneau, Ak 99803
Attn: T. Neubauer

National Renewable Energy Laboratory (2)
1617 Cole Blvd.
Golden, CO 80401-3393
Attn: J. Ohi
L. Goldstein

New York Power Authority
1633 Broadway
New York, NY 10019
Attn: B. Chezar

Northern States Power
414 Nicollet Mall
Minneapolis, MN 55401
Attn: M. Rogers

Oglethorpe Power Company
2100 E. Exchange Place
P.O. box 1349
Tucker, GA 30085-1349
Attn: K. Scruggs

Omnion Power Corporation
P.O. Box 879
East Troy, WI 53120
Attn: H. Meyer

Pacific Gas & Electric (4)
3400 Crow Canyon Road
San Ramon, CA 94583
Attn: G. Ball
R. Winter
B. Norris
J. Meglen

Power Technologies, Inc.
1 Sierragate Plaza, Suite 340
Roseville, CA 95678
Attn: H. Clark

Puerto Rico Power Authority
G.P.O. Box 4267
San Juan, Puerto Rico 00936-426
Attn: W. Torres

R&D Associates
2100 Washington Blvd.
Arlington, VA 22204-5706
Attn: J. Thompson

Robicon Corporation
100 Sagamore Hill Road
Pittsburgh, PA 15239
Attn: A. Maruschak

Sacramento Municipal Utility District
6201 S. Street
Sacramento, CA 95817
Attn: L. Wittrup

Salt River Project
MS PAB 357, Box 52025
Phoenix, AZ 85072-2025
Attn: H. Lundstrom

San Diego Gas & Electric Company
P.O. Box 1831
San Diego, CA 92112
Attn: J. Wight

W. J. Schafer Associates
303 Lindbergh Avenue
Livermore, CA 94550-9551
Attn: S. Schoenung

R. K. Sen & Associates
3808 Veazey Street NW
Washington, DC 20016
Attn: R. Sen

Silent Power, Inc.
163 West 1700 South
Salt Lake City, UT 84115
Attn: J. Rasmussen

Silent Power, Inc. (5)
489 Devon Park Drive
Suite 315
Wayne, PA 19087
Attn: W. Auxer
A. Koenig (3)
G. Smith

Silent Power, Ltd. (2)
Davy Road, Astmoor
Runcorn, Cheshire
UNITED KINGDOM WA7 1PZ
Attn: W. Jones
M. McNamee

Southern California Edison
2244 Walnut Grove Avenue
P.O. Box 800
Rosemeade, CA 91770
Attn: A. Rodriguez

Stuart Kuritzky
347 Madison Avenue
New York, NY 10017

Superconductivity, Inc.
2114 Eagle Drive
Middleton, WI 53562
Attn: J. Emerick

United Engineers and Contractors
700 South Ash St.
P.O. Box 5888
Denver, CO 80217
Attn: A. Randall

University of Missouri - Rolla
112 Electrical Engineering Building
Rolla, MO 65401-0249
Attn: M. Anderson

University of New Mexico
Dept. of Chemistry
Albuquerque, NM 87131-1096
Attn: L. Deck

University of Wisconsin - Madison
Dept. of Electrical & Computer Eng.
1415 Johnson Drive
Madison, WI 53706
Attn: D. Divan

U.S. Department of Energy (21)
Office of Energy Management
CE-142 FORSTL
Washington, DC 20585
Attn: R. Eaton (20)
K. Klunder

U.S. Department of Energy (9)
Office of Propulsion Systems
CE-321 FORSTL
Washington, DC 20585
Attn: K. Barber
J. Brogan
E. Dowgiallo
K. Heitner
A. Landgrebe
R. Miner
D. O'Hara
P. Patil
R. Sutula

U.S. Department of Energy (2)
Albuquerque Operations Office
Energy Technologies Division
Albuquerque, NM 87115
Attn: G. Buckingham (2)

U.S. Windpower, Inc.
6952 Preston Avenue
Livermore, CA 94550
Attn: D. Richardson

Westinghouse STC
1310 Beulah Road
Pittsburgh, PA 15235
Attn: H. Saunders

W. R. Grace & Company
62 Whittemore Avenue
Cambridge, MA 02140
Attn: S. Strzempko

Yuasa-Exide
P.O. Box 14205
Reading, PA 19612-4205
Attn: F. Tarantino

Zaininger Engineering Co., Inc.
1590 Oakland Road, Suite B211
San Jose, CA 95131
Attn: H. Zaininger

1811 R. Clough
1811 C. Arnold
1812 C. Renschler
1812 R. Assink
2000 H. Schmitt
2500 G. Beeler

2504 R. Clark
2504 L. Lachenmeyer
2522 K. Grothaus
2523 D. Doughty
2525 P. Butler (20)
2525 A. Akhil
2525 J. Braithwaite
2525 N. Clark
2525 J. Freese
2525 R. Jungst
2525 S. Klassen
3714 J. Kerr, Attn: D. Wilt
6200 B. Marshall
6204 N. Magnani
6213 T. Bickell
6218 W. Bower
6218 R. Bonn
8523-2 Central Technical Files
7141 Technical Library (5)
7151 Technical Publications
7613-2 Document Processing for DOE/OSTI (10)

THIS PAGE INTENTIONALLY LEFT BLANK